超対称ランダウ・ギンツブルグ模型の赤外臨界点の数値的研究

森川, 億人

出版情報：Kyushu University, 2020, 博士（理学）, 課程博士
バージョン：
権利関係：

Ph.D. Thesis

Numerical study of infrared criticality of the supersymmetric Landau–Ginzburg model

超対称ランダウ・ギンツブルグ模型の赤外臨界点の数値的研究

Okuto Morikawa

Department of Physics, Kyushu University,
744 Motooka, Nishi-ku, Fukuoka, 819-0395, Japan

December 20, 2020

Abstract

In sufficiently low energies, that is, at the infrared (IR) fixed point, quantum field theories are expected to be scale invariant. Such a scale-invariant theory would be described by a conformal field theory (CFT). If a quantum field theory gives rise to a nontrivial CFT at the IR fixed point, the original theory is called the Landau–Ginzburg (LG) description of the CFT, or the LG model. In particular, as an example of the supersymmetric LG model, it is believed that the two-dimensional $\mathcal{N} = (2, 2)$ Wess–Zumino (2D $\mathcal{N} = 2$ WZ) model corresponds to the 2D $\mathcal{N} = 2$ superconformal field theory (SCFT). This conjecture of the LG description has been theoretically analyzed from various aspects. It is, however, difficult to prove this theoretical conjecture directly, since the coupling constant becomes strong at the IR region. Moreover, because this is the lower-dimensional massless system, the perturbation theory possesses severe IR divergences. For these reasons, the LG description is a remarkable non-perturbative phenomenon.

This issue is closely related to superstring theory. Superstring theory is expected to describe quantum gravity, and provide a candidate for a theory of everything, which unifies all fundamental forces. In superstring theory, we observe a four-dimensional spacetime, while there exists an extra six-dimensional space, which is compactified into the Calabi–Yau (CY) manifold. Then, scattering amplitudes in a superstring theory with the CY compactification can be computed from an $\mathcal{N} = 2$ SCFT, by which the world sheet theory is described. However to pursue this strategy is quite difficult because such a SCFT is in general not a solvable minimal model. Thus, it is hard to carry out any computation for a general CY manifold and to treat phenomena relating to the dynamics of spacetime. The LG description, on the other hand, realizes a strongly-interacting Lagrangian with the superpotential corresponding to the geometry of the CY manifold; we can deform the geometry of the superstring compactification by manipulating the superpotential. Therefore, if we can analyze such a strongly-interacting field theory directly, the study of the LG model would be a new approach to look into superstring theory.

An useful approach to this issue may be provided by a non-perturbative calculational method such as the lattice field theory. A quantum field theory is defined as a discretized theory on a spacetime lattice. Implementation of such a lattice formulation on the computer enables us to calculate physical quantities from first principles. As is well recognized, however, the spacetime lattice is generally incompatible with spacetime symmetries such as the supersymmetry (SUSY). Although those symmetries are expected to restore in the continuum limit, this is an obstacle to the lattice study on supersymmetric field theories. Despite this difficulty, there are some recent numerical studies for the WZ model with the cubic superpotential; the scaling dimension and the central charge in the corresponding A_2 minimal model were measured. These numerical studies achieved a triumph of the lattice field theory, and

provides a non-perturbative evidence of the WZ/minimal-model correspondence.

In this thesis, we numerically study the 2D $\mathcal{N} = 2$ WZ model, by using the formulation by Kamata and Suzuki. This formulation is based on the Nicolai map and the momentum cutoff regularization; allowing the action to be non-local, the theory preserves the full set of SUSY even with a finite cutoff, as well as the translational invariance. We focus on the following three numerical studies: (A) the numerical simulation of the ADE-type theories and verification of the theoretical conjecture; (B) the continuum limit analysis of the scaling dimension based on the finite-size scaling; (C) the application to the torus compactification of superstring theory.

(A) We apply the SUSY-preserving formulation to the following various ADE-type theories: the A_2, A_3, D_3, D_4, E_6 ($\cong A_2 \otimes A_3$), and E_7 models. In some aspects, we extend and improve the theoretical and numerical analyses in the preceding works. First, to study the DE minimal models and further applications, the method is generalized to one with multiple superfields and more complicated superpotentials. Second, for the A_2 minimal model, numerical accuracy is quite improved. Third, we numerically measure the scaling dimension, by using the two-point function of the scalar field in the momentum space. Also we numerically measure the central charge, by using the two-point function of the supercurrent and that of the energy-momentum tensor. Our results are consistent with the conjectured WZ/minimal-model correspondence.

(B) We develop an extrapolation method to take the continuum and infinite-volume limit, while any extrapolation has been not done in the preceding numerical studies. Then, we perform a precision measurement of the scaling dimension in the A_2-type theory. This result implies the restoration of the locality in the continuum limit.

(C) We apply the above method to non-minimal SCFTs. For simplicity we consider the complex one-dimensional torus compactification. This theory may be simply described by the $A_2 \otimes A_2 \otimes A_2$ minimal model. To deform the geometry of the compactification, we add a would-be marginal operator to the superpotential; then, the central charge is believed not to depend on this deformation. We numerically observe the central charge being constant under this deformation, which provides the non-perturbative evidence of the conjecture.

These studies show a coherence picture which is consistent with the conjecture of the LG description of SCFT, and support the validity of our formulation. This kind of numerical approach, when further developed, will come in useful to study superstring theory.

This thesis is based on the following papers:

- O. Morikawa and H. Suzuki,
  "Numerical study of the $\mathcal{N} = 2$ Landau–Ginzburg model,"
  PTEP **2018** no.8, (2018) 083B05, `arXiv:1805.10735 [hep-lat]`.

- O. Morikawa,
  "Numerical study of the $\mathcal{N} = 2$ Landau–Ginzburg model with two superfields,"
  JHEP **12** (2018) 045, `arXiv:1810.02519 [hep-lat]`.

- O. Morikawa,
  "Continuum limit in numerical simulations of the $\mathcal{N} = 2$ Landau–Ginzburg model,"
  PTEP **2019** no.10, (2019) 103B03, `arXiv:1906.00653 [hep-lat]`.

Contents

List of Figures

List of Tables

Acknowledgements

First of all, I would like to show my profound gratitude to my supervisor, Prof. Hiroshi Suzuki, for his continuous supports. He always encouraged me on my research since I was an undergraduate student. He suggested a lot of interesting and exciting topics to study, and was willing to provide valuable feedback on them. From his insightful comments and the extensive discussions with him, I learned various ideas on physics and sincere attitudes as a researcher.

I am grateful to Prof. Koji Harada, Prof. Takashi Hara, and Prof. Yoshifumi R. Shimizu, for their valuable advice. They also supported my research as the advisory committee. I would like to extend my thanks to Prof. Koji Tsumura, Prof. Ken-ichi Okumura, and Prof. Takuma Matsumoto, for their kind words and the wide-ranging discussions.

I would like to express my appreciation to Prof. Hisao Suzuzki for giving me various ideas about applications of my research to superstring theory, Prof. Hiroto So and Prof. Noboru Kawamoto for instructing me in supersymmetry on the lattice. I was encouraged by their comments and useful discussions with them. I show my gratitude to Dr. Issaku Kanamori, Dr. Daisuke Kadoh, Dr. Akio Tomiya, and Dr. Katsumasa Nakayama for meaningful discussions on the lattice simulation. My gratefulness would go to the members of WHOT-QCD Collaboration for their hospitality.

I was supported other members in Theory of Elementary Particles Laboratory; and other people in Theoretical Nuclear Physics Laboratory and Theory of Subatomic Physics and Astrophysics Laboratory. I especially would like to express my thanks to my three seniors: Dr. Hiromasa Takaura, Dr. Aya Kasai, and Mr. Hiroki Makino. They kindly taught me many aspects of physics about which I had dubious ideas. They are also the collaborators on my project, and have sophisticated skills based on a deep physical viewpoint, which was very helpful in my research. My thanks also go to Dr. Masahiro Ishii, Dr. Junpei Sugano, Dr. Takehiro Hirakida, Mr. Kenji Hieda, Mr. Shoya Ogawa, and Mr. Yushin Yamada, for their fruitful comments in casual conversation.

I show my appreciation to Ms. Yuki Yamaji, Ms. Megumi Ieda, Ms. Atsuko Sono, Ms. Mayumi Takaki, Ms. Mariko Ishii, Ms. Mariko Komiya, and Ms. Mako Nagata for their practical supports.

The numerical computations in this thesis were partially carried out by supercomputer system ITO of Research Institute for Information Technology (RIIT) at Kyushu University. The work was supported by Grant-in-Aid for Scientific Research (KAKENHI) Grant Number JP18J20935 from the Japan Society for the Promotion of Science (JSPS).

Chapter 1

Introduction

1.1 Landau–Ginzburg description of the conformal field theory

The dynamics of elementary particles is described by a theoretical framework, quantum field theory. Its microscopic structure at short distances or in high energies effects long-distance or low-energy physics in a complicated way because of quantum radiations. An effective way to analyze this has been developed by renormalization group (RG) transformation [1]. The flow of RG transformations, which is called the RG flow, governs the behavior of a quantum field theory under some rigid scale transformations, which act as the "coarse-graining" between different scales.

In an extremely low-energy scale, that is, at the infrared (IR) fixed point of the RG flow, any quantum field theory is expected to possess the scale invariance, while all massive modes are decoupled. Such a scale-invariant theory would be described by a conformal field theory (CFT) [2]. If a quantum field theory gives rise to a nontrivial CFT at the IR fixed point, the original field theory is called the Landau–Ginzburg (LG) description of the CFT [3], or the LG model. The LG description thus provides a Lagrangian-level realization of CFT, and is characterized by a nontrivial critical behavior under the RG flow. Originally, this idea of the LG model was introduced as a phenomenological model to describe superconductivity [4]; in this context, we use the free energy instead of the Lagrangian. Such critical phenomena are of great interest in a wide range of physics.

Although the existence of such a Lagrangian is not always obvious, if we know it, techniques developed in quantum field theory provide a quite important tool to clarify conformally invariant systems. As another famous example, the Feigin–Fuks (integral) representation [5,6] gives a free-field Lagrangian on curved spacetime. Feigin and Fuks employed this to explore the unitary representation of the Virasoro algebra, and proved the Kac determinant formula in an elegant way (see Chap. 2). Analyses of the Lagrangian such as their technique have come in useful [7, 8] for performing many computations explicitly and understanding the systems intuitively.

It is also important to consider the fermionic extension of the conformal symmetry by the supersymmetry (SUSY) [9–11], which is a symmetry under swapping bosons and fermions. This extended symmetry, superconformal symmetry, is realized in the two-dimensional (2D) world sheet theory of superstring theory, which is expected to describe quantum gravity [12–

14], and provide a candidate for a theory of everything unifying all fundamental forces.[1] In superstring theory, because of the consistency of the theory, we observe a four-dimensional spacetime, while there exists an extra six-dimensional space [17–23]. Requiring the SUSY on the four-dimensional spacetime, the extra dimensions are considered to be compactified into the Calabi–Yau (CY) manifold [24, 25]. Then, we have a 2D $\mathcal{N} = 2$ superconformal field theory (SCFT) on the world sheet.[2] Scattering amplitudes in a superstring theory with the CY compactification can be computed from this SCFT. We can pursue this strategy if such a SCFT is a solvable minimal model or a tensor product of minimal models (Gepner model [26, 27]), but it is in general not the case. Thus, it is hard to carry out any computation for a general CY manifold, and treat phenomena which relate to the dynamics of the compactification.

Now, an alternative approach may be provided by the LG description of SCFT, while a 2D $\mathcal{N} = 2$ LG model becomes a $\mathcal{N} = 2$ SCFT at infrared criticality. It is believed [26–37] that an example of this is given by the 2D $\mathcal{N} = 2$ massless Wess–Zumino (WZ) model with a quasi-homogeneous superpotential, which can be obtained by the dimensional reduction of the four-dimensional WZ model [38]. It is known that the structure of the superpotential is closely related to the geometry of the CY manifold [39–42]. One can easily change the superpotential, which causes the deformation of the geometry of the superstring compactification.

The above theoretical conjecture of the LG description has been studied from various aspects, which support this correspondence [39, 43–52]. For example, Refs. [43, 46, 48] argue the RG flow for the WZ model with the monomial superpotential, $W(\Phi) \propto \Phi^{n+1}$, which corresponds to the A_n minimal model of the $\mathcal{N} = 2$ SCFT; the correspondence between the superpotential and the ADE minimal model is classified in Ref. [44]. See Refs. [53, 54] for reviews. It is, however, difficult to prove this theoretical conjecture directly, since the 2D $\mathcal{N} = 2$ massless WZ model is strongly coupled at low energies. Moreover, because this is the lower-dimensional massless system, the perturbation theory suffers from IR divergences. The LG description is thus truly a non-perturbative phenomenon.

1.2 Lattice field theory and the numerical approaches

A non-perturbative calculational method may be provided by the lattice field theory [55]. The lattice field theory is the most well-developed framework to study non-perturbative phenomena in quantum field theories; it provides the lattice regularization that the continuum spacetime is discretized as the set of points called the lattice. Then, a quantum field theory is defined as a discretized theory on the spacetime lattice with finite degrees of freedom. Implementation of such a formulation on the lattice (lattice formulation) on a computer enables us to calculate physical quantities of interest from first principles. As is well recognized, however, the lattice formulation is in general not compatible with the SUSY, because the SUSY is one of spacetime symmetries; schematically

$$\{Q, \bar{Q}\} \sim \partial, \tag{1.1}$$

where Q ($\bar{Q}$) is the charge associated with the SUSY (supercharge), and the derivative ∂ denotes the translation. (We will discuss this anti-commutation relation in Chap. 3.) While

[1] The original string theory was considered as a theory of hadrons mainly from 1968 to 1975. For these studies, see Ref. [15] for a review. For developments in 1980s, Ref. [16] gives a detailed review.

[2] Here, we consider the 2D $\mathcal{N} = (2, 2)$ supersymmetry, and not $\mathcal{N} = (2, 0)$. For more details, see Chap. 3.

the SUSY must be a crucial element to study the above LG description, as a usual way, lattice parameters should be fine-tuned so that the lattice formulation yields the target SUSY-invariant theory in the continuum limit; this fact complicates actual numerical studies [56–59].[3]

Despite this difficulty, recently, the authors of Ref. [61] studied the case of a cubic superpotential $W = \Phi^3$, which is considered to correspond the A_2 minimal model; they measured the scaling dimension of the scalar field in the IR limit by using a lattice formulation of Ref. [62].[4] In Ref. [61], one can observe good agreement of the scaling dimension with that of the A_2 minimal model. The formulation of Ref. [62] exactly preserves one nilpotent SUSY at finite lattice spacing (not full SUSY)[5], and the vacuum energy is canceled even on the lattice thanks to the existence of the so-called Nicolai or Nicolai–Parisi–Sourlas map [69–72]. Because of this preserved SUSY, and since this lower-dimensional theory is super-renormalizable, it can be argued, to all orders of perturbation theory, that the full set of the SUSY is automatically restored in the continuum limit [73,74]. The study of Ref. [61] thus achieved a triumph of the lattice field theory, and paved the way for the numerical investigation of the LG model.

Somewhat later, the authors of Ref. [75] examined the same A_2-type WZ model with a cubic superpotential by using the formulation from Ref. [76]; they measured not only the scaling dimension but also the central charge. The formulation in Ref. [76] is based on the Nicolai map and a momentum cutoff regularization. A remarkable feature is that the formulation preserves the full SUSY as well as the translational invariance even with a finite cutoff. Owing to this fact, it is straightforward to construct the Noether current associated with spacetime symmetries, for instance the supercurrent for the SUSY.[6] Then, from the numerical simulation of the two-point function of the supercurrent, the central charge was observed, which is fairly consistent with the A_2 minimal model.

The latter formulation is (almost) identical to the dimensional reduction of the lattice formulation [77] of the 4D $\mathcal{N} = 1$ WZ model on the basis of the SLAC derivative [78, 79]. Although this formulation exactly preserves SUSY, it is well recognized that it breaks the locality because of the SLAC derivative. For the 2D *massive* $\mathcal{N} = 2$ WZ model, because of the exactly preserved SUSY and because this theory is super-renormalizable, it can be argued [76], to all orders of perturbation theory, that the locality is automatically restored in the continuum limit. Although, strictly speaking, the theoretical basis of the formulation for the *massless* WZ model is not obvious, the above numerical results support the validity of the formulation, and the restoration of the locality. This is an interesting observation left as a future problem.

1.3 Numerical study of the 2D $\mathcal{N} = 2$ WZ model

In this thesis, following on from the study of Ref. [75], we numerical study the 2D $\mathcal{N} = 2$ WZ model by employing the SUSY-invariant formulation of Ref. [76]. We extend and improve the

[3] Ref. [60] is a recent review of the SUSY on the lattice, which refers to lattice formulations of the 2D $\mathcal{N} = 2$ WZ model.

[4] References [63–67] are preceding studies on the 2D massive $\mathcal{N} = 2$ WZ model.

[5] This feature is common to the lattice formulation studied in Ref. [68].

[6] In a lattice formulation such as that in Ref. [61,62], the explicit expression of the Noether current associated with spacetime symmetries is quite nontrivial because the regularization breaks such symmetries and the Noether's theorem cannot work well.

theoretical and numerical analyses in Ref. [75] in several aspects.

To obtain further support for the conjectured LG correspondence and the validity of the formulation, we study the following higher critical models: the A_3, D_3, D_4, $E_6 \cong A_2 \otimes A_3$, E_7 models, as well as the A_2 model [80, 81]. First, the method in Ref. [75] is then generalized to the WZ model with multiple superfields and more complicated superpotentials. Second, the numerical accuracy and the effective number of configurations in the Monte Carlo simulation are quite improved. Third, for the scaling dimension, we use the two-point function of the scalar field in the momentum space instead of the susceptibility of Ref. [75]. We also measure the central charge by using the two-point function not only of the supercurrent but also of the energy–momentum tensor (EMT). In Ref. [75], it was found that the EMT correlation function was too noisy to extract the central charge; in this thesis, we settle this problem by using SUSY Ward–Takahashi relations. It turns out that our prescription for the correlation function of the EMT is rather useful to measure the central charge. We also calculate the "effective central charge" as in Ref. [75] that is an analogue of the Zamolodchikov C-function [82, 83]. All these results for typical ADE-type theories show a coherence picture, which is consistent with the conjectured WZ/minimal-model correspondence.

In this thesis, we also consider an extrapolation method to take the continuum limit [84]. Although the SCFT is defined as the continuum theory with the infinite volume, the results of the preceding works and ours above are not extrapolated to the continuum/infinite-volume limits. Moreover, one can find that the computation of the scaling dimension in Ref. [75] is quite sensitive to a ultraviolet (UV) ambiguity because of the locality breaking. To justify numerical studies based on the formulation, it should be observed that such a UV ambiguity disappear in the continuum/infinite-volume limit. We develop the finite-size scaling analysis in Refs. [61, 75] into a continuum-limit extrapolation method. The extrapolation also carries out the infinite volume limit. We then apply this extrapolation method to the above numerical approach. We study the A_2-type WZ model with the cubic superpotential, and perform a precision measurement of the scaling dimension by using this extrapolation method. This is a more reliable result, and is rather consistent with the conjectured A_2-type correspondence.

Finally, we apply the present numerical approach to the SCFT which is not a minimal model. For simplicity the complex one-dimensional torus compactification is studied. In a simple way, this theory is described by the Gepner model, $A_2 \otimes A_2 \otimes A_2$, which corresponds to the superpotential of the form $x^3 + y^3 + z^3$. If we add a term xyz to the superpotential, which does not correspond a Gepner model but is still quasi-homogeneous, the geometry of the compactification is deformed. This term xyz is believed to be a marginal operator, and so the central charge would not depend on this deformation. As mentioned above, however it is difficult to treat such deformations in the compactification in usual analyses of superstring theory; this is an interesting non-perturbative problem. We numerically simulate the WZ model with this superpotential, while the deformation parameter is varied; the central charge is directly measured. From our result we see the central charge being constant under this deformation, which provides the non-perturbative evidence of the conjecture.

All these studies are consistent with the theoretical conjecture of the LG/SCFT correspondence, and support the validity of the formulation of Ref. [76]. In view of the LG/CY correspondence [39–42], we hope that this kind of numerical method, when further developed, will eventually provide a computation method for scattering amplitudes in a superstring theory, whose world sheet theory is not necessarily a Gepner model.

1.4 Organization of the thesis

This thesis is organized as follows: In Chap. 2, we give a review of 2D CFT to introduce the necessary ideas we will use later. We also review the SUSY and the superconformal symmetry in Chap. 3, by using explicit computations in the 2D WZ model. Especially, we derive the explicit form of the important Noether currents: the supercurrent, the EMT, and the $U(1)$ current; we show that those currents form the superconformal multiplet in the massless free WZ model. In Chap. 4, we discuss the RG, and the LG description of CFT together with the LG/CY correspondence. We then introduce the Zamolodchikov's c-theorem and its SUSY-analogue. In Chap. 5, we examine the SUSY-invariant formulation studied in Ref. [76]. To provide consistency checks of the simulation based on this, we show that the Witten index and some SUSY WT relations are reproduced. Chapter 6 is the main part of this thesis; we investigate the WZ model at IR criticality and give our numerical results. In the first two sections, we focus on the ADE-type WZ model, which corresponds to the minimal model of SCFT. We measure the scaling dimension from the scalar correlator and the central charge from the two-point functions of the above Noether currents. In Sect. 6.3, we develop the continuum-limit analysis, and perform precision measurement of the scaling dimension. Finally, in Sect. 6.4, we measure the central charge under the deformation of the torus compactification. Chapter 7 is devoted to the conclusions. In Appendix A, we present a fast algorithm for the practical numerical computation.

Chapter 2

Conformal field theory

2.1 Conformal transformation

Let us briefly introduce basic ideas of the conformal field theory (CFT) [2]. The most part in this chapter is based on the discussion in Ref. [53, 85]. In what follows, in d-dimensions, Green indices, μ, ν, ... run over 0, 1, ..., $d-1$; repeated indices are not summed over.

If for manifolds M and M' a differentiable mapping $\varphi : M \to M'$ is a one-to-one mapping and the inverse φ^{-1} is differentiable, then φ is called a diffeomorphism. Given a Riemann metric $ds^2 = \sum_{\mu,\nu} g_{\mu\nu}(x) dx^\mu dx^\nu$ on the manifold M, a diffeomorphism from M to M

$$g_{\mu\nu}(x) \to g'_{\mu\nu}(x') = e^{\omega(x)} g_{\mu\nu}(x) \tag{2.1}$$

is known as a conformal transformation, where $\omega(x)$ is an arbitrary real function. The set of all conformal transformations forms the conformal group. As usual, a Killing vector v^μ is given as an infinitesimal generator of the isometry group, such that the metric is invariant

$$\delta g_{\mu\nu}(x) = 0 \tag{2.2}$$

under an infinitesimal transformation $x^\mu \to x^\mu + \delta x^\mu = x^\mu + \epsilon v^\mu(x)$. Now, from Eq. (2.1), let us consider an infinitesimal coordinate transformation, under which the mapped Riemann metric is *conformally equivalent* to the original one:

$$\delta g_{\mu\nu}(x) \propto g_{\mu\nu}(x). \tag{2.3}$$

In other words, the metric is invariant under a coordinate transformation $x^\mu \to x^\mu + \epsilon v^\mu(x)$ and a local rescaling of the metric known as the Weyl transformation [86, 87]

$$g_{\mu\nu}(x) \to g'_{\mu\nu}(x) = e^{\omega(x)} g_{\mu\nu}(x). \tag{2.4}$$

Then, v^μ is called a conformal Killing vector, and is an infinitesimal generator of the conformal group.

If a field theory has the conformal symmetry, which is a invariance under conformal transformations, the theory is called a conformal field theory. Since any conformal transformation induces the Weyl transformation, conformal field theories on curved spacetime is invariant under Weyl transformations; this is the Weyl symmetry.

	v^μ
translation	a^μ
rotation	$\sum_\nu \omega^\mu{}_\nu x^\nu$ $(\omega_{\mu\nu} = -\omega_{\nu\mu})$
scaling transformation (dilatation)	λx^μ
special conformal transformation	$\|x\|^2 b^\mu - 2(b \cdot x)x^\mu$

Table 2.1: Infinitesimal conformal transformation in d-dimensional Euclidean space ($d > 2$)

In the d-dimensional Euclidean space, we obtain the conformal Killing equation as

$$\partial_\mu v_\nu(x) + \partial_\nu v_\mu(x) = \frac{2}{d} \sum_\rho \partial_\rho v^\rho(x) \delta_{\mu\nu}. \tag{2.5}$$

Table 2.1 shows the set of the Killing vectors in the d-dimensional Euclidean spacetime with $d > 2$. We note that, for $d > 2$, there exists a finite number of generators. On the other hand, if we set $d = 2$, the conformal Killing equation reduces to

$$\bar{\partial} v^z = 0, \tag{2.6}$$

where we have introduced the complex coordinate $z = x^0 + ix^1$, and

$$v^z \equiv v^0 + iv^1, \qquad v^{\bar{z}} \equiv v^0 - iv^1, \tag{2.7}$$

$$\partial \equiv \frac{\partial}{\partial z} = \frac{1}{2}(\partial_0 - i\partial_1), \qquad \bar{\partial} \equiv \frac{\partial}{\partial \bar{z}} = \frac{1}{2}(\partial_0 + i\partial_1). \tag{2.8}$$

Therefore v^z is a holomorphic function, and $v^{\bar{z}}$ is an anti-holomorphic function; the number of generators is infinite. From the infinitesimal transformations for $d = 2$, a finite conformal transformation is given by

$$z \to z' = f(z), \tag{2.9}$$

where $f(z)$ is holomorphic. In what follows, mainly, we will consider a CFT on the 2D Euclid space.

2.2 Primary fields and correlation functions

It is convenient to introduce a conformal weight, which characterize under conformal transformations the behavior of local operators, and to define an important class of local operators called a primary field. The conformal weight is defined as follows: There exists a local operator $\mathcal{O}$ such that, under the rigid transformation

$$z' = \zeta z, \qquad \zeta \in \mathbb{C}, \tag{2.10}$$

it behaves as

$$\mathcal{O}'(z', \bar{z}') = \zeta^{-h} \bar{\zeta}^{-\bar{h}} \mathcal{O}(z, \bar{z}). \tag{2.11}$$

Then, $(h, \bar{h})$ are called the conformal weights of $\mathcal{O}$. Local operators like $\mathcal{O}$ (2.11) are the eigenstates under Eq. (2.10), and form a basis of local operators. Especially, for a rotation $\zeta = e^{i\theta}$ with $\theta \in \mathbb{R}$,

$$\mathcal{O}'(z', \bar{z}') = e^{-i\theta(h-\bar{h})}\mathcal{O}(z, \bar{z}), \tag{2.12}$$

and for a scaling transformation $\zeta = \lambda \in \mathbb{R}$,

$$\mathcal{O}'(z', \bar{z}') = \lambda^{-(h+\bar{h})}\mathcal{O}(z, \bar{z}). \tag{2.13}$$

Thus, $h - \bar{h}$ is known as a spin, and $h + \bar{h}$ is a scaling dimension. A local operator $\mathcal{O}$ is known as a primary field if it transforms as

$$\mathcal{O}'(z', \bar{z}') = (\partial z')^{-h}(\bar{\partial}\bar{z}')^{-\bar{h}}\mathcal{O}(z, \bar{z}) \tag{2.14}$$

under a general conformal transformation $z \to z' = z'(z)$.

Next, let us consider an N-point function of basis vectors $\mathcal{O}_i$ in the vector space spanned by local operators:

$$\langle \mathcal{O}_{i_1}(z_1, \bar{z}_1) \dots \mathcal{O}_{i_N}(z_N, \bar{z}_N) \rangle. \tag{2.15}$$

When $(z_1,\ \bar{z}_1)$ gets close to $(z_2,\ \bar{z}_2)$ rather than $(z_n,\ \bar{z}_n)$ with $n \geq 3$, the product, $\mathcal{O}_{i_1}\mathcal{O}_{i_2}$, is approximately given as a local operator; $\mathcal{O}_{i_1}$ and $\mathcal{O}_{i_2}$ "fuse" together. The fused operator can be expanded by an arbitrary basis of local operators. Then, schematically, we have the so-called fusion rule as

$$[\mathcal{O}_i] \times [\mathcal{O}_j] = \sum_k N^k{}_{ij}[\mathcal{O}_k], \tag{2.16}$$

where $N^k{}_{ij} = 0$ or 1. This rule implies that, if $N^k{}_{ij} = 0$, $\mathcal{O}_k$ cannot contribute the fusion of $\mathcal{O}_i$ and $\mathcal{O}_j$. More concretely, one may expand this product as

$$\mathcal{O}_i(z_1, \bar{z}_1)\mathcal{O}_j(z_2, \bar{z}_2) = \sum_k c^k{}_{ij}(z_1 - z_2, \bar{z}_1 - \bar{z}_2)\mathcal{O}_k(z_2, \bar{z}_2). \tag{2.17}$$

This expansion is termed the operator product expansion (OPE). Of course, if $N^k{}_{ij} = 0$, then $c^k{}_{ij} = 0$. It is now simple to take the basis of local operators (2.11). Straightforwardly, we can obtain

$$c^k{}_{ij}(z, \bar{z}) = z^{h_k - h_i - h_j}\bar{z}^{\bar{h}_k - \bar{h}_i - \bar{h}_j}C^k{}_{ij}. \tag{2.18}$$

Here $C^k{}_{ij}$ is a constant. We will often focus on a dominant part in OPE at short distance, that is, singular terms with $h_k - h_i - h_j < 0$ or $\bar{h}_k - \bar{h}_i - \bar{h}_j < 0$. We then use "$\sim$" in place of "$=$," which implies "$=$" up to non-singular terms.

2.3 Energy–momentum tensor

In what follows, let us focus on the energy–momentum tensor (EMT), which is a Noether current associated with the translation. On a curved spacetime, one define the EMT by the variation of the metric $\delta g_{\mu\nu}$,

$$\delta\langle \mathcal{O}(x) \rangle = -\frac{1}{4\pi}\int d^2y\, \sqrt{g(y)} \sum_{\mu,\nu} \delta g_{\mu\nu}(y)\langle T_{\mu\nu}(y)\mathcal{O}(x) \rangle, \tag{2.19}$$

where $g(x) = \det g_{\mu\nu}(x)$; the Weyl transformation $\delta g_{\mu\nu} = 2\delta\omega g_{\mu\nu}$ gives rise to

$$\delta\langle\mathcal{O}(x)\rangle = -\frac{1}{2\pi}\int d^2y\,\sqrt{g(y)}\,\delta\omega(y)\sum_\mu\langle T_{\mu\mu}(y)\mathcal{O}(x)\rangle. \tag{2.20}$$

Thus the Weyl invariance implies that the EMT should be traceless,

$$\sum_\mu T_{\mu\mu} = 0. \tag{2.21}$$

In the complex coordinates, we note that

$$T_{zz} = \frac{1}{4}(T_{11} - iT_{12} - iT_{21} - T_{22}), \tag{2.22}$$

$$T_{z\bar{z}} = \frac{1}{4}(T_{11} + iT_{12} - iT_{21} + T_{22}), \tag{2.23}$$

$$T_{\bar{z}z} = \frac{1}{4}(T_{11} - iT_{12} + iT_{21} + T_{22}), \tag{2.24}$$

$$T_{\bar{z}\bar{z}} = \frac{1}{4}(T_{11} + iT_{12} + iT_{21} - T_{22}). \tag{2.25}$$

From the fact that the EMT is a traceless symmetric tensor, $T_{\mu\nu} = T_{\nu\mu}$ and Eq. (2.21), we have the traceless condition in the complex coordinates,

$$T_{z\bar{z}} = T_{\bar{z}z} = 0. \tag{2.26}$$

Thus, the conservation law, $\sum_\mu \partial_\mu T_{\mu\nu} = 0$, is rewritten by

$$\bar{\partial}T_{zz} = 0, \qquad\qquad \partial T_{\bar{z}\bar{z}} = 0. \tag{2.27}$$

These imply that we have the holomorphic part $T_{zz} = T(z)$, and anti-holomorphic one $T_{\bar{z}\bar{z}} = \bar{T}(\bar{z})$.

Naively, since $T_{\mu\nu}$ is a tensor field, one may consider T ($\bar{T}$) is a primary field, which is a generalization of tensor. On a curved background, however, because of the scalar curvature R, the conformal symmetry (or the traceless condition) is broken by quantum effects,

$$\sum_\mu T_{\mu\mu} = -\frac{c}{12}R. \tag{2.28}$$

This is called the trace anomaly or Weyl anomaly, and c is the central charge [88, 89].[1] This anomalous effect lead to the fact that the EMT is not a primary field. To see this, let us examine the OPE between the local operator and T.

First, given a continuum symmetry and its associated Noether current j_μ, we have the Ward–Takahashi (WT) relation [91, 92] as

$$\sum_\mu \frac{\partial}{\partial x_\mu}\langle j_\mu(x)\mathcal{O}(y)\rangle = \frac{1}{i\epsilon}\langle\delta\mathcal{O}(y)\delta^d(x-y)\rangle, \tag{2.29}$$

[1] For a historical review, see Ref. [90].

where $\delta\mathcal{O}$ is the variation of $\mathcal{O}$ under the corresponding infinitesimal transformation, and ϵ is a small parameter. The EMT with T and $\bar{T}$ generates the infinitesimal transformation $x_\mu \to x_\mu + \epsilon v_\mu$; then

$$\mathrm{Res}_{z\to 0}\, iv^z(z)T(z)\mathcal{O}(0,0) + \overline{\mathrm{Res}}_{\bar{z}\to 0}(-i)v^{\bar{z}}(\bar{z})\bar{T}(\bar{z})\mathcal{O}(0,0) = \frac{1}{i\epsilon}\delta\mathcal{O}(0,0). \tag{2.30}$$

This is the integral representation of the conformal WT relation [93]. Here Res and $\overline{\mathrm{Res}}$ mean residues, which is the coefficients of $1/z$ and $1/\bar{z}$, respectively. For a local operator $\mathcal{O}$ with the conformal weights $(h,\, \bar{h})$, from the behavior under the global transformation (2.11) and the translation $\delta\mathcal{O} = -\sum_\mu \epsilon v_\mu \partial_\mu \mathcal{O}$, the OPE between $\mathcal{O}$ and T is given by

$$T(z)\mathcal{O}(0,0) \sim \cdots + \frac{h}{z^2}\mathcal{O}(0,0) + \frac{1}{z}\partial\mathcal{O}(0,0). \tag{2.31}$$

Especially, when $\mathcal{O}$ is a primary field, from Eq. (2.14), we have

$$T(z)\mathcal{O}(0,0) \sim \frac{h}{z^2}\mathcal{O}(0,0) + \frac{1}{z}\partial\mathcal{O}(0,0). \tag{2.32}$$

The OPE between $\mathcal{O}$ and $\bar{T}$ is clear by now.

Similarly, the OPE of T itself is given by

$$T(z)T(0) \sim \frac{c}{2z^4} + \frac{2}{z^2}T(0) + \frac{1}{z}\partial T(0), \tag{2.33}$$

and for $\bar{T}$

$$\bar{T}(\bar{z})\bar{T}(0) \sim \frac{\bar{c}}{2\bar{z}^4} + \frac{2}{\bar{z}^2}\bar{T}(0) + \frac{1}{\bar{z}}\bar{\partial}\bar{T}(0). \tag{2.34}$$

$T(z)\bar{T}(0)$ is non-singular. Usually, we assume $\bar{c} = c$.[2] Equation (2.33) is not identical to Eq. (2.32), and hence, we find that T and $\bar{T}$ with $c \neq 0$ are not primary fields. The first term proportional to the central charge c comes from the trace anomaly (2.28). This can be seen roughly as follows: From the conservation law,

$$\bar{\partial}T_{zz} + \partial T_{z\bar{z}} = 0, \tag{2.35}$$

we have the OPE of $\partial T_{z\bar{z}}$ as

$$\begin{aligned}
\partial T_{z\bar{z}}(z_1,\bar{z}_1)\partial T_{z\bar{z}}(z_2,\bar{z}_2) &= \bar{\partial}T_{zz}(z_1,\bar{z}_1)\partial T_{z\bar{z}}(z_2,\bar{z}_2) \\
&= \partial_{\bar{z}_1}\partial_{\bar{z}_2}\left[\frac{c}{2(z_1-z_2)^4} + \dots\right] \qquad (2.36)\\
&= \frac{c\pi}{6}\partial_{z_1}^2\partial_{z_2}\partial_{\bar{z}_2}\delta(z_1-z_2,\bar{z}_1-\bar{z}_2) + \dots, \qquad (2.37)
\end{aligned}$$

where we have used

$$\bar{\partial}\partial \ln|z|^2 = \bar{\partial}\frac{1}{z} = 2\pi\delta^2(z,\bar{z}), \tag{2.38}$$

[2] If $c \neq \bar{c}$, the gravitation anomaly exists. Thus, by quantum effects, the invariance under coordinate transformations is broken.

and $\delta^2(z,\bar{z}) = \frac{1}{2}\delta(x_0)\delta(x_1)$. Therefore we estimate

$$T_{z\bar{z}}(z_1,\bar{z}_1)T_{z\bar{z}}(z_2,\bar{z}_2) \sim \frac{c\pi}{6}\partial_{z_1}\partial_{\bar{z}_2}\delta(z_1-z_2,\bar{z}_1-\bar{z}_2) + \dots \tag{2.39}$$

Inserting the operator $\sum_\mu T_{\mu\mu}$ into Eq. (2.20), we have

$$\sum_\mu \delta\langle T_{\mu\mu}(x)\rangle = -\frac{1}{2\pi}\int d^2y\,\sqrt{g(y)}\,\delta\omega(y)\sum_{\mu,\nu}\langle T_{\mu\mu}(y)T_{\nu\nu}(x)\rangle \tag{2.40}$$

$$= \frac{c}{6}\int d^2y\,\sqrt{g(y)}\,\delta\omega(y)\sum_\mu \partial_\mu^y\partial_\mu^y\delta(y_0-x_0)\delta(y_1-x_1) \tag{2.41}$$

$$= \frac{c}{6}\sum_\mu \partial_\mu\partial_\mu\delta\omega(x). \tag{2.42}$$

In the conformal gauge $g_{\mu\nu} = e^{2\omega}\delta_{\mu\nu}$, on the other hand, the scalar curvature is give by

$$R = -2e^{-2\omega}\sum_\mu \partial_\mu\partial_\mu\omega. \tag{2.43}$$

Then, we finally obtain

$$\sum_\mu \delta\langle T_{\mu\mu}(x)\rangle = -\frac{c}{12}\delta R. \tag{2.44}$$

This is identical to the trace anomaly (2.28).

2.4 Virasoro algebra

In this section, we consider the holomorphic part $T(z)$ only, while one can discuss the anti-holomorphic part in the same way. Our goal here is to obtain the minimal series of CFT. Let us consider the Laurent expansion for $T(z)$ about $z = 0$,

$$T(z) = \sum_{n\in\mathbb{Z}}\frac{L_n}{z^{n+2}}. \tag{2.45}$$

The coefficient L_n is termed the Virasoro generator. Inversely, the Virasoro generator can be written in terms of $T(z)$ by

$$L_n = \frac{1}{2\pi i}\oint dz\, z^{n+1}T(z). \tag{2.46}$$

From the OPE of T itself (2.33), the Virasoro generator satisfies the following commutation relation:

$$[L_m, L_n] = (m-n)L_{m+n} + \frac{c}{12}m(m^2-1)\delta_{m+n,0}. \tag{2.47}$$

This is the Virasoro algebra [94], which is the central extension of the Witt algebra with $c = 0$. The expansion of $T(z)T(0)$ gives a representation of the Virasoro algebra in terms of the OPE.

Because of the invariance of $\langle 0|0\rangle$ under coordinate transformations, the vacuum expectation value of $T(z)$ should vanish,

$$\langle 0|T(z)|0\rangle = 0, \tag{2.48}$$

that is, for $^\forall n \in \mathbb{Z}$,

$$\langle 0|L_n|0\rangle = 0. \tag{2.49}$$

It is, however, inconsistent with the Virasoro algebra that we assume $L_n|0\rangle = 0$ for all n when $c \neq 0$. Now, noting that the Hermiticity of the EMT (or unitarity of the theory) leads to

$$L_n^\dagger = L_{-n}, \tag{2.50}$$

it is sufficient to impose that

$$L_n|0\rangle = 0 \qquad (n \geq 0) \tag{2.51}$$

It is important to consider the behavior of the Virasoro generator acting on the primary state, which is defined by

$$|c,h\rangle = \lim_{z\to 0} \mathcal{O}(z)|0\rangle, \tag{2.52}$$

where $\mathcal{O}$ is a primary field with $(h,\, 0)$. By using the OPE between the primary field and T (2.32), the Virasoro generator acts on the primary state as

$$L_n|c,h\rangle = 0 \qquad (n \geq 1), \tag{2.53}$$

$$L_0|c,h\rangle = h|c,h\rangle. \tag{2.54}$$

Such a state is also called the highest weight state.

From the above relation, L_n $(n > 0)$ is a lowering (annihilation) operator, and $L_{-n} = L_n^\dagger$ is a raising (creation) operator. n in L_{-n} is the level of the excitation. An eigenstate of L_0 that Virasoro raising operators act on the primary state

$$L_{-n_1} L_{-n_2} \ldots L_{-n_r}|c,h\rangle \tag{2.55}$$

is called the descendant with the level $N = \sum_i n_i$ and the weight $h + N$. The Verma module $V(c,h)$ [95, 96] is then defined by a vector space spanned by the primary state $|c,h\rangle$ and its descendants. All states with the level N in $V(c,h)$ span the subspace $V_N(c,h)$. The dimension of $V_N(c,h)$, $p(N) \equiv \dim V_N(c,h)$, is the number of integer partitions of N, and hence,

$$\sum_{N=0}^{\infty} p(N) q^N = \prod_{k=1}^{\infty} \frac{1}{1-q^k} \tag{2.56}$$

$$= 1 + q + 2q^2 + 3q^3 + \ldots \tag{2.57}$$

We now take the basis of $V_N(c,h)$ as Eq. (2.55) with $n_1 \geq n_2 \geq \cdots \geq n_r > 0$. Let us define the $p(N) \times p(N)$ Gram matrix, $\mathcal{M}_N(c,h)$

$$\mathcal{M}_N(c,h) = \begin{pmatrix} \langle c,h|L_1^N \\ \langle c,h|L_1^{N-2}L_2 \\ \vdots \\ \langle c,h|L_N \end{pmatrix} \begin{pmatrix} L_{-1}^N|c,h\rangle & L_{-2}L_{-1}^{N-2}|c,h\rangle & \ldots & L_{-N}|c,h\rangle \end{pmatrix}. \tag{2.58}$$

$\det \mathcal{M}_N(c,h)$ is called the Kac determinant. If the Verma module is unitary, $\mathcal{M}_N(c,h)$ is positive definite.

A descendant $|\chi\rangle \in V_N(c,h)$ $(N>0)$, such that

$$L_n|\chi\rangle = 0 \qquad (n>0), \tag{2.59}$$

is the null vector. This state is orthogonal to any state $|v\rangle \in V(c,h)$, that is, $\langle\chi|v\rangle = 0$. Especially, $\langle\chi|\chi\rangle = 0$. When a null vector in $V_N(c,h)$ exists, a raw/column vector in $\mathcal{M}_N(c,h)$ vanishes identically; then $\det \mathcal{M}_N(c,h) = 0$. Generally, if $\det \mathcal{M}_N(c,h) = 0$, there exists a null vector with the level N in the Verma module. Since a physical state $|\psi\rangle$ vanishes by acting with the Virasoro lowering operator, $(\langle\psi| + \langle\chi|)(|\psi\rangle + |\chi\rangle) = \langle\psi|\psi\rangle$. We identify these two states as

$$|\psi\rangle \cong |\psi\rangle + |\chi\rangle. \tag{2.60}$$

The Hilbert space obtained from physical states, $\mathcal{H}_{\text{phys}}$, includes the extra degrees of freedom $\mathcal{H}_{\text{null}}$ because of the existence of null vectors. $\mathcal{H}_{\text{null}}$ indicates the gauge symmetry, and the identification (2.60) corresponds to the gauge transformation.

The explicit form of the Kac determinant is given in Refs. [5, 6, 97], by

$$\det \mathcal{M}_N(c,h) = K_N \prod_{1\le rs\le N} (h - h_{r,s})^{p(N-rs)}, \tag{2.61}$$

$$K_N = \prod_{1\le rs\le N} [(2r)^s s!]^{p(N-rs)-p(N-r(s+1))}, \tag{2.62}$$

$$h_{r,s} = \frac{c-1}{24} + \frac{1}{4}(r\alpha_+ + s\sigma_-)^2, \tag{2.63}$$

$$\alpha_\pm = \frac{1}{\sqrt{24}}(\sqrt{1-c} \pm \sqrt{25-c}). \tag{2.64}$$

Using the central charge $c \in \mathbb{C}$ in terms of the parameter $\mu \in \mathbb{C}$,

$$c = 1 - \frac{6}{\mu(\mu+1)}, \tag{2.65}$$

we can rewrite as

$$\alpha_+ = \sqrt{\frac{2(\mu+1)}{\mu}}, \qquad \alpha_- = -\sqrt{\frac{2\mu}{\mu+1}}, \tag{2.66}$$

$$h_{r,s} = \frac{[(\mu+1)r - \mu s]^2 - 1}{4\mu(\mu+1)}. \tag{2.67}$$

If the conformal weight h is identical to $h_{r,s}$, there exists a null vector with the level $N = rs$.

When $0 \le c < 1$, let us take c and h as

$$c = c_{p,p'} = 1 - \frac{6(p-p')^2}{pp'}, \tag{2.68}$$

$$\alpha_+ = \sqrt{\frac{2p'}{p}}, \qquad \alpha_- = -\sqrt{\frac{2p}{p'}}, \tag{2.69}$$

$$h_{r,s} = h_{p-r,p'-s} = \frac{(p'r - ps)^2 - (p'-p)^2}{4pp'}, \tag{2.70}$$

where the integers p and p' are coprime, and $1 \leq r \leq p-1$, $1 \leq s \leq p'-1$. In this case, the Kac determinant has zero points. The OPEs between the set of primary fields with $\{h_{r,s}\}$ are closed; the number of the primary fields is given by the finite number $(p-1)(p'-1)$. This theory with the finite number of the primary fields is called the minimal model.

Unitary representations of CFT can exists for $c \geq 1$ and $h \geq 0$, or in the minimal model with $p = m$, $p' = m+1$ ($p' - p = 1$); the central charge and the conformal weights in the unitary minimal model is given by

$$c = 1 - \frac{6}{m(m+1)}, \qquad m = 2, 3, \ldots, \tag{2.71}$$

$$h_{r,s} = \frac{[(m+1)r - ms]^2 - 1}{4m(m+1)}, \tag{2.72}$$

where $1 \leq r \leq m-1$, $1 \leq s \leq m$. Note that $h_{r,s} = h_{m-r,m+1-s}$. There are many statistical systems, which provide the minimal model at criticality:

- $m = 3$, $c = 1/2$: Ising model,
- $m = 4$, $c = 7/10$: Tricritical Ising model,
- $m = 5$, $c = 4/5$: 3-state Potts model.

Such statistical systems exist for all unitary minimal models [98, 99].

Chapter 3

Supersymmetry and superconformal multiplet

3.1 Supersymmetry and the WZ model

As already mentioned, it is believed that the LG description of 2D $\mathcal{N}=2$ SCFT is provided by the 2D $\mathcal{N}=2$ WZ model [38]. This model is invariant under supersymmetry (SUSY), which is a symmetry under swapping bosons and fermions. Supersymmetric theories possess a fermionic extension of Poincarè symmetry (and internal symmetries); SUSY is a type of spacetime symmetries. Superconforml symmetry is a SUSY-extension of the conformal symmetry. In this chapter, utilizing the WZ model we will give a review of the SUSY and the superconformal symmetry.

3.1.1 4D $\mathcal{N}=1$ supersymmetry

To obtain the 2D $\mathcal{N}=2$ WZ action, it is convenient to consider the dimensional reduction of the 4D $\mathcal{N}=1$ WZ model. Let A be a complex scalar, ψ_α a left-handed Weyl spinor, and F an auxiliary field. The term "$\mathcal{N}=1$" means that there exists a single supercharge Q_α ($\bar{Q}_{\dot{\alpha}}$), which swaps A, ψ and F as

$$(A, A^*) \leftrightarrow (\psi_\alpha, \bar{\psi}_{\dot{\alpha}}) \leftrightarrow (F, F^*). \tag{3.1}$$

We note that the 2-component Weyl spinor is an irreducible representation of the Lorentz group in four dimensions. By introducing Grassmann coordinates θ^α and $\bar{\theta}^{\dot{\alpha}}$, we can define the WZ model in the so-called superspace $(x, \theta, \bar{\theta})$, whose action is given by

$$S = \int d^4x\, d^4\theta\, \bar{\Phi}\Phi - \int d^4x\, d^2\theta\, W(\Phi) - \int d^4x\, d^2\bar{\theta}\, W(\bar{\Phi}). \tag{3.2}$$

Here Φ is the chiral superfield

$$\Phi(x, \theta, \bar{\theta}) = A(y) + \sqrt{2}\sum_{\alpha=1}^{2}\theta^\alpha\psi_\alpha(y) + \sum_{\alpha=1}^{2}\theta^\alpha\theta_\alpha F(y), \tag{3.3}$$

and the coordinate y is given by

$$y_M = x_M + i\sum_{\alpha=1}^{2}\sum_{\dot{\alpha}=\dot{1}}^{\dot{2}}\theta^{\alpha}\sigma_{M\alpha\dot{\alpha}}\bar{\theta}^{\dot{\alpha}} \qquad \text{for } M = 0,\ 1,\ 2,\ 3, \tag{3.4}$$

where σ_0 is the unit matrix and $\sigma_{1,2,3}$ the Pauli matrices; $W(\Phi)$ or $W(\bar{\Phi})$ in Eq. (3.2) is the superpotential assumed to be a polynomial of the superfield Φ or $\bar{\Phi}$.

The above action (3.2) is invariant under the SUSY transformation

$$\delta_\xi\Phi = \sum_{\alpha=1}^{2}\xi^{\alpha}Q_{\alpha}\Phi - \sum_{\dot{\alpha}=\dot{1}}^{\dot{2}}\bar{\xi}^{\dot{\alpha}}\bar{Q}_{\dot{\alpha}}\Phi, \tag{3.5}$$

where ξ ($\bar{\xi}$) is a Grassmann parameter, and

$$Q_{\alpha} = \frac{\partial}{\partial\theta^{\alpha}} + \sum_{\mu}\sum_{\dot{\beta}=\dot{1}}^{\dot{2}} i\sigma^{\mu}_{\alpha\dot{\beta}}\bar{\theta}^{\dot{\beta}}\partial_{\mu}, \qquad \bar{Q}_{\dot{\alpha}} = -\frac{\partial}{\partial\bar{\theta}^{\dot{\alpha}}} - \sum_{\mu}\sum_{\beta=1}^{2} i\theta^{\beta}\sigma^{\mu}_{\beta\dot{\alpha}}\partial_{\mu}. \tag{3.6}$$

For the component fields (A, ψ, F), the transformation is rewritten by

$$\delta_\xi A = \sum_{\beta=1}^{2}\xi^{\beta}\sqrt{2}\psi_{\beta}, \tag{3.7}$$

$$\delta_\xi\psi_{\alpha} = \sum_{\beta}^{2}\xi^{\beta}\sqrt{2}\epsilon_{\beta\alpha}F - \sum_{\dot{\beta}=\dot{1}}^{\dot{2}}\bar{\xi}^{\dot{\beta}}\sum_{\mu}(-i\sqrt{2})\sigma^{\mu}_{\alpha\dot{\beta}}\partial_{\mu}A, \tag{3.8}$$

$$\delta_\xi F = -\sum_{\dot{\beta}=\dot{1}}^{\dot{2}}\bar{\xi}^{\dot{\beta}}\sum_{\mu}\sum_{\gamma=1}^{2} i\sqrt{2}\partial_{\mu}\psi^{\gamma}\sigma^{\mu}_{\gamma\dot{\beta}}, \tag{3.9}$$

where $\epsilon_{12} = -\epsilon_{21} = 1$ and $\epsilon_{11} = \epsilon_{22} = 0$. These SUSY transformations fulfill the following anti-commutation relations:

$$\{Q_{\alpha}, \bar{Q}_{\dot{\beta}}\} = \sum_{\mu}(-2i)\sigma^{\mu}_{\alpha\dot{\beta}}\partial_{\mu}, \tag{3.10}$$

$$\{Q_{\alpha}, Q_{\beta}\} = \{\bar{Q}_{\dot{\alpha}}, \bar{Q}_{\dot{\beta}}\} = 0. \tag{3.11}$$

In the first line, two SUSY transformations lead to the translation. We can see that the supercharge and the generators of the Poincarè group fulfill the simplest SUSY-extension of the Poincarè algebra. From the second line, the supercharge Q ($\bar{Q}$) is nilpotent.

One of the most important quantities in supersymmetric field theories is the Witten index [100, 101], which is a topological invariant relating to the vacuum structure of the theory. The Witten index is defined by the difference between the numbers of bosonic states n_b and fermionic states n_f:

$$\Delta \equiv n_b - n_f. \tag{3.12}$$

In supersymmetric theories, the number of non-zero energy bosonic states is identical to that of non-zero energy fermionic states. Thus, the Witten index is the difference between the numbers of bosonic and fermionic vacua. By using the fermion number operator $\mathcal{F}$, which act on a bosonic state as $\mathcal{F} = 0$ and on a fermionic state as $\mathcal{F} = 1$, we can formally define the Witten index as

$$\Delta = \mathrm{Tr}(-1)^{\mathcal{F}} e^{-\beta H}, \tag{3.13}$$

where H is the Hamiltonian, and β is the inverse temperature; in terms of the path integral,

$$\Delta = \int [d\Phi]\, e^{-S[\Phi]}, \tag{3.14}$$

where we impose periodic boundary conditions for bosons and fermions. It is known that the Witten index has the following properties:

1. $\Delta \geq 0$.
2. $\Delta = 1$ in a massive free theory.
3. If $\Delta \neq 0$ the SUSY cannot be broken.
4. If Δ does not depend on β and the physical box size, it can be computed in the limit that configurations are constant, where β and the box can vanish (ultralocal limit).
5. In general Δ is not an integer, but still remains as the topological index.
6. If not mass gap exist, Δ can be ill-defined or infinite.

3.1.2 2D $\mathcal{N} = 2$ WZ model

Let us consider the dimensional reduction of the above 4D WZ action. We then identify the two coordinates x_0 and x_1 with the 2D ones, and eliminate the dependence on x_2 and x_3. In two dimensions, a minimal spinor representation is a 1-component Majorana–Weyl spinor. The 4D Weyl representation ψ_α consists of two 2D Weyl spinors, ψ_1 ($\bar{\psi}_{\dot{1}}$) and ψ_2 ($\bar{\psi}_{\dot{2}}$), each of which can decompose two Majorana–Weyl spinors. Then, there are two supercharges, Q_1 and $\bar{Q}_{\dot{1}}$, and two ones, Q_2 and $\bar{Q}_{\dot{2}}$, respectively. This is called the $\mathcal{N} = (2, 2)$ supersymmetry; we will abbreviate it as the $\mathcal{N} = 2$ SUSY.

We define a 2D Dirac fermion by

$$\psi \equiv \begin{pmatrix} \psi_1 \\ \bar{\psi}_{\dot{2}} \end{pmatrix}, \qquad \bar{\psi}\gamma_0 \equiv (\bar{\psi}_{\dot{1}}, \psi_2), \tag{3.15}$$

and the 2D Dirac matrices by

$$\gamma_0 = \begin{pmatrix} 0 & 1 \\ 1 & 0 \end{pmatrix}, \qquad \gamma_1 = \begin{pmatrix} 0 & i \\ -i & 0 \end{pmatrix}. \tag{3.16}$$

In terms of the complex coordinates, these are written by

$$\gamma_z = \begin{pmatrix} 0 & 1 \\ 0 & 0 \end{pmatrix}, \qquad \gamma_{\bar{z}} = \begin{pmatrix} 0 & 0 \\ 1 & 0 \end{pmatrix}. \tag{3.17}$$

The Euclidean action of the 2D $\mathcal{N} = 2$ WZ model is given by[1]

$$S = \int d^2x \left[4\partial A^* \bar{\partial} A - F^* F - F^* \frac{W(A)^*}{\partial A^*} - F \frac{W(A)}{\partial A} + \bar{\psi}\gamma_0 \begin{pmatrix} 2\partial & \frac{\partial^2 W(A)}{\partial (A^*)^2} \\ \frac{\partial^2 W(A)}{\partial A^2} & 2\bar{\partial} \end{pmatrix} \psi \right]. \tag{3.18}$$

As we will see later, we need to construct the WZ model with multiple superfields. Let the WZ model contain N_Φ superfields, $\{\Phi_I\}_{I=1,\ldots,N_\Phi}$. The 4D action in the superspace (3.2) is generalized to

$$S = \int d^4x\, d^4\theta \sum_I \bar{\Phi}_I \Phi_I - \int d^4x\, d^2\theta\, W(\{\Phi\}) - \int d^4x\, d^2\bar{\theta}\, W(\{\bar{\Phi}\}), \tag{3.19}$$

and the 2D WZ action (3.18) to

$$S = \int d^2x \sum_I \left[4\partial A_I^* \bar{\partial} A_I - F_I^* F_I - F_I^* \frac{W(\{A\})^*}{\partial A_I^*} - F_I \frac{W(\{A\})}{\partial A_I} + (\bar{\psi}\gamma_0)_I \sum_J \begin{pmatrix} 2\delta_{IJ}\partial & \frac{\partial^2 W(\{A\})}{\partial A_I^* \partial A_J^*} \\ \frac{\partial^2 W(\{A\})}{\partial A_I \partial A_J} & 2\delta_{IJ}\bar{\partial} \end{pmatrix} \psi_J \right]. \tag{3.20}$$

The superpotential $W(\{\Phi\})$ ($W(\{\bar{\Phi}\})$) is a multi-variable polynomial of $\{\Phi_I\}$ ($\{\bar{\Phi}_I\}$).

The SUSY transformation in the 2D $\mathcal{N} = 2$ WZ model in Eq. (3.18) or (3.20) is given by

$$\delta_\xi \varphi(x) = \sum_{\alpha=1}^{2} \xi^\alpha Q_\alpha \varphi(x) - \sum_{\dot{\alpha}=\dot{1}}^{\dot{2}} \bar{\xi}^{\dot{\alpha}} \bar{Q}_{\dot{\alpha}} \varphi(x), \tag{3.21}$$

where φ stands for A, ψ, or F (or a generic field). Here, omitting the factor of root-two in Eqs. (3.7)–(3.9), Q_α ($\alpha = 1, 2$) is defined by

$$Q_1 \bar{\psi}_{\dot{1}}(x) = -2\bar{\partial} A^*(x), \qquad Q_1 A^*(x) = 0, \tag{3.22}$$
$$Q_1 F^*(x) = 2\bar{\partial} \bar{\psi}_{\dot{2}}(x), \qquad Q_1 \bar{\psi}_{\dot{2}}(x) = 0, \tag{3.23}$$
$$Q_1 A(x) = \psi_1(x), \qquad Q_1 \psi_1(x) = 0, \tag{3.24}$$
$$Q_1 \psi_2(x) = F(x), \qquad Q_1 F(x) = 0, \tag{3.25}$$

and

$$Q_2 \bar{\psi}_{\dot{2}}(x) = -2\partial A^*(x), \qquad Q_2 A^*(x) = 0, \tag{3.26}$$
$$Q_2 F^*(x) = -2\partial \bar{\psi}_{\dot{1}}(x), \qquad Q_2 \bar{\psi}_{\dot{1}}(x) = 0, \tag{3.27}$$
$$Q_2 A(x) = \psi_2(x), \qquad Q_2 \psi_2(x) = 0, \tag{3.28}$$
$$Q_2 \psi_1(x) = -F(x), \qquad Q_2 F(x) = 0. \tag{3.29}$$

[1]The Euclidean action of the auxiliary field in the WZ model has the "wrong sign", that is, the sign is opposite to the Gaussian one. In this sense, the functional integral containing the Euclidean action of the auxiliary field is merely a formal expression. We understand that the auxiliary field is always expressed by using the equation of motion. The functional integral then becomes perfectly well defined under this understanding. Our computation below is based on such a well-defined functional integral.

On the other hand, $\bar{Q}_{\dot{\alpha}}$ ($\dot{\alpha} = \dot{1}, \dot{2}$) is defined by

$$\bar{Q}_{\dot{1}}\psi_1(x) = -2\bar{\partial}A(x), \qquad \bar{Q}_{\dot{1}}A(x) = 0, \tag{3.30}$$
$$\bar{Q}_{\dot{1}}F(x) = -2\bar{\partial}\psi_2(x), \qquad \bar{Q}_{\dot{1}}\psi_2(x) = 0, \tag{3.31}$$
$$\bar{Q}_{\dot{1}}A^*(x) = \bar{\psi}_{\dot{1}}(x), \qquad \bar{Q}_{\dot{1}}\bar{\psi}_{\dot{1}}(x) = 0, \tag{3.32}$$
$$\bar{Q}_{\dot{1}}\bar{\psi}_{\dot{2}}(x) = -F^*(x), \qquad \bar{Q}_{\dot{1}}F^*(x) = 0, \tag{3.33}$$

and

$$\bar{Q}_{\dot{2}}\psi_2(x) = -2\partial A(x), \qquad \bar{Q}_{\dot{2}}A(x) = 0, \tag{3.34}$$
$$\bar{Q}_{\dot{2}}F(x) = 2\partial\psi_1(x), \qquad \bar{Q}_{\dot{2}}\psi_1(x) = 0, \tag{3.35}$$
$$\bar{Q}_{\dot{2}}A^*(x) = \bar{\psi}_{\dot{2}}(x), \qquad \bar{Q}_{\dot{2}}\bar{\psi}_{\dot{2}}(x) = 0, \tag{3.36}$$
$$\bar{Q}_{\dot{2}}\bar{\psi}_{\dot{1}}(x) = F^*(x), \qquad \bar{Q}_{\dot{2}}F^*(x) = 0. \tag{3.37}$$

These transformations obey anti-commutation relations,

$$\{Q_1, \bar{Q}_{\dot{1}}\} = -2\bar{\partial}, \tag{3.38}$$
$$\{Q_2, \bar{Q}_{\dot{2}}\} = -2\partial, \tag{3.39}$$
$$\{Q_1, \bar{Q}_{\dot{2}}\} = \{Q_2, \bar{Q}_{\dot{1}}\} = 0, \tag{3.40}$$
$$\{Q_\alpha, Q_\beta\} = \{\bar{Q}_{\dot{\alpha}}, \bar{Q}_{\dot{\beta}}\} = 0. \tag{3.41}$$

The WZ model above is also invariant under two $U(1)$ transformations. The first one is the following transformation ($\gamma \in \mathbb{R}$),

$$\delta_\gamma A(x) = 0, \qquad \delta_\gamma F(x) = 0, \tag{3.42}$$
$$\delta_\gamma\psi(x) = \delta_\gamma \begin{pmatrix}\psi_1\\ \bar{\psi}_{\dot{2}}\end{pmatrix}(x) = i\gamma \begin{pmatrix}\psi_1\\ \bar{\psi}_{\dot{2}}\end{pmatrix}(x), \quad \delta_\gamma(\bar{\psi}\gamma_0)^T(x) = \delta_\gamma \begin{pmatrix}\bar{\psi}_{\dot{1}}\\ \psi_2\end{pmatrix}(x) = -i\gamma \begin{pmatrix}\bar{\psi}_{\dot{1}}\\ \psi_2\end{pmatrix}(x). \tag{3.43}$$

We assign the $U(1)$ charge $+1$ to ψ, and -1 to $\bar{\psi}$. It will turn out that the associated $U(1)$ current together with the supercurrent and the EMT forms the superconformal multiplet. The other one is the so-called R-symmetry. In the case of $N_\Phi = 1$ and $W(\Phi) = \lambda\Phi^n/n$, the $U(1)_R$ transformation is given by

$$A(x) \to \exp\left[i\gamma/n\right] A(x), \tag{3.44}$$
$$\psi_\alpha(x) \to \exp\left[-i\gamma(n-2)/2n\right] \psi_\alpha(x), \tag{3.45}$$
$$\bar{\psi}_{\dot{\alpha}}(x) \to \exp\left[i\gamma(n-2)/2n\right] \bar{\psi}_{\dot{\alpha}}(x), \tag{3.46}$$
$$F(x) \to \exp\left[-i\gamma(n-1)/n\right] F(x). \tag{3.47}$$

Note that, even in the free-field limit $\lambda \to 0$, the $U(1)_R$ current can be neither holomorphic nor anti-holomorphic; it is not a member of the expected superconformal multiplet.

3.2 Spacetime symmetries and the Noether currents

We consider the basic spacetime symmetries of the 2D $\mathcal{N} = 2$ WZ model: SUSY, the translation, and the $U(1)$ symmetry. Our goal in this section is to derive the associated Noether currents: the supercurrent, the EMT, and the $U(1)$ current. In general, a Noether current is obtained as follows: Suppose that there exists a symmetry transformation $\varphi(x) \to \varphi(x) + \delta\varphi(x)$.

Then under the localized transformation

$$\varphi(x) \to \varphi(x) + \rho(x)\delta\varphi(x), \tag{3.48}$$

the action changes as

$$\delta S = -\frac{i}{2\pi}\int d^2x \sum_\mu j_\mu(x)\partial_\mu\rho(x). \tag{3.49}$$

Here $j_\mu(x)$ is the expected Noether current, which satisfies the conservation law

$$\sum_\mu \partial_\mu j_\mu(x) = 0. \tag{3.50}$$

From this derivation, we can obtain the Noether currents associated with the SUSY transformation δ_ξ (3.21), the translation

$$\delta_v\varphi(x) = -\sum_\mu v_\mu\partial_\mu\varphi(x), \tag{3.51}$$

and the $U(1)$ transformation δ_γ (3.43). It is convenient to define

$$j_\mu(x) = \begin{cases} -i\left(\xi^1\bar{S}^+_\mu(x) + \xi^2 S^-_\mu(x) + \bar{\xi}^{\dot{1}}\bar{S}^-_\mu(x) + \bar{\xi}^{\dot{2}}S^+_\mu(x)\right), \\ i\sum_\nu v_\nu T_{\mu\nu}(x), \\ \gamma J_\mu(x). \end{cases} \tag{3.52}$$

Here $S^\pm_\mu$ and $\bar{S}^\pm_\mu$ denote the supercurrents, $T_{\mu\nu}$ is the EMT, and J_μ is the $U(1)$ current. The superscripts $\pm$ of the supercurrent denote the $U(1)$ charge ±1.

Now we can derive the explicit form of the Noether currents. That of the supercurrent and the EMT, however, is ambiguous. This is because we have freedom to add a term X_μ, which is divergence-free $\sum_\mu \partial_\mu X_\mu$ and/or is proportional to the equation of motion. To remove this ambiguity it is natural to consider the $\mathcal{N}=2$ superconformal multiplet in the *massless free WZ model*, which is an $\mathcal{N}=2$ SCFT with $c=3$. The multiplet formed by the above Noether currents fulfills the $\mathcal{N}=2$ super-Virasoro algebra, as we will see in the next section. We then impose that the EMT is traceless,

$$\sum_\mu T_{\mu\mu} = 0, \tag{3.53}$$

that is,

$$T_{z\bar{z}} = T_{\bar{z}z} = 0, \tag{3.54}$$

and the supercurrent is gamma-traceless,

$$\sum_\mu \gamma_\mu \begin{pmatrix} \bar{S}^\pm_\mu \\ S^\pm_\mu \end{pmatrix} = 0, \tag{3.55}$$

that is,

$$S^{\pm}_{\bar{z}} = \bar{S}^{\pm}_{z} = 0, \tag{3.56}$$

for the massless free case, $W = 0$.

It is, however, still ambiguous to obtain the explicit form of EMT. Because of this, it is difficult to find the desired EMT, starting from the canonical EMT obtained by the variation δ_v (3.51). A better strategy is the following: We note that the Noether current obtained under the infinitesimal conformal transformation $z \to z + v_z(z)$ ($\bar{z} \to \bar{z} + v_{\bar{z}}(\bar{z})$) must be related to the traceless EMT. This transformation is an exact symmetry of the massless free WZ model. We now consider the infinitesimal transformation

$$\delta'_v A(x) = -\sum_{\mu} v_\mu \partial_\mu A(x), \tag{3.57}$$

$$\delta'_v \psi_1(x) = -\sum_{\mu} v_\mu \partial_\mu \psi_1(x) - \frac{1}{2}(\bar{\partial} v_{\bar{z}})\psi_1(x), \tag{3.58}$$

$$\delta'_v \bar{\psi}_{\dot{1}}(x) = -\sum_{\mu} v_\mu \partial_\mu \bar{\psi}_{\dot{1}}(x) - \frac{1}{2}(\bar{\partial} v_{\bar{z}})\bar{\psi}_{\dot{1}}(x), \tag{3.59}$$

$$\delta'_v \psi_2(x) = -\sum_{\mu} v_\mu \partial_\mu \psi_2(x) - \frac{1}{2}(\partial v_z)\psi_2(x), \tag{3.60}$$

$$\delta'_v \bar{\psi}_{\dot{2}}(x) = -\sum_{\mu} v_\mu \partial_\mu \bar{\psi}_{\dot{2}}(x) - \frac{1}{2}(\partial v_z)\bar{\psi}_{\dot{2}}(x), \tag{3.61}$$

$$\delta'_v F(x) = -\sum_{\mu} v_\mu \partial_\mu F(x). \tag{3.62}$$

If $v_z = v_z(z)$ and $v_{\bar{z}} = v_{\bar{z}}(\bar{z})$ in the massless free WZ model, these transformations coincide with the conformal transformation, where the conformal weights are (0, 0) for A and F, (0, 1/2) for ψ_1 and $\bar{\psi}_{\dot{1}}$, and (1/2, 0) for ψ_2 and $\bar{\psi}_{\dot{2}}$; this gives rise to the traceless EMT for the free field case. When v_μ is constant, this is just the translation $\delta'_v = \delta_v$ (3.51). When $v_\mu \propto \epsilon_{\mu\nu} x_\nu$, this is the infinitesimal Lorentz transformation. Since these transformation is a symmetry of the WZ model, the variation of the action with the localized parameter $v_\mu(x)$ gives rise to a conserved Noether current, which is a combination of the canonical EMT, the Lorentz current, and the equation of motion. In this way, we can obtain the EMT which fulfills the above requirements.

Following the above definition, we have the supercurrent [75]

$$S^+ \equiv S^+_z = \sum_I 4\pi \bar{\psi}_{\dot{2}I} \partial A_I, \qquad S^+_{\bar{z}} = \sum_I 2\pi \psi_{1I} \frac{\partial W(\{A\})}{\partial A_I}, \tag{3.63}$$

$$S^- \equiv S^-_z = \sum_I (-4\pi) \psi_{2I} \partial A^*_I, \qquad S^-_{\bar{z}} = \sum_I 2\pi \bar{\psi}_{\dot{1}I} \frac{\partial W(\{A\})^*}{\partial A^*_I}, \tag{3.64}$$

$$\bar{S}^+_z = \sum_I (-2\pi) \bar{\psi}_{\dot{2}I} \frac{\partial W(\{A\})^*}{\partial A^*_I}, \qquad \bar{S}^+ \equiv \bar{S}^+_{\bar{z}} = \sum_I (-4\pi) \psi_{1I} \bar{\partial} A^*_I, \tag{3.65}$$

$$\bar{S}^-_z = \sum_I (-2\pi) \psi_{2I} \frac{\partial W(\{A\})}{\partial A_I}, \qquad \bar{S}^- \equiv \bar{S}^-_{\bar{z}} = \sum_I 4\pi \bar{\psi}_{\dot{1}I} \bar{\partial} A_I, \tag{3.66}$$

and the EMT

$$
\begin{aligned}
T_{\mu\nu} = \sum_I \Bigg\{ & -2\pi \partial_\mu A_I^* \partial_\nu A_I - 2\pi \partial_\nu A_I^* \partial_\mu A_I \\
& + \pi \delta_{\mu\nu} \Bigg[2 \sum_\rho \partial_\rho A_I^* \partial_\rho A_I - 2F_I^* F_I - 2F_I^* \frac{\partial W(\{A\})^*}{\partial A_I^*} - 2F_I \frac{\partial W(\{A\})}{\partial A_I} \\
& \qquad + \sum_J \left(\frac{\partial^2 W(\{A\})^*}{\partial A_I^* \partial A_J^*} \bar{\psi}_{\dot{1}I} \bar{\psi}_{\dot{2}J} + \frac{\partial^2 W(\{A\})}{\partial A_I \partial A_J} \psi_{2I} \psi_{1J} \right) \Bigg] \\
& - \pi (\delta_{0\mu} - i\delta_{1\mu})(\delta_{0\nu} - i\delta_{1\nu}) \left(\bar{\psi}_{\dot{1}I} \bar{\partial} \psi_{1I} - \bar{\partial} \bar{\psi}_{\dot{1}I} \psi_{1I} \right) \\
& \qquad - \pi (\delta_{0\mu} + i\delta_{1\mu})(\delta_{0\nu} + i\delta_{1\nu}) \left(\psi_{2I} \partial \bar{\psi}_{\dot{2}I} - \partial \psi_{2I} \bar{\psi}_{\dot{2}I} \right) \Bigg\}.
\end{aligned} \tag{3.67}
$$

The explicit form of the $U(1)$ current is given by

$$
J \equiv J_z = \sum_I 2\pi \bar{\psi}_{\dot{2}I} \psi_{2I}, \tag{3.68}
$$

$$
\bar{J} \equiv J_{\bar{z}} = \sum_I 2\pi \psi_{1I} \bar{\psi}_{\dot{1}I}. \tag{3.69}
$$

The EMT can be written in the complex coordinates as

$$
T \equiv T_{zz} = \sum_I \left(-4\pi \partial A_I^* \partial A_I - \pi \psi_{2I} \partial \bar{\psi}_{\dot{2}I} + \pi \partial \psi_{2I} \bar{\psi}_{\dot{2}I} \right), \tag{3.70}
$$

$$
\bar{T} \equiv T_{\bar{z}\bar{z}} = \sum_I \left(-4\pi \bar{\partial} A_I^* \bar{\partial} A_I^* - \pi \bar{\psi}_{\dot{1}I} \bar{\partial} \psi_{1I} + \pi \bar{\partial} \bar{\psi}_{\dot{1}I} \psi_{1I} \right), \tag{3.71}
$$

$$
\begin{aligned}
T_{z\bar{z}} = T_{\bar{z}z} = \sum_I \Bigg[& -\pi F_I^* F_I - \pi F_I^* \frac{\partial W(\{A\})^*}{\partial A_I^*} - \pi F_I \frac{\partial W(\{A\})}{\partial A_I} \\
& + \sum_J \left(\frac{\pi}{2} \frac{\partial^2 W(\{A\})^*}{\partial A_I^* \partial A_J^*} \bar{\psi}_{\dot{1}I} \bar{\psi}_{\dot{2}J} + \frac{\pi}{2} \frac{\partial^2 W(\{A\})}{\partial A_I \partial A_J} \psi_{2I} \psi_{1J} \right) \Bigg].
\end{aligned} \tag{3.72}
$$

Noting that $F_I = -\partial W^*/\partial A_I^*$ under the equation of motion, when $W = 0$, the (gamma-) traceless condition is satisfied clearly.

It can be confirmed that the above expressions of the supercurrent, the EMT, and the $U(1)$ current are related by the SUSY transformation. For instance, $S^\pm$, T, and J, satisfies

$$
T = \frac{1}{4} Q_2 S^\pm - \frac{1}{4} \bar{Q}_{\dot{2}} S^\pm, \tag{3.73}
$$

$$
S^+ = \bar{Q}_{\dot{2}} J, \qquad\qquad S^- = Q_2 J \tag{3.74}
$$

This fact also provides support for the above Noether currents.

3.3 $\mathcal{N}=2$ super-Virasoro algebra

3.3.1 OPEs of the superconformal multiplet

We focus on the massless free WZ model with $W(\Phi)=0$,

$$S=\int d^2x\left[4\partial A^*\bar\partial A+2\bar\psi_{\dot 1}\partial\psi_1+2\psi_2\bar\partial\bar\psi_{\dot 2}\right]. \tag{3.75}$$

Here we have eliminated the auxiliary field F. This would be a free $\mathcal{N}=2$ SCFT. In this section, let us confirm that the above Noether currents satisfy the $\mathcal{N}=2$ super-Virasoro algebra as expected.

We immediately find that from equations of motion,

$$\bar\partial\partial A=0, \tag{3.76}$$
$$\partial\psi_1=0,\qquad \partial\bar\psi_{\dot 1}=0, \tag{3.77}$$
$$\bar\partial\psi_2=0,\qquad \bar\partial\bar\psi_{\dot 2}=0, \tag{3.78}$$

A should be a sum of holomorphic and anti-holomorphic functions, $(\psi_1,\bar\psi_{\dot 1})$ is anti-holomorphic, and $(\psi_2,\bar\psi_{\dot 2})$ holomorphic. Under the conformal transformation $z\to z'$, we have

$$A'(z',\bar z')=A(z,\bar z), \tag{3.79}$$
$$\psi_1'(\bar z')=(\bar\partial\bar z')^{-1/2}\psi_1(\bar z),\qquad \bar\psi_{\dot 1}'(\bar z')=(\bar\partial\bar z')^{-1/2}\bar\psi_{\dot 1}(\bar z), \tag{3.80}$$
$$\psi_2'(z')=(\partial z')^{-1/2}\psi_2(z),\qquad \bar\psi_{\dot 2}'(z')=(\partial z')^{-1/2}\bar\psi_{\dot 2}(z). \tag{3.81}$$

The SUSY transformation given in Eqs. (3.22)–(3.37) is now called the superconformal transformation. Since the conformal (superconformal) transformation does not mix holomorphic and anti-holomorphic functions, transformations by Q_1 (3.22)–(3.25) and $\bar Q_{\dot 1}$ (3.26)–(3.29) are holomorphic, those by Q_2 (3.30)–(3.33) and $\bar Q_{\dot 2}$ (3.34)–(3.37) are anti-holomorphic. Noting that

$$\bar\partial\partial\ln|z|^2=\pi\delta(x_0)\delta(x_1), \tag{3.82}$$

The OPEs between the component fields are given by[2]

$$A(z,\bar z)A^*(0,0)\sim-\frac{1}{4\pi}\ln|z|^2, \tag{3.83}$$
$$\psi_1(\bar z)\bar\psi_{\dot 1}(0)\sim\frac{1}{2\pi}\frac{1}{\bar z}, \tag{3.84}$$
$$\bar\psi_{\dot 2}(z)\psi_2(0)\sim\frac{1}{2\pi}\frac{1}{z}, \tag{3.85}$$
$$(\text{otherwise})\sim 0. \tag{3.86}$$

[2]In string theory, the following normalization is conventional: $\varphi\to(1/\sqrt{2\pi})\varphi$. Then we see the overall factor $1/2\pi$ in the action (3.75), while coefficients of the OPEs (3.83)–(3.85) are simplified.

We summarize explicit expressions for the Noether currents in the massless free limit. In the holomorphic sector the supercurrent, the EMT and the $U(1)$ current are

$$S^+(z) = 4\pi\bar{\psi}_{\dot{2}}(z)\partial A(z), \tag{3.87}$$
$$S^-(z) = -4\pi\psi_2(z)\partial A^*(z), \tag{3.88}$$
$$T(z) = -4\pi\partial A^*(z)\partial A(z) - \pi\psi_2(z)\partial\bar{\psi}_{\dot{2}}(z) + \pi\partial\psi_2(z)\bar{\psi}_{\dot{2}}(z), \tag{3.89}$$
$$J(z) = 2\pi\bar{\psi}_{\dot{2}}(z)\psi_2(z), \tag{3.90}$$

and in the anti-holomorphic sector,

$$\bar{S}^+(\bar{z}) = -4\pi\psi_1(\bar{z})\bar{\partial}A^*(\bar{z}), \tag{3.91}$$
$$\bar{S}^-(\bar{z}) = 4\pi\bar{\psi}_{\dot{1}}(\bar{z})\bar{\partial}A(\bar{z}), \tag{3.92}$$
$$\bar{T}(\bar{z}) = -4\pi\bar{\partial}A^*(\bar{z})\bar{\partial}A(\bar{z}) - \pi\bar{\psi}_{\dot{1}}(\bar{z})\bar{\partial}\psi_1(\bar{z}) + \pi\bar{\partial}\bar{\psi}_{\dot{1}}(\bar{z})\psi_1(\bar{z}), \tag{3.93}$$
$$\bar{J}(\bar{z}) = 2\pi\psi_1(\bar{z})\bar{\psi}_{\dot{1}}(\bar{z}). \tag{3.94}$$

Using these, we find that the holomorphic Noether currents fulfill the OPEs of the $\mathcal{N} = 2$ super-Virasoro algebra,

$$T(z)T(0) \sim \frac{c}{2z^4} + \frac{2}{z^2}T(0) + \frac{1}{z}\partial T(0), \tag{3.95}$$
$$T(z)S^\pm(0) \sim \frac{3}{2z^2}S^\pm(0) + \frac{1}{z}\partial S^\pm(0), \tag{3.96}$$
$$T(z)J(0) \sim \frac{1}{z^2}J(0) + \frac{1}{z}\partial J(0), \tag{3.97}$$
$$S^\pm(z)S^\pm(0) \sim 0, \tag{3.98}$$
$$S^+(z)S^-(0) \sim \frac{2c}{3z^3} + \frac{2}{z^2}J(0) + \frac{2}{z}T(0) + \frac{1}{z}\partial J(0), \tag{3.99}$$
$$J(z)S^\pm(0) \sim \pm\frac{1}{z}S^\pm(0), \tag{3.100}$$
$$J(z)J(0) \sim \frac{c}{3z^2}, \tag{3.101}$$

where the central charge is $c = 3$ corresponding to a free $\mathcal{N} = 2$ SCFT.

3.3.2 $\mathcal{N} = 2$ minimal model

Finally, the minimal series of the SCFT is discussed. We should remark that there are two chooses of boundary conditions for the fermion [17–19]; for instance,

$$\text{Neveu–Schwarz (NS) sector} : \psi_2(e^{2\pi i}z) = +\psi_2(z), \tag{3.102}$$
$$\text{Ramond (R) sector} : \psi_2(e^{2\pi i}z) = -\psi_2(z). \tag{3.103}$$

Noting that ψ has the conformal weight $h = 1/2$, its Laurent expansion is given by

$$\psi_2(z) = \sum_r \frac{\psi_{2,r}}{z^{r+\frac{1}{2}}}, \tag{3.104}$$

where $r \in \mathbb{Z} + \frac{1}{2}$ in the NS sector, and $r \in \mathbb{Z}$ in the R sector. There exist minimal models of $\mathcal{N} = 2$ SCFT at $c < 3$, while non-SUSY minimal models at $c < 1$. Unitary representations can exist for $c \geq 3$, or in unitary minimal models [102]

$$\hat{c} = \frac{c}{3} = \frac{k}{k+2}, \qquad \text{for } k = 1, 2, \ldots \tag{3.105}$$

In the NS sector, the conformal weights and $U(1)$ charges are

$$h_{\ell,m} = \frac{\ell(\ell+2) - m^2}{4(k+2)}, \tag{3.106}$$

$$Q_{\ell,m} = \frac{m}{k+2}, \tag{3.107}$$

and in the R sector, on the other hand,

$$h_{\ell,m} = \frac{\ell(\ell+2) - (m \pm 1)^2}{4(k+2)} + \frac{1}{8}, \tag{3.108}$$

$$Q_{\ell,m} = \frac{m \pm 1}{k+2} \mp \frac{1}{2}. \tag{3.109}$$

Here ℓ and m are integers, such that

$$0 \leq \ell \leq k, \qquad\qquad -\ell \leq m \leq \ell. \tag{3.110}$$

Chapter 4

Renormalization group and Landau–Ginzburg description

4.1 Renormalization group

So far, we have took into account (S)CFTs, which includes the invariance under scale transformations. In this section, we discuss the scaling behavior of more general quantum field theories, which is governed by the renormalization group (RG). The most part of this chapter is based on Ref. [53].

To see the behavior under scaling transformations of a d-dimensional quantum field theory, suppose that a complete set of local operators $\mathcal{O}_i(x)$ behaves as

$$\delta\mathcal{O}_i(x) = -\sum_j \Delta_i{}^j \mathcal{O}_j(x) \tag{4.1}$$

under an infinitesimal scale transformation. Then, the scaling transformation for a correlation function is given by

$$\begin{aligned}\delta\left\langle \prod_m \mathcal{O}_m(x_m) \right\rangle = &-\frac{1}{2\pi}\int d^dx \left\langle \sum_\mu T_{\mu\mu}(x) \prod_m \mathcal{O}_m(x_m) \right\rangle \\ &- \sum_{j,k} \Delta_k{}^j \left\langle \mathcal{O}_j(x_k) \prod_{m\neq k} \mathcal{O}_m(x_m) \right\rangle .\end{aligned} \tag{4.2}$$

The first term on the right hand side comes from the variation of the action under the scaling. The trace of the EMT can be expanded in terms of the complete set $\{\mathcal{O}_i\}$,

$$\int d^dx \sum_\mu T_{\mu\mu} = -2\pi {\sum_i}' \int d^dx\, \beta^i(g)\mathcal{O}_i(x). \tag{4.3}$$

Here $\sum_i'$ is the summation over operators with dimension less than or equal to d. Writing a general renormalizable action

$$S = {\sum_i}' g^i \int d^dx\, \mathcal{O}_i(x), \tag{4.4}$$

where g^i is a coupling constant, we obtain the RG equation as

$$\delta \left\langle \prod_m \mathcal{O}_m(x_m) \right\rangle = -{\sum_i}' \beta^i(g) \frac{\partial}{\partial g^i} \left\langle \prod_m \mathcal{O}_m(x_m) \right\rangle - \sum_{j,k} \Delta_k{}^j \left\langle \mathcal{O}_j(x_k) \prod_{m \neq k} \mathcal{O}_m(x_m) \right\rangle. \tag{4.5}$$

It can be absorbed into the definition of $\Delta_i{}^j$ that contact terms between the trace of the EMT and other local operators, and g^i-derivatives acting on local operators. We find that the RG equation states

$$\text{Scaling transformation} = \text{Running of couplings} + \text{Mixing of local operators}. \tag{4.6}$$

Even if the classical action is scale invariant, the total quantum system can possess nontrivial dependence on the scale. We mean by the "scale invariance" that the theory is invariant under RG transformations. This scale invariance may be realized in the quantum field theory with a fixed parameter of the coupling, $g^i = g^i_*$; it is a fixed point under the RG flow, where the coupling is truly constant. Sufficiently low-energy physics is expected to be at the IR fixed point, while all massive modes are decoupled. The similarity between the scale invariance and conformal symmetry appears to imply that such a scale-invariant theory would be described by a CFT. Especially, any 2D unitary scale-invariant theory has the conformal symmetry [82, 103]. It is, however, not the case for all field theories [104].

4.2 Zamolodchikov's c-theorem

In a 2D theory without conformal symmetry, the traceless condition is not satisfied; $T_{z\bar{z}}$ does not vanish, and T_{zz} ($T_{\bar{z}\bar{z}}$) is not (anti-) holomorphic. We cannot define the central charge in the Virasoro algebra. However, we can generalize the idea of the central charge in such a field theory. First, noting that the two-point function of T_{zz} in a CFT is given by

$$\langle T_{zz}(z) T_{zz}(0) \rangle = \frac{c}{2z^4} \tag{4.7}$$

because of rotational invariance, we can define a function $F(\tau)$ with $\tau = \ln z\bar{z}$ such that [103, 105]

$$\langle T_{zz}(z,\bar{z}) T_{zz}(0,0) \rangle = \frac{F(\tau)}{z^4}. \tag{4.8}$$

At the fixed point of RG transformations, where the theory has the conformal invariance, $2F$ is identical to the central charge c itself. The discussion in the previous section leads to the fact that $2F(\tau) \to c$ in an extremely low-energy region, $\tau \to \infty$. Second, we also define G and H by

$$\langle T_{zz}(z,\bar{z}) T_{z\bar{z}}(0,0) \rangle = \frac{G(\tau)}{4z^3\bar{z}}, \tag{4.9}$$

$$\langle T_{z\bar{z}}(z,\bar{z}) T_{z\bar{z}}(0,0) \rangle = \frac{H(\tau)}{z^2\bar{z}^2}, \tag{4.10}$$

where G and H are the functions of τ because of rotational invariance [103, 105]. From the conservation law $\bar{\partial}T_{zz} + \partial T_{z\bar{z}} = 0$, one obtains

$$4\frac{dF}{d\tau} + \frac{dG}{d\tau} - 3G = 0, \tag{4.11}$$

$$4\frac{dG}{d\tau} - 4G + \frac{dH}{d\tau} - 2H = 0. \tag{4.12}$$

Then we can find

$$\frac{d}{d\tau}\left(2F - G - \frac{3}{8}H\right) = -\frac{3}{4}H. \tag{4.13}$$

The form in the parentheses of the left hand side is called the Zamolodchikov C-function [82]:

$$C \equiv 2F - G - \frac{3}{8}H. \tag{4.14}$$

The unitarity (or the reflection positivity) indicates that H is non-negative [106, 107]. Thus $C(\tau)$ is a monotonically decreasing function of τ. At $\tau \to \infty$, $C(\tau)$ is stationary and identical to c because $T_{z\bar{z}} = 0$.

There also exists the supersymmetric version of the Zamolodchikov C-function in terms of the supercurrent, instead of the EMT [83]. We discuss this in the 2D $\mathcal{N} = 2$ WZ model. The supercurrent (3.63)–(3.66),

$$S_z^+ = 4\pi\bar{\psi}_{\dot{2}}\partial A, \qquad S_{\bar{z}}^+ = 2\pi\psi_1 W'(A), \tag{4.15}$$

$$S_z^- = -4\pi\psi_2\partial A^*, \qquad S_{\bar{z}}^- = 2\pi\bar{\psi}_{\dot{1}} W'(A)^*, \tag{4.16}$$

satisfies the conservation law

$$\bar{\partial}S_z^{\pm} + \partial S_{\bar{z}}^{\pm} = 0. \tag{4.17}$$

For a superconformal system, $S_{\bar{z}}^{\pm} = 0$ and

$$\left\langle S_z^{\pm}(z) S_z^{\pm}(0)\right\rangle = 0, \tag{4.18}$$

$$\left\langle S_z^{+}(z) S_z^{-}(0)\right\rangle = \frac{2c}{3z^3}. \tag{4.19}$$

Now, introducing w and q by

$$w(z,\bar{z}) \equiv S_z^+(z,\bar{z}) + S_z^-(z,\bar{z}), \qquad q(z,\bar{z}) \equiv -S_{\bar{z}}^+(z,\bar{z}) - S_{\bar{z}}^-(z,\bar{z}), \tag{4.20}$$

we define general forms as

$$\langle w(z,\bar{z}) w(0,0)\rangle = \frac{f(\tau)}{z^3}, \tag{4.21}$$

$$\langle w(z,\bar{z}) q(0,0)\rangle = \langle q(z,\bar{z}) w(0,0)\rangle = \frac{g(\tau)}{z^2\bar{z}}, \tag{4.22}$$

$$\langle q(z,\bar{z}) q(0,0)\rangle = \frac{h(\tau)}{z\bar{z}^2} \tag{4.23}$$

Here owing to rotational invariance, f, g, and h are functions of τ only. From Eq. (4.17), we can obtain

$$\frac{df}{d\tau} - \frac{dg}{d\tau} + 2g = 0, \tag{4.24}$$

$$\frac{dg}{d\tau} - \frac{dh}{d\tau} - g + h = 0, \tag{4.25}$$

and

$$\frac{d}{d\tau}\left(f + g - 2h\right) = -2h. \tag{4.26}$$

Thus we again see that the SUSY-analogue of the Zamolodchikov C-function,

$$\chi \equiv \frac{3}{4}\left(f + g - 2h\right), \tag{4.27}$$

is a monotonically decreasing function of τ because $h(\tau)$ is non-negative. As $\tau \to \infty$, we observe $S_{\tilde{z}}^{\pm} = 0$ and $\chi = c$.

4.3 Landau–Ginzburg description

In this section, we introduce the Landau–Ginzburg (LG) model. Originally, the so-called Ginzburg–Landau theory is considered to describe superconductivity [4]. This is realized by introducing a complex order parameter, on the basis of the mean field approximation to second-order phase transitions. We first consider an order parameter $\eta \in \mathbb{R}$, such that $\eta = 0$ for the ordered phase, and $\eta \neq 0$ for the disordered phase. Suppose that the free energy, $F(T, \eta)$ at a temperature T can be expanded by the order parameter η, and is symmetric under $\eta \to -\eta$. Then we obtain

$$F(T, \eta) = F(T, 0) + C_2(T)\eta^2 + C_4(T)\eta^4 + \cdots . \tag{4.28}$$

Now we regard η as a type of "wave function," $\psi \in \mathbb{C}$. and replace η with ψ, and η^2 with $|\psi|^2$; then the free energy is rewritten by

$$F(T, \psi) = F(T, 0) + C_2(T)|\psi|^2 + C_4(T)|\psi|^4 + \cdots . \tag{4.29}$$

When the wave function ψ depends on positions in the space, the kinetic term

$$-\frac{\hbar^2}{2m}|\nabla\psi|^2 \tag{4.30}$$

is supposed to add to the free energy. To minimize F under variations of ψ leads to the Ginzburg–Landau equation.

In the context of field theory, we consider the (Euclidean) Lagrangian, instead of the free energy. For example,

$$\mathcal{L} = \frac{1}{2}(\partial\phi)^2 + \lambda_1\phi^2 + \lambda_2\phi^4. \tag{4.31}$$

In the IR limit, tuning λ_1 to zero (massless), this model becomes the critical theory that is the $m = 3$ minimal model in Chap 2. (That is, this model belongs to the same universality class as the Ising model.) Similarly, the model with ϕ^{2m-2}, instead of ϕ^4, corresponds to the mth minimal model [3]. Such a (strongly-interacting) Lagrangian realization of CFT is the LG description of CFT and the LG model. This provides a intuitive picture of its operator content; a primary field $\mathcal{O}_{r,s}$ with the conformal weight $h_{r,s}$ given in Chap. 2 is identified with

$$\phi^n = \mathcal{O}_{n+1,n+1}, \qquad (0 \le n \le m-2). \tag{4.32}$$

Let us take into account the 2D $\mathcal{N} = 2$ SUSY. Especially, the 2D $\mathcal{N} = 2$ WZ model (3.18)

$$S = \int d^2x \Bigg[4\partial A^* \bar{\partial} A - F^*F - F^*W'(A)^* - FW'(A) + (\bar{\psi}_{\dot{1}}, \psi_2) \begin{pmatrix} 2\partial & W''(A)^* \\ W''(A) & 2\bar{\partial} \end{pmatrix} \begin{pmatrix} \psi_1 \\ \bar{\psi}_{\dot{2}} \end{pmatrix} \Bigg] \tag{4.33}$$

with the superpotential

$$W(\Phi) = \frac{\lambda}{k+2}\Phi^{k+2} \qquad \text{for } k = 1,\, 2,\, \ldots, \tag{4.34}$$

is believed to provide the LG description of the kth $\mathcal{N} = 2$ unitary minimal model in Chap. 3. For example, in Ref. [52], an evidence is provided by the analysis of a generalization of the Witten index,

$$Z(q, \bar{q}, \gamma_L, \gamma_R) = \mathrm{Tr}(-1)^F q^{H_L} \bar{q}^{H_R} \exp\left(i\gamma_L J_{0,L} + i\gamma_R J_{0,R}\right), \tag{4.35}$$

where H is the Hamiltonian, and J_0 is the $U(1)$ charge, the subscript L denote the left-mover part, and R does the right-mover part; q, $\bar{q}$, and $\gamma_{L,R}$ are arbitrary constants. Although this can be computed in the $\mathcal{N} = 2$ minimal model, it is difficult in the WZ model. Now, for the case of $\gamma_R = 0$, we define the elliptic genus by

$$Z(q, \bar{q}, \gamma_L, 0) = \mathrm{tr}(-1)^F q^{H_L} \bar{q}^{H_R} \exp\left(i\gamma_L J_{0,L}\right). \tag{4.36}$$

In the WZ model, this partition function implies that the boundary condition along time is twisted by $\exp(i\gamma_L J_{0,L})$. The most salient feature is that the elliptic genus is invariant under $W(\Phi) \to \epsilon W(\Phi)$ with $\epsilon \ge 0$, so it is a topological number; in the free-field limit $\epsilon \to 0$, this becomes computable. It turns out [52] that the elliptic genus in the minimal model is identical to that in the WZ model.

For the WZ model with multiple superfields (3.20), the superpotential $W(\{\Phi_I\})$ should be quasi-homogeneous,

$$W(\{\Lambda^{\omega_I}\Phi_I\}) = \Lambda W(\{\Phi_I\}). \tag{4.37}$$

We can see this as follows: Suppose that $W = \Phi^m + \Phi^n$ $(m < n)$ for simplicity. Rescaling the metric induces $\int d^2z\, d^2\theta \to \lambda \int d^2z\, d^2\theta$, and hence, we have

$$\int d^2z\, d^2\theta\, W(\Phi) = \lambda \int d^2z\, d^2\theta\, \left(\Phi^m + \Phi^n\right). \tag{4.38}$$

We can absorb the overall factor λ into the redefinition of the superfield as $\Phi \to \lambda^{-1/m}\Phi$, and consider the IR limit, which indicates the strong-coupling limit $\lambda \to \infty$. Then we see

$$\int d^2z\, d^2\theta\, W(\Phi) = \int d^2z\, d^2\theta\, \left(\Phi^m + \lambda^{-n/m}\Phi^n\right) \tag{4.39}$$

$$\overset{\lambda\to\infty}{\to} \int d^2z\, d^2\theta\, \Phi^m. \qquad (m < n) \tag{4.40}$$

The IR behavior thus is governed by the quasi-homogeneous part of the superpotential with the lowest weight.[1] The explicit WZ/minimal-model correspondence is tabulated in Table. 4.1, where the quasi-homogeneous superpotential is classified [44].

Algebra	Superpotential	Central charge
A_n	x^{n+1}, $n \geqq 1$	$3 - 6/(n+1)$
D_n	$x^{n-1} + xy^2$, $n \geqq 3$	$3 - 6/2(n-1)$
E_6	$x^3 + y^4$	$3 - 6/12$
E_7	$x^3 + xy^3$	$3 - 6/18$
E_8	$x^3 + y^5$	$3 - 6/30$

Table 4.1: ADE classification

4.4 Gepner model and Calabi–Yau compactification

A low-energy effective theory of the heterotic superstring theory is given by a ten-dimensional $\mathcal{N} = 1$ supergravity, which includes the graviton together with its superpartner, gravitino. We now assume that the $\mathcal{N} = 1$ SUSY remains in the flat four-dimensional spacetime, while the extra six-dimensions are compactified. Then, the compactified space should be a Calabi–Yau (CY) manifold. In this last section, let us consider the relation between the LG model and the CY compactification of the superstring theory.

In superstring theory, the compactification into a complex d-dimensional CY manifold can be described by an $\mathcal{N} = 2$ SCFT with $\hat{c} = c/3 = d$. Such a theory may be a product of minimal models, $\mathcal{M}_{k_i}^{\mathcal{N}=2}$ with $m = k_i$ ($i = 1, 2, \ldots, N$),

$$\otimes\mathcal{M}_{k_i}^{\mathcal{N}=2}, \qquad \hat{c} = \sum_i^N \frac{k_i}{k_i + 2} = 3. \tag{4.41}$$

This is called the Gepner model.[2] For simplicity, we consider the Gepner model with $k_i = k$ for $^\forall i$,

$$\frac{Nk}{k+2} = 3. \tag{4.42}$$

[1] Thanks to the non-renormalization theorem [108–110], the superpotential is expected to receive no modifications under quantum radiations. It is, however, not clear that the perturbative non-renormalization theorem can apply to the present model, because the perturbation theory suffers from the IR divergences.

[2] This definition is not yet a superstring theory itself, but consistent with the type II or heterotic superstring. The consistency with the spacetime SUSY requires that the $U(1)$ charge takes only integers.

and then we have

$$(k, N) = (1, 9),\ (2, 6),\ (3, 5),\ (6, 4). \tag{4.43}$$

For example, if $(k, N) = (3, 5)$, the CY manifold is the quintic in $\mathbb{C}P^4$,

$$G(z) = z_1^5 + z_2^5 + z_3^5 + z_4^5 + z_5^5 = 0. \tag{4.44}$$

On the other hand, the LG description of the $k = 3$ minimal is provided by the WZ model with $W = \Phi^5$. The LG model corresponding to (4.44) has the superpotential

$$W(\{\Phi\}) = \Phi_1^5 + \Phi_2^5 + \Phi_3^5 + \Phi_4^5 + \Phi_5^5. \tag{4.45}$$

Note that the forms of Eqs. (4.44) and (4.45) are identical.

A simple way to see this correspondence is as follows: At the IR fixed point, the critical theory is determined by the form of the superpotential; then we consider the partition function as

$$Z = \int \prod_I [d\Phi_I]\ e^{\int d^2z\, d^2\theta\, W(\{\Phi\}) + \text{h.c.}}. \tag{4.46}$$

Because W is quasi-homogeneous as in Eq. (4.37), we can change the variables from $\{\Phi\}$ to $\{X\}$, such that $W(\Phi_1, \Phi_2, \ldots, \Phi_N) = X_1 W(1, X_2, \ldots, X_N)$. Integrating over X_1, we have

$$Z \sim \int \prod_{I>1} [dX_I]\ \delta(W(1, X_2, \ldots, X_N)). \tag{4.47}$$

Possible configurations are thus constrained to be on the hypersurface defined by $W = 0$, which forms the CY manifold.

As another example of the LG/CY correspondence, we show that the non-linear sigma model on the CY manifold and the LG model are related each other through a phase transition [42, 53]. By the dimensional reduction of a four-dimensional $\mathcal{N} = 1$ supersymmetric theory, we construct a 2D $\mathcal{N} = 2$ theory. Let V be a $U(1)$ vector superfield, P and Φ_I ($I = 1$, 2, …, 5) chiral superfields with the superpotential

$$W = PG(\Phi). \tag{4.48}$$

Here G is identical to the form of Eq. (4.45). We assign the $U(1)$ charge $q_\Phi = 1$ to Φ_I and $q_P = -5$ to P. Especially, we can add the Fayet–Iliopoulos term [111]

$$-r \int d^2x \int d^4\theta\, V, \tag{4.49}$$

to the action, where r is the Fayet–Iliopoulos parameter. The dimensional reduction of the above setup induces the potential

$$\begin{aligned} U = |G(\phi)|^2 + |p|^2 \sum_I \left| \frac{\partial G}{\partial \phi_I} \right|^2 + \frac{e^2}{2} \left(r + 5|p|^2 - \sum_I |\phi_I|^2 \right)^2 \\ + 2(A_2^2 + A_3^2) \left(\sum_I |\phi_I|^2 + 25|p|^2 \right), \end{aligned} \tag{4.50}$$

where e denote the gauge coupling, A_2 and A_3 are the scalar fields coming from the gauge field in four dimensions. The scalar component of each superfield is written as its lower case letter. For a smoothness condition, we impose that the five equations,

$$\frac{\partial G}{\partial \phi_I} = 0, \tag{4.51}$$

have only one simultaneous solution, $\phi_I = 0$ for $^\forall i$.

Let us consider configurations of the fields, which minimize the potential. First, when $r > 0$, the second term in the potential (4.50) vanishes if $p = 0$ or $\phi_I = 0$. The cancellation condition of the third term is

$$p = 0, \qquad \sum_I |\phi_I|^2 = r. \tag{4.52}$$

From the fourth term, we have $\sigma = 0$. As a consequence, we obtain

$$G(\phi) = 0. \tag{4.53}$$

The fields $\{\phi_i\}$ are regarded as the coordinates on the manifold defined by Eq. (4.53), which is called the target space. When we consider a curved target space, the theory is a non-linear sigma model.

Second, we focus on the case of $r < 0$. From the second and third terms, we see

$$|p|^2 = \frac{r}{5}, \qquad \phi_I = 0, \tag{4.54}$$

and from the fourth term $\sigma = 0$. Fluctuations of p are massive, while those of ϕ_I leads to the LG model with the massless superpotential

$$W = \langle p \rangle G(\Phi). \tag{4.55}$$

We find that, for a same theory, there exist the CY phase for $r > 0$, and the LG phase for $r < 0$.[3]

As mentioned in Introduction, if the world sheet theory is described by a Gepner model, scattering amplitudes in the superstring theory can be computed from the the SCFT, but it is in general not the case. Thus, it is quite difficult to carry out computations for a general CY manifold, and treat the deformation of the compactification. On the other hand, the superpotential $W(\Phi)$ of the LG model can be arbitrary changed, while the CY manifold is deformed in the same way as we discussed in this section. Recall again, however, that the LG description is a strongly-interacting field theory (and perturbation techniques is hindered by the IR divergences).

[3]Although $r = 0$ is a singular point, we can perform analytical continuation through $r = 0$ by adding

$$i\frac{\theta}{2\pi}\int F_{\mu\nu} dx^\mu \wedge dx^\nu, \tag{4.56}$$

if θ is non-zero at $r = 0$.

Chapter 5

Numerical approach based on the Nicolai map

5.1 Formulation

5.1.1 Momentum cutoff regularization

In this and next chapters, as an alternative approach to study the LG model, we attempt studying a non-perturbative numerical method on the basis of the lattice field theory. To quantize the 2D $\mathcal{N} = 2$ WZ action in Eq. (3.20), we employ the formulation studied in Ref. [76], which is based on a momentum cutoff regularization and the Nicolai mapping. First of all, suppose that the system we consider is defined in a 2D Euclidean box of physical size $L_0 \times L_1$. The Fourier mode of a generic field $\varphi(x)$ is then defined by

$$\varphi(x) = \frac{1}{L_0 L_1} \sum_p e^{ipx} \varphi(p), \qquad \varphi(p) = \int d^2x \, e^{-ipx} \varphi(x), \tag{5.1}$$

where the momentum is discretized as

$$p_\mu = \frac{2\pi}{L_\mu} n_\mu, \qquad \text{for } n_\mu \in \mathbb{Z}. \tag{5.2}$$

Note that

$$\varphi^*(p) = \varphi(-p)^*. \tag{5.3}$$

The WZ action in the momentum space is given by

$$\begin{aligned} S = \frac{1}{L_0 L_1} \sum_p \sum_I \Bigg[& 4p_z A_I^*(-p) p_{\bar{z}} A_I(p) - F_I^*(-p) F_I(p) \\ & - F_I(-p) \frac{\partial W(\{A\})}{\partial A_I}(p) - F_I^*(-p) \frac{\partial W(\{A\})^*}{\partial A_I^*}(p) \\ & + (\bar{\psi}\gamma_0)_I(-p) \sum_J \begin{pmatrix} 2\delta_{IJ} p_z & \frac{\partial^2 W(\{A\})^*}{\partial A_I^* \partial A_J^*} * \\ \frac{\partial^2 W(\{A\})}{\partial A_I \partial A_J} * & 2\delta_{IJ} p_{\bar{z}} \end{pmatrix} \psi_J(p) \Bigg], \end{aligned} \tag{5.4}$$

where

$$p_z \equiv \frac{1}{2}(p_0 - ip_1), \qquad p_{\bar{z}} \equiv \frac{1}{2}(p_0 + ip_1), \tag{5.5}$$

and "$*$" denotes the convolution

$$(\varphi_1 * \varphi_2)(p) \equiv \frac{1}{L_0 L_1} \sum_q \varphi_1(q)\varphi_2(p-q), \tag{5.6}$$

It is understood that the field products in $\partial W(\{A\})/\partial A_I$ and $\partial W(\{A\})/\partial A_I \partial A_J$ are defined by this convolution. After eliminating F by the equation of motion, the action yields

$$S = S_B + \frac{1}{L_0 L_1} \sum_p \sum_{I,J} (\bar{\psi}\gamma_0)_I(-p) \begin{pmatrix} 2i\delta_{IJ}p_z & \frac{\partial^2 W(\{A\})^*}{\partial A_I^* \partial A_J^*} * \\ \frac{\partial^2 W(\{A\})}{\partial A_I \partial A_J} * & 2i\delta_{IJ}p_{\bar{z}} \end{pmatrix} \psi_J(p), \tag{5.7}$$

where S_B is the bosonic part of the total action

$$S_B = \frac{1}{L_0 L_1} \sum_p \sum_I N_I^*(-p) N_I(p), \tag{5.8}$$

and the new variables $\{N(p)\}$ is defined by

$$N_I(p) \equiv 2ip_z A_I(p) + \frac{\partial W(\{A\})^*}{\partial A_I^*}(p). \tag{5.9}$$

This new variables $N_I(p)$ specify the so-called Nicolai map [69–72]; the change of variables from $\{A\}$ to $\{N\}$ simplifies the weight of the functional integral drastically, as we will see soon.

To define the functional integral of this system, we now introduce the momentum cutoff Λ as

$$|p_\mu| \le \Lambda \qquad \text{for } \mu = 0 \text{ and } 1, \tag{5.10}$$

and the "lattice spacing" a as

$$\Lambda \equiv \frac{\pi}{a}. \tag{5.11}$$

All dimensionful quantities are then measured in units of a. Although an underlying "lattice space" is not always assumed here, we will use the parameter a to take the "continuum limit" $a \to 0$, which removes the UV cutoff, $\Lambda \to \infty$. If L_μ/a is an even integer, the discretized momentum is given by

$$p_\mu = \frac{2\pi}{L_\mu} n_\mu \qquad \text{for } n_\mu = 0, \pm 1, \ldots, \pm\frac{L_\mu}{2a}. \tag{5.12}$$

Then we define the partition function by

$$\mathcal{Z} = \int \prod_{|p_\mu| \le \pi/a} \prod_I \left[dA_I(p) dA_I^*(p) \prod_{\alpha=1}^{2} d\psi_{\alpha I}(p) \prod_{\dot{\alpha}=\dot{1}}^{\dot{2}} d\bar{\psi}_{\dot{\alpha} I}(p) \right] e^{-S}. \tag{5.13}$$

When the integers L_μ/a are odd, the spacetime lattice is imposed by periodic boundary conditions; then, this formulation is nothing but the dimensional reduction of the lattice formulation of the 4D $\mathcal{N}=1$ WZ model [77], which is based on the SLAC derivative [78, 79].

The original classical action in the coordinate space is invariant under SUSY transformations, translations, $U(1)$ transformations. These transformations, δ_ξ (3.21), δ_v (3.57)–(3.62), and δ_γ (3.43), act on field variables linearly and do not mix different momenta. Hence, the restriction on the Fourier modes in Eq. (5.10) is preserved. As the consequence, the above formulation in Eq. (5.13) manifestly preserves these spacetime symmetries [76]. This fact enables us to use the explicit form of the supercurrent given in Eqs. (3.63)–(3.66), the EMT in Eq. (3.67), the $U(1)$ current in Eqs. (3.68) and (3.69) in numerical simulations.

We note that this regularization sacrifices the locality of the theory. Unfortunately, it is well recognized that the SLAC derivative in general plagued by some pathology [112–114]; the locality is not automatically restored in the continuum limit in four dimensions. See Ref. [115] for an analysis of the issue of the exactly preserved SUSY and the locality. For the *massive* 2D $\mathcal{N}=2$ WZ model, on the other hand, the authors of Ref. [76] argue, thanks to the preserved SUSY, that the locality is automatically restored in the continuum limit to all orders of perturbation theory. For the *massless* case, however, because perturbation techniques are hindered by the IR divergences, it is not clear whether the restoration of the locality is automatically accomplished. Strictly speaking, the theoretical basis of the numerical simulation below is not quite obvious. Nevertheless, the numerical results of Ref. [75] and ours below suggest the validity of the formulation. We leave understanding this observed validity as a future problem.

5.1.2 Nicolai map

The above definition of the regularized partition function of the 2D $\mathcal{N}=2$ WZ model allows the Nicolai or Nicolai–Parisi–Sourlas map [69–72], which renders the path-integral weight Gaussian [76].[1] The point is that the Dirac determinant in Eq. (5.7) coincides with the Jacobian of the transformation $(A_I, A_I^*) \to (N_I, N_I^*)$ defined in Eq. (5.9), up to the sign:

$$\det \begin{pmatrix} 2i\delta_{IJ}p_z & \frac{\partial^2 W(\{A\})^*}{\partial A_I^* \partial A_J^*} * \\ \frac{\partial^2 W(\{A\})}{\partial A_I \partial A_J} * & 2i\delta_{IJ}p_{\bar{z}} \end{pmatrix} = \det \frac{\partial(\{N\},\{N^*\})}{\partial(\{A\},\{A^*\})}. \tag{5.14}$$

Hence, integrating over the fermion fields, the partition function is represented as

$$\begin{aligned} \mathcal{Z} &= \int \prod_{|p_\mu|\le \pi/a} \prod_I [dA_I(p) dA_I^*(p)]\ e^{-S_B} \det \frac{\partial(\{N\},\{N^*\})}{\partial(\{A\},\{A^*\})} \\ &= \int \prod_{|p_\mu|\le \pi/a} \prod_I [dN_I(p) dN_I^*(p)]\ e^{-S_B} \sum_k \operatorname{sign} \det \frac{\partial(\{N\},\{N^*\})}{\partial(\{A\},\{A^*\})}\bigg|_{\{A\}=\{A\}_k}. \end{aligned} \tag{5.15}$$

where $\{A\}_k$ ($k = 1, 2, \dots$) is a set of solutions of the equations

$$2ip_z A_I(p) + \frac{\partial W(\{A\})^*}{\partial A_I^*}(p) - N_I(p) = 0, \qquad p_\mu = \frac{2\pi}{L_\mu} n_\nu, \qquad |n_\mu| \le \frac{L_\mu}{2}, \tag{5.16}$$

[1] This is the common feature to the lattice formulation in Refs. [61, 62].

Note that e^{-S_B} (5.8) is Gaussian in terms of the variables (N_I, N_I^*).

From the representation in Eq. (5.15), we can carry out the following simulation algorithm [63] (see also Ref. [116]):

1. Generate complex random numbers $N_I(p)$ for each p_μ and I, whose real and imaginary parts obey the Gaussian distribution.

2. Solve numerically the multi-variable algebraic equations (5.16) with respect to $\{A\}$ and (ideally) find all the solutions $\{A\}_k$ $(k = 1, 2, \dots)$.

3. Calculate the following sums over k:

$$\sum_k \operatorname{sign}\det \frac{\partial(\{N\},\{N^*\})}{\partial(\{A\},\{A^*\})}\bigg|_{\{A\}=\{A\}_k}, \tag{5.17}$$

$$\sum_k \operatorname{sign}\det \frac{\partial(\{N\},\{N^*\})}{\partial(\{A\},\{A^*\})}\,\mathcal{O}(A,A^*)\bigg|_{\{A\}=\{A\}_k}, \tag{5.18}$$

   where $\mathcal{O}$ is an observable of interest. In Appendix A, we present a fast algorithm for the computation of the Jacobian.

4. Repeat steps (1)–(3) and compute the averages over $\{N_I(p)\}$:

$$\Delta \equiv \left\langle \sum_i \operatorname{sign}\det \frac{\partial(\{N\},\{N^*\})}{\partial(\{A\},\{A^*\})}\bigg|_{\{A\}=\{A\}_k} \right\rangle, \tag{5.19}$$

$$\langle\mathcal{O}\rangle = \frac{1}{\Delta}\left\langle \sum_i \operatorname{sign}\det \frac{\partial(\{N\},\{N^*\})}{\partial(\{A\},\{A^*\})}\,\mathcal{O}(A,A^*)\bigg|_{\{A\}=\{A\}_k} \right\rangle. \tag{5.20}$$

Here, Δ is the correctly normalized partition function, that is, the Witten index, $\mathrm{tr}(-1)^{\mathcal{F}}$, discussed in Chap. 3.[2] The Witten index counts the number of vacua; for instance, if $W(\{A\})$ is a polynomial of degree $n+1$, we should have $\Delta = n$; we see $\Delta = n$ for A_n, D_n, and E_n-type theories. We find that, in practical numerical simulations, the statistical error of Δ is much smaller than that of the numerator in Eq. (5.20). Hence, one can estimate the statistical error of the average $\langle\mathcal{O}\rangle$ by a simple error-propagation rule in the ratio.

One can generate Gaussian random numbers easily without any undesired autocorrelation. A remarkable feature is that this algorithm is completely free from any notable autocorrelation and the critical slowing down. Also, although $\operatorname{sign}\det \frac{\partial(\{N\},\{N^*\})}{\partial(\{A\},\{A^*\})} \pm 1$, this signs do not cause any sign problem, at least for $\Delta > 0$. This is because the distribution of $\operatorname{sign}\det \frac{\partial(\{N\},\{N^*\})}{\partial(\{A\},\{A^*\})}$ is well-biased to a positive number to reproduce $\Delta > 0$; we will see this behavior in the numerical simulation below.

[2] If there exists the inverse of the Nicolai map locally, then the Witten index is nothing but the winding number of the Nicolai map, that is, the (almost) number of distinct configurations of A for a fixed N [72]. Also for the WZ model with multiple superfield, if the condition

$$\det \frac{\partial^2 W}{\partial A_I \partial A_J} \neq 0 \tag{5.21}$$

satisfies almost everywhere, the Nicolai map is surjective and the Witten index is well-defined.

Unfortunately, in step (2), for a given N_I, we do not know a priori how many solutions $A_{I,k}$ of Eq. (5.16) exist. Therefore, it is quit difficult to judge whether all the solutions are found or not. The best thing we can do is to increase the possible number of initial trial solutions in the solver algorithm; the stability of the number of solutions under the increase of trial ones provides a consistency check. Other consistency checks can be provided by the observation of Δ and SUSY WT relations. Any physical quantities we compute cannot be free from the systematic error coming from "undiscovered solutions." It is difficult to estimate this systematic error at this time, and the quoted values of the numerical results should be taken with this reservation.

5.2 Simulation setup and classification of configurations

Let us consider the ADE-type WZ model of Eq. (5.7) with the quasi-homogeneous superpotential given in Table 4.1

$$W(\Phi) = \frac{\lambda}{n}\Phi^n \qquad \text{for } A_n \text{ with } n = 2,\, 3, \tag{5.22}$$

which sometimes be written in the abbreviated forms as $W = \Phi^3$ and $W = \Phi^4$, respectively, and

$$W(\{\Phi\}) = \frac{\lambda_1}{n}\Phi_1^n + \frac{\lambda_2}{2}\Phi_1\Phi_2^2 \qquad \text{for } D_n \text{ with } n = 3,\, 4, \tag{5.23}$$

$$W(\{\Phi\}) = \frac{\lambda_1}{3}\Phi_1^3 + \frac{\lambda_2}{3}\Phi_1\Phi_2^3 \qquad \text{for } E_7. \tag{5.24}$$

We set the coupling constants

$$a\lambda = a\lambda_1 = a\lambda_2 = 0.3, \tag{5.25}$$

which is identical to those in Refs. [61,75]. For any forms of the superpotential, for simplicity, the box size

$$L \equiv L_0 = L_1, \tag{5.26}$$

is supposed to be even integers. We generate 640 configurations of $\{N\}$ obeying the Gaussian distribution e^{-S_B}. The size of L is taken as even integers from 8 to 36 for A_2, from 8 to 30 for A_3 [80]; 8, 16, 24, 32, 40, and 44 for D_3; 8, 16, 24, 32, 36, 40 and 42 for D_4; 8, 16, and 24 for E_7 [81].

Given a configuration of N_I, we numerically solve the algebraic equation (5.16) with respect to A_I by employing the Newton–Raphson (NR) method.[3] We then generate the initial value of the real and imaginary parts of $A_I(p)$ by the Gaussian random number with unit variance as in Ref. [75]. We set the convergence threshold as

$$\sqrt{\frac{\sum_p \left|2ip_z A_I(p) + (\partial W(\{A\})^*/\partial A_I^*)(p) - N_I(p)\right|^2}{\sum_q |N_I(q)|^2}} < 10^{-14}, \tag{5.27}$$

[3]For the generation of the configurations of N_I and A_I and $\operatorname{sign}\det\frac{\partial(N,N^*)}{\partial(A,A^*)}$, we used a `C++` library `Eigen` [117]. In particular, we extensively used the class `PartialPivLU`.

for all obtained configurations, while the authors in Ref. [75] set this upper bound 10^{-13}. By this norm of the residue, we estimate the quality of the obtained configuration A_I.

For a fixed configuration of N_I, we increase the number of initial trial configurations of A_I until we obtain *convergent* 100 solutions for A_I allowing repetition of identical solutions. A initial configuration, which is generated randomly, does not necessarily converge to a solution along iterations in the NR method, so sometimes it diverges and does not provide any solution. In Ref. [75], the number of *initial trial configurations* is kept fixed to 100 but this choice sometimes misses some solutions, especially for A_3, D_n, and E_n. This setup is another improvement compared to the setup of Ref. [75]. Two solutions $A_{I,1}$ and $A_{I,2}$ are regarded as identical if the norm of the difference of those satisfies

$$\sqrt{\frac{\sum_p |A_{I,1}(p) - A_{I,2}(p)|^2}{\sum_q |A_{I,1}(q)|^2}} < \begin{cases} 10^{-13} & \text{for } A_n, \\ 10^{-11} & \text{for } D_n,\ E_n, \end{cases} \tag{5.28}$$

while the upper bound is equal to 10^{-11} in Ref. [75].

We tabulate the classification of configurations we obtained in Tables 5.1–5.3 for A_2 ($W = \Phi^3$); in Tables 5.4–5.6 for A_3 ($W = \Phi^4$); in Tables 5.7 and 5.8 for D_3; in Tables 5.9 and 5.10 for D_4; in Table 5.11 for E_7. The symbol $(n_+, n_-)_{n_+-n_-}$ implies the following: For a configuration $\{N(p)\}$, we find $(n_+ + n_-)$ solutions, $\{A(p)\}_k$ ($k = 1, \ldots, n_+ + n_-$); the n_+ solutions take $\operatorname{sign}\det \frac{\partial(N,N^*)_i}{\partial(A,A^*)_j} = +1$ and the n_- solutions take -1. The subscript $n_+ - n_-$ stands for the contribution of that configuration of N_I to Δ in Eq. (5.19). In these tables, the number of obtained configurations for each setup is shown. Table 5.3, for example, shows that for $L = 36$ we had 13 configurations of N with $(3, 1)_2$ out of 640 configurations.

In the tables, to indicate the quality of the obtained configurations, we list the numerical results of Δ defined in Eq. (5.19), which should reproduce the Witten index: $\Delta = n$ for A_2, D_n, E_n. For A_2 and D_3, our simulation gives $\Delta = 2$ and 3 exactly for all box sizes, respectively. For the other models, Δ deviates from the expected Witten index but only slightly; from this, one might roughly estimate that the systematic error from the solution search, that is, the possibility that some solutions are missed, is less than 1% even for E_7.

For the same purpose, we also list the numerical results of the one-point function,

$$\delta \equiv \frac{\langle S_B \rangle}{(L_0/a + 1)(L_1/a + 1)} - 1, \tag{5.29}$$

where S_B is the bosonic part of the action defined in Eq. (5.8). The one-point function δ should identically vanish if the SUSY is preserved [64, 75].[4]

We also show the computation time in core · hour on an Intel Xeon E5 2.0 GHz for A_2, A_3, D_3 and D_4 with $L/a = 8, \ldots, 32, 40$; an Intel Xeon Gold 3.0 GHz for D_4 with $L/a = 36$, 42 and E_7.

The hot spot in our computation is the LU decomposition carried out in the NR iteration, whose computational time scales as $\propto N^3$ for a matrix of size N. Thus, we expect that the computational time scales as $\propto (L/a)^6$ as a function of the lattice size L/a. The actual computational time for A_2 and A_3 is depicted in Fig. 5.1; this is fairly well explained by this theoretical expectation.

[4]For the calculation of δ and succeeding numerical analyses, we used the programming language `Julia` [118–120].

Table 5.1: Classification of configurations for A_2 ($W = \Phi^3$).

L/a	8	10	12	14	16
$(2,0)_2$	640	640	640	639	639
$(3,1)_2$	0	0	0	1	1
Δ	2	2	2	2	2
δ	0.0070(44)	−0.0046(36)	0.0019(30)	−0.0020(25)	−0.0003(23)
core · hour [h]	0.77	2.23	5.5	12.37	25.62

Table 5.2: Classification of configurations for A_2 ($W = \Phi^3$) (continued).

L/a	18	20	22	24	26
$(2,0)_2$	634	636	634	637	635
$(3,1)_2$	6	4	6	3	5
Δ	2	2	2	2	2
δ	−0.0000(20)	−0.0015(19)	−0.0006(17)	0.0001(16)	−0.0026(15)
core · hour [h]	48.97	87.03	143.83	236.62	405.28

Table 5.3: Classification of configurations for A_2 ($W = \Phi^3$) (continued).

L/a	28	30	32	34	36
$(2,0)_2$	634	626	633	628	627
$(3,1)_2$	6	14	7	12	13
Δ	2	2	2	2	2
δ	−0.0002(13)	0.0000(13)	0.0014(12)	0.0008(11)	0.0007(11)
core · hour [h]	649.78	963.93	1382.07	1936.52	2699.42

Table 5.4: Classification of configurations for A_3 ($W = \Phi^4$).

L/a	8	10	12	14
$(3,0)_3$	638	638	638	638
$(4,1)_3$	2	2	2	2
$(5,2)_3$	0	0	0	0
$(4,0)_4$	0	0	0	0
$(5,1)_4$	0	0	0	0
$(2,0)_2$	0	0	0	0
Δ	3	3	3	3
δ	0.0003(45)	0.0035(36)	0.0001(30)	−0.0015(26)
core · hour [h]	3.73	12.8	36.1	89.55

Table 5.5: Classification of configurations for A_3 ($W = \Phi^4$) (continued).

L/a	16	18	20	22
$(3,0)_3$	634	635	632	627
$(4,1)_3$	6	5	6	13
$(5,2)_3$	0	0	2	0
$(4,0)_4$	0	0	0	0
$(5,1)_4$	0	0	0	0
$(2,0)_2$	0	0	0	0
Δ	3	3	3	3
δ	0.0006(25)	0.0014(20)	0.0024(20)	0.0023(18)
core $\cdot$ hour [h]	202.65	425.23	872.03	1661.22

Table 5.6: Classification of configurations for A_3 ($W = \Phi^4$) (continued).

L/a	24	26	28	30
$(3,0)_3$	625	616	614	615
$(4,1)_3$	15	23	20	22
$(5,2)_3$	0	0	2	0
$(4,0)_4$	0	1	3	2
$(5,1)_4$	0	0	1	0
$(2,0)_2$	0	0	0	1
Δ	3	3.002(2)	3.006(3)	3.002(3)
δ	0.0000(16)	0.0004(16)	0.0023(17)	$-0.0010(15)$
core $\cdot$ hour [h]	2917.48	5004.37	8273.47	12905.13

Table 5.7: Classification of configurations for D_3.

L/a	8	16	24
$(3,0)_3$	640	640	638
$(4,1)_3$	0	0	2
$(5,2)_3$	0	0	0
Δ	3	3	3
δ	0.0016(30)	0.0015(16)	$-0.0007(11)$
core$\cdot$hour [h]	1.60	63.78	649.73

Table 5.8: Classification of configurations for D_3 (continued).

L/a	32	40	44
$(3,0)_3$	639	633	632
$(4,1)_3$	1	7	7
$(5,2)_3$	0	0	1
Δ	3	3	3
δ	0.00019(85)	−0.00078(69)	−0.00092(63)
core·hour [h]	3440.33	13426.08	25623.00

Table 5.9: Classification of configurations for D_4.

L/a	8	16	24	32
$(4,0)_4$	640	638	629	626
$(5,1)_4$	0	2	9	13
$(6,2)_4$	0	0	2	1
$(7,3)_4$	0	0	0	0
$(4,1)_3$	0	0	0	0
$(5,0)_5$	0	0	0	0
$(10,6)_4$	0	0	0	0
Δ	4	4	4	4
δ	−0.0028(31)	0.0018(17)	−0.0020(11)	−0.00095(84)
core·hour [h]	1.73	72.28	847.83	5220.60

Table 5.10: Classification of configurations for D_4 (continued).

L/a	36	40	42
$(4,0)_4$	604	606	603
$(5,1)_4$	23	24	35
$(6,2)_4$	12	8	9
$(7,3)_4$	1	0	0
$(4,1)_3$	0	1	0
$(5,0)_5$	0	1	0
$(10,6)_4$	0	0	1
Δ	4	4.000(2)	4
δ	−0.00008(73)	−0.00025(87)	0.00019(64)
core·hour [h]	4328.58	22264.12	12272.93

Table 5.11: Classification of configurations for E_7.

L/a	8	16	24
$(7,0)_7$	639	628	582
$(8,1)_7$	1	10	20
$(6,0)_6$	0	2	27
$(7,1)_6$	0	0	5
$(8,0)_8$	0	0	3
$(8,2)_6$	0	0	2
$(9,2)_7$	0	0	1
Δ	7	6.997(2)	6.952(9)
δ	−0.0013(32)	−0.0004(16)	0.0009(17)
core·hour [h]	1.30	60.28	750.92

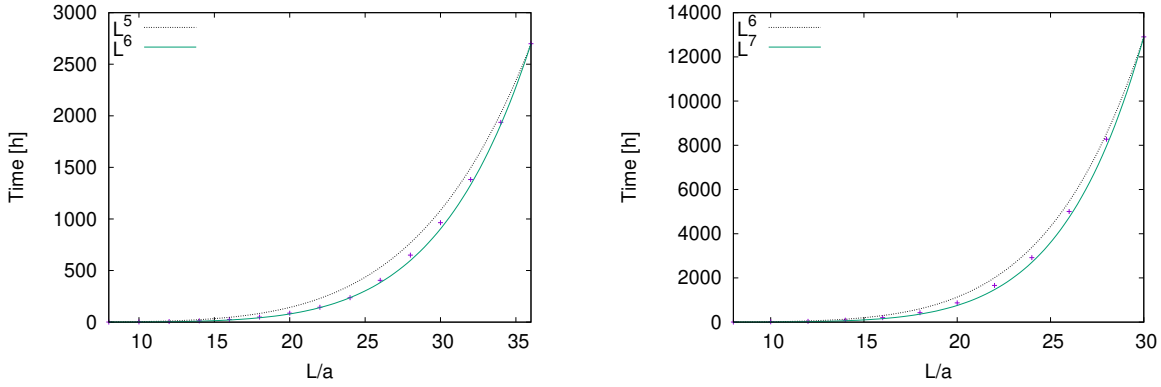

(a) A_2. (b) A_3.

Figure 5.1: Computational time as a function of the lattice size.

5.3 SUSY Ward–Takahashi relation

As mentioned above, our formulation exactly preserves SUSY even with a finite cutoff. Thus, barring the statistical error and the systematic error associated with the solution search, SUSY WT relations should *hold exactly* for any parameter. The observation of these relations thus provides a useful check of our simulation and gives a rough idea of the magnitude of the statistical and systematic errors.

The simplest SUSY WT relation is $\delta = 0$ for δ in Eq. (5.29), and in Tables 5.1–5.11 we have observed that this relation is reproduced quite well in our simulation. In this section, we present results on two further SUSY WT relations on two-point correlation functions which follow from the identities [75][5]

$$\left\langle Q_1(A(p)\bar{\psi}_{\dot{1}}(-p))\right\rangle = 0, \tag{5.30}$$

$$\langle Q_2(F^*(p)\psi_1(-p))\rangle = 0, \tag{5.31}$$

where the explicit form of the SUSY transformation is given in Chapter 3.

First, Eq. (5.30) yields

$$2ip_{\bar{z}} \left\langle A(p)A^*(-p)\right\rangle = -\left\langle \psi_1(p)\bar{\psi}_{\dot{1}}(-p)\right\rangle, \tag{5.32}$$

whose real and imaginary parts are

$$p_1 \left\langle A(p)A^*(-p)\right\rangle = \mathrm{Re}\left\langle \psi_1(p)\bar{\psi}_{\dot{1}}(-p)\right\rangle, \tag{5.33}$$

$$p_0 \left\langle A(p)A^*(-p)\right\rangle = -\,\mathrm{Im}\left\langle \psi_1(p)\bar{\psi}_{\dot{1}}(-p)\right\rangle. \tag{5.34}$$

In Figs. 5.2–5.5 we plot correlation functions in these relations as functions of $-\pi \le ap_0 \le \pi$. The box size is the maximal one, that is, $L/a = 36$ for A_2 and $L/a = 30$ for A_3. The spatial momentum p_1 is fixed to be $p_1 = \pi/a$ (the largest positive value) or $p_1 = 2\pi/L$ (the smallest positive value). In the figures, the left panel corresponds to the real part relation of Eq. (5.33) and the right one to the imaginary part of Eq. (5.34). In the plots, "bosonic" implies the correlation function on the left-hand side of the WT relation and "fermionic" implies the correlation function on the right-hand side. Errors are statistical only.

Next, Eq. (5.31) gives the relation

$$\left\langle F(p)F^*(-p)\right\rangle = -2ip_z \left\langle \psi_1(p)\bar{\psi}_{\dot{1}}(-p)\right\rangle, \tag{5.35}$$

and the real and imaginary parts are given by

$$\left\langle F(p)F^*(-p)\right\rangle = -p_1\,\mathrm{Re}\left\langle \psi_1(p)\bar{\psi}_{\dot{1}}(-p)\right\rangle + p_0\,\mathrm{Im}\left\langle \psi_1(p)\bar{\psi}_{\dot{1}}(-p)\right\rangle, \tag{5.36}$$

$$0 = -p_0\,\mathrm{Re}\left\langle \psi_1(p)\bar{\psi}_{\dot{1}}(-p)\right\rangle - p_1\,\mathrm{Im}\left\langle \psi_1(p)\bar{\psi}_{\dot{1}}(-p)\right\rangle. \tag{5.37}$$

In Figs. 5.6–5.9 we plot correlation functions in the real part relation of Eq. (5.36); the other conditions and conventions are the same as above. For the computation of the left-hand side of Eq. (5.36) we have used the representation[6]

$$\begin{aligned}\left\langle F(p)F^*(-p)\right\rangle &= \left\langle W'(A)^*(p)W'(A)(-p)\right\rangle - L_0L_1 \\ &= \left\langle |N(p) - (ip_0 + p_1)A(p)|^2\right\rangle - L_0L_1.\end{aligned} \tag{5.41}$$

[5] In the present system, SUSY cannot be spontaneously broken because of the non-zero Witten index.

[6] A way to derive this relation is to introduce the source term for the auxiliary field:

$$S_J = \frac{1}{L_0L_1}\sum_p \left[F^*(-p)J(p) + J^*(-p)F(p)\right]. \tag{5.38}$$

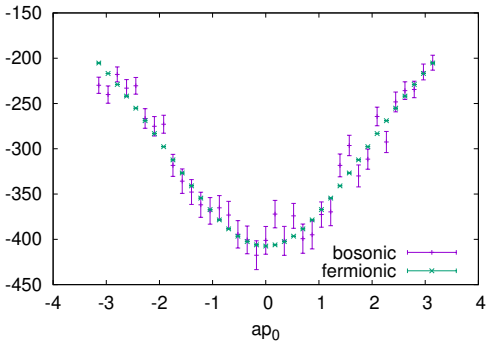

(a) Real part (5.33).

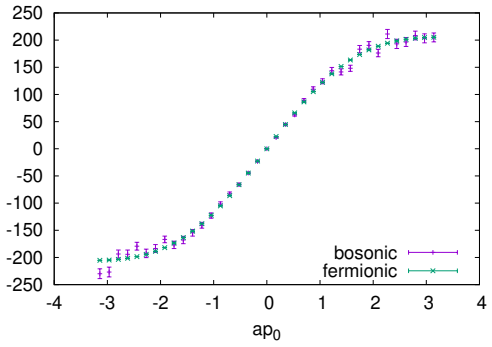

(b) Imaginary part (5.34).

Figure 5.2: SUSY WT relation of Eq. (5.32) for A_2, $L/a = 36$, and $ap_1 = \pi$.

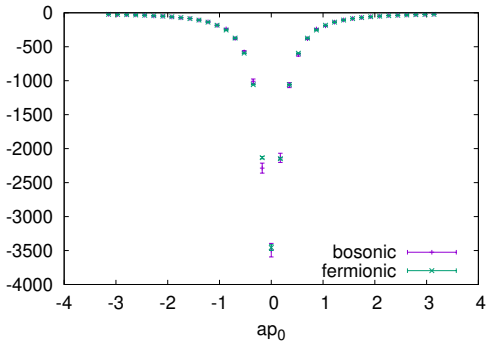

(a) Real part (5.33).

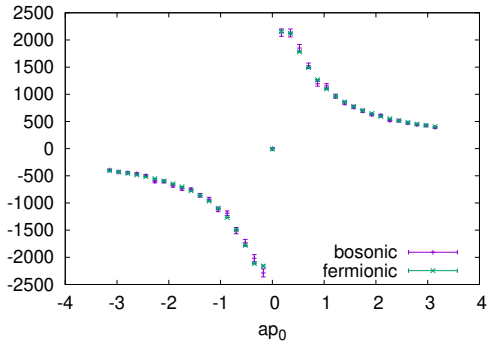

(b) Imaginary part (5.34).

Figure 5.3: SUSY WT relation of Eq. (5.32) for A_2, $L/a = 36$, and $ap_1 = \pi/18$.

If the WT relations hold exactly, the "bosonic" points and the "fermionic" points in the plots should coincide with each other. Overall, we observe good agreements within 1σ, as

Then, after a (formal) Gaussian integration over the auxiliary field, this term changes to

$$S_J \to \frac{1}{L_0 L_1} \sum_p \left[-W'(A)(-p)J(p) - J^*(-p)W'(A)^*(p) + J^*(-p)J(p) \right]. \tag{5.39}$$

Therefore,

$$\begin{aligned} &\langle F^*(-p)F(p) \rangle \\ &= (L_0 L_1)^2 \frac{\delta}{\delta J(p)} \frac{\delta}{\delta J^*(-p)} \\ &\quad \times \left\langle \exp\left\{ \frac{1}{L_0 L_1} \sum_q \left[W'(A)(-q)J^*(q) + J(-q)W'(A)^*(q) - J(-q)J^*(q) \right] \right\} \right\rangle \Bigg|_{J=0, J^*=0} \\ &= \langle W'(A)^*(p)W'(A)(-p) \rangle - L_0 L_1. \end{aligned} \tag{5.40}$$

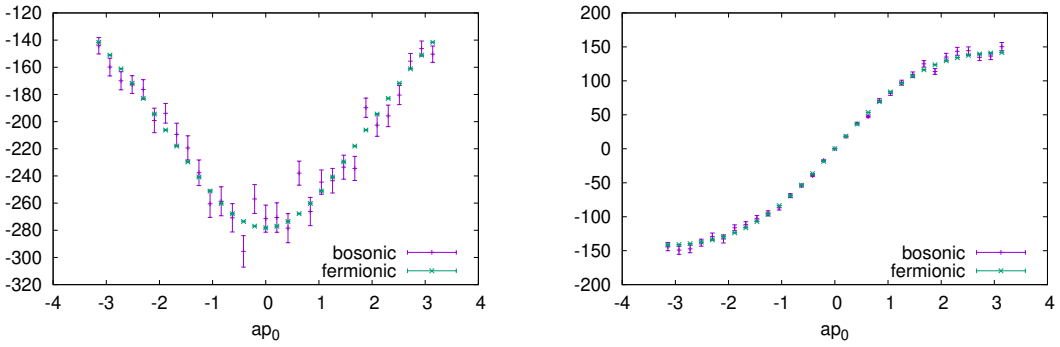

(a) Real part (5.33). (b) Imaginary part (5.34).

Figure 5.4: SUSY WT relation of Eq. (5.32) for A_3, $L/a = 30$, and $ap_1 = \pi$.

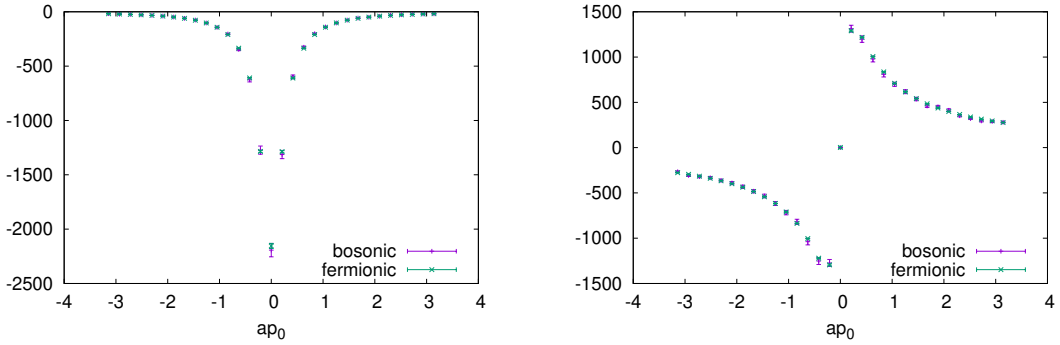

(a) Real part (5.33). (b) Imaginary part (5.34).

Figure 5.5: SUSY WT relation of Eq. (5.32) for A_3, $L/a = 30$, and $ap_1 = \pi/15$.

expected. However, there still exist some deviations of order 2σ, especially in the real-part WT relations at the largest spatial momentum $ap_1 = \pi$. To argue that these deviations are a result of statistical fluctuations and not due to the omission of some solutions in our solution search, we carried out the measurements corresponding to the left panels of Figs. 5.2 and 5.6, respectively but for $L/a = 8$, by changing the number of configurations by four times, that is, 640 and 2560. The results are shown in Figs. 5.10 and 5.11. We see that although for 640 configurations there exist some discrepancies between the "bosonic" and "fermionic" ones of order 2σ, when we increase the number of configurations by four times, the statistical error is halved and the discrepancies of the central values actually decrease. From this behavior, we think that the observed discrepancies in the WT relations are due to statistical fluctuations and they eventually disappear as the number of configurations is increased sufficiently.

Finally, we mention a general tendency of the statistical error in the correlation functions we found through the numerical simulation. Particularly in the high momentum region, the correlation functions of the scalar field suffer from larger statistical fluctuations than those of the fermion field (as seen in the left panel of Fig. 5.2). Actually, because of this problem we

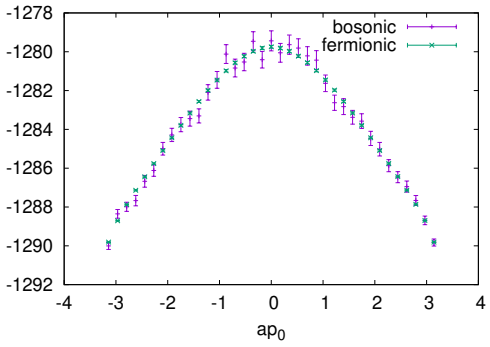

Figure 5.6: SUSY WT relation of Eq. (5.36) for A_2, $L/a = 36$, and $ap_1 = \pi$.

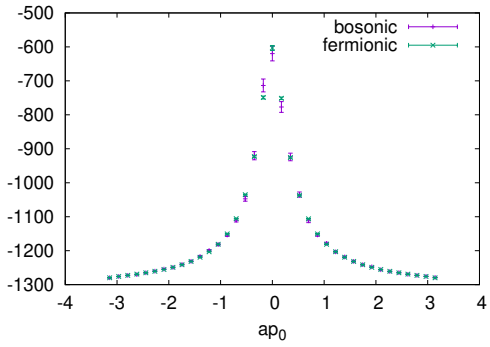

Figure 5.7: SUSY WT relation of Eq. (5.36) for A_2, $L/a = 36$, and $ap_1 = \pi/18$.

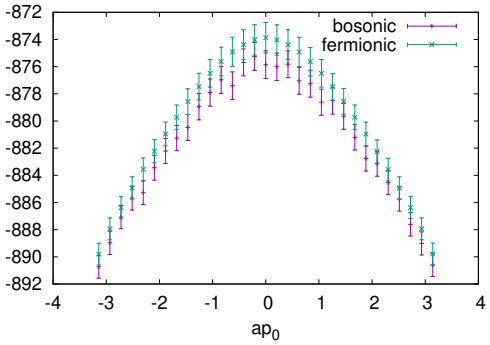

Figure 5.8: SUSY WT relation of Eq. (5.36) for A_3, $L/a = 30$, and $ap_1 = \pi$.

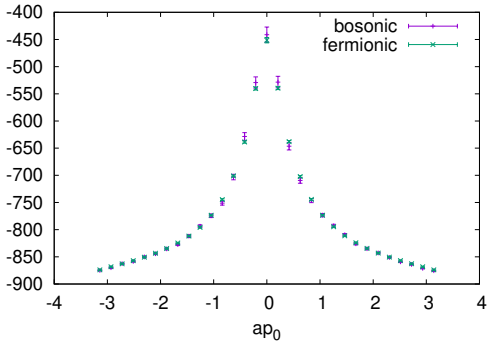

Figure 5.9: SUSY WT relation of Eq. (5.36) for A_3, $L/a = 30$, and $ap_1 = \pi/15$.

could not directly examine four-point SUSY WT relations including a four-point correlation function of A and A^*. On the other hand, if we assume the validity of SUSY WT relations, we can use them to rewrite some noisy correlation functions into less noisy ones. This technique will be employed frequently in the following sections.

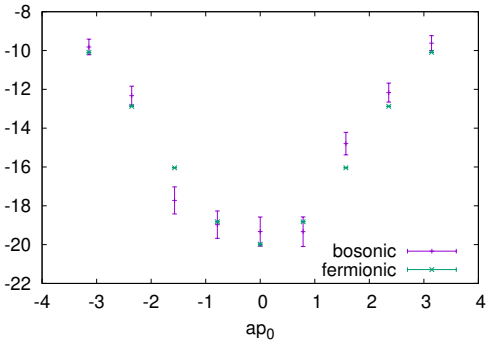

(a) Number of configurations: 640.

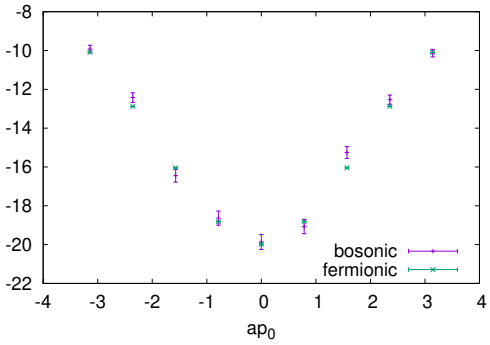

(b) Number of configurations: 2560.

Figure 5.10: SUSY WT relation of Eq. (5.33) for A_2, $L/a = 8$ and $ap_1 = \pi$.

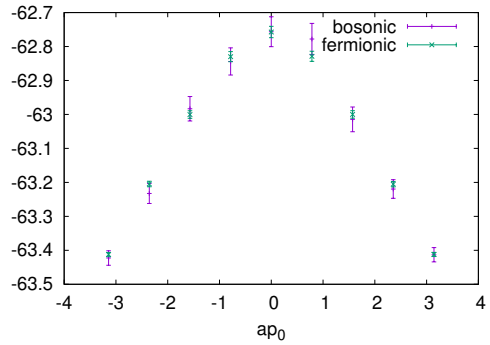

(a) Number of configurations: 640.

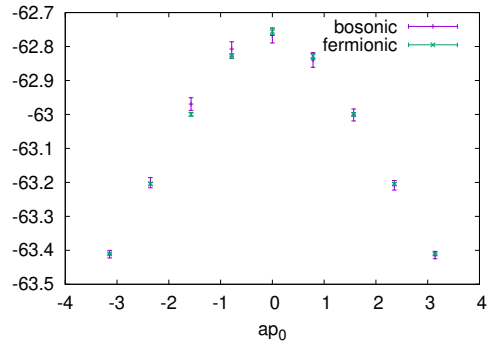

(b) Number of configurations: 2560.

Figure 5.11: SUSY WT relation of Eq. (5.36) for A_2, $L/a = 8$ and $ap_1 = \pi$.

Chapter 6

Numerical simulation of correlation functions

6.1 Scaling dimension

In this section, we measure the scaling dimension of the scalar field in the IR limit from the two-point correlation function [80]. If the expected LG correspondence for the WZ model with $W = \Phi^n$ holds, the chiral superfield is identified with the chiral primary field in the A_{n-1} minimal model with the conformal dimension

$$h = \bar{h} = \frac{1}{2n}. \tag{6.1}$$

Thus the two-point function of the scalar field is expected to behave as

$$\langle A(x)A^*(0)\rangle \propto \frac{1}{z^{2h}\bar{z}^{2\bar{h}}}, \tag{6.2}$$

for large $|z|$. To obtain the value of the scaling dimension $h + \bar{h}$, in Ref. [75], the authors computed the susceptibility

$$\chi_\phi \equiv \frac{1}{a^2}\int_{L_0 L_1} d^2x \ \langle A(x)A^*(0)\rangle \,. \tag{6.3}$$

To avoid the UV ambiguity at the contact point $x \sim 0$, a small region around $x = 0$ was excised [61]. Then, for the scaling dimension, they obtained

$$1 - h - \bar{h} = 0.616(25)(13). \tag{6.4}$$

The expected value is $1 - h - \bar{h} = 2/3 = 0.666\ldots$ for the A_2 minimal model. It turns out, however, that the susceptibility in Eq. (6.3) is quite sensitive to the size of the excised region with the formulation of Ref. [75]; Section 6.3 addresses this issue in the context of the continuum limit.

Here, we instead directly study the correlation function in the momentum space $\langle A(p)A^*(-p)\rangle$. The Fourier transformation of Eq. (6.2) reads (assuming $h = \bar{h}$)

$$\langle A(p)A^*(-p)\rangle \propto \frac{1}{(p^2)^{1-h-\bar{h}}}, \tag{6.5}$$

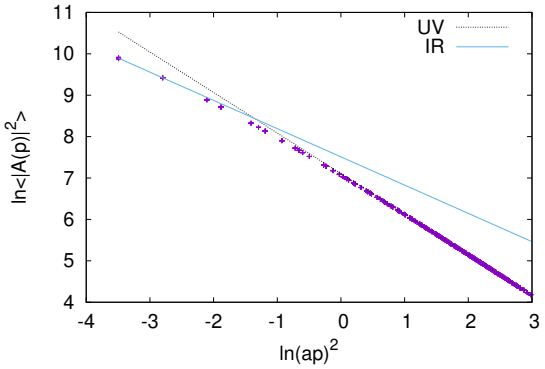

(a) A_2, $L/a = 36$.

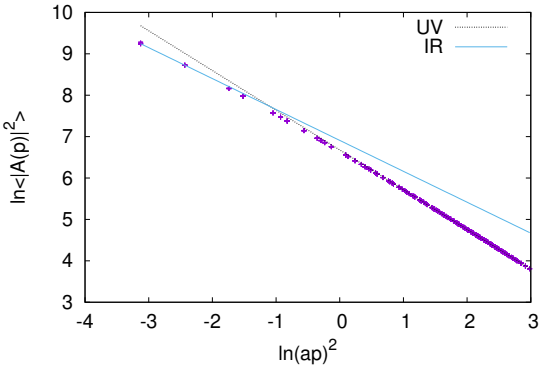

(b) A_3, $L/a = 30$.

Figure 6.1: $\ln\langle A(p)A^*(-p)\rangle$ as a function of $\ln(ap)^2$ for A_2 and A_3. The broken and solid lines are linear fits in the UV and IR regions, respectively.

Table 6.1: Scaling dimensions obtained for A_2 and A_3 from the linear fit in the IR region $\frac{2\pi}{L} \leq |p| < \frac{4\pi}{L}$.

Algebra	L/a	χ^2/d.o.f.	$1-h-\bar{h}$	Expected value
A_2	36	0.506	0.682(10)(7)	0.666...
A_3	30	0.358	0.747(11)(12)	0.75

for $|p|$ small.

Also since the SUSY WT relation of Eq. (5.32) shows that

$$\left\langle \psi_1(p)\bar{\psi}_{\dot{1}}(-p)\right\rangle = -2ip_{\bar{z}}\left\langle A(p)A^*(-p)\right\rangle \tag{6.6}$$

instead of the two-point function of the scalar field, we may use the two-point function of the fermion field, which is less noisy, as already mentioned.

Figure 6.1 shows $\ln\langle A(p)A^*(-p)\rangle$ as a function of $\ln(ap)^2$ in the case of the maximal box size, that is, $L/a = 36$ for A_2 and $L/a = 30$ for A_3, respectively. We also show the fitting lines in the UV region $\frac{\pi}{\sqrt{2}} \leq a|p| < \pi$ and in the IR region $\frac{2\pi}{L} \leq |p| < \frac{4\pi}{L}$. Table 6.1 summarizes the scaling dimension obtained from the linear fit in the IR region, which is one of our main results in this section. Recall, however, that those numbers may contain the systematic error associated with the solutions undiscovered by the NR method.

It may be of some interest to see how the values are changed if we do not include a few percent of "strange solutions" in Tables 5.1–5.6, such as $(3,1)_2$ in Table 5.1. Thus, we have computed the scaling dimension $1-h-\bar{h}$ by using only the $(2,0)_2$-type solutions for A_2 ($L/a = 36$) and the $(3,0)_3$-type solutions for A_3 ($L/a = 30$). The result is:

$$1-h-\bar{h} = 0.6716(82) \qquad \text{for } A_2, \tag{6.7}$$

$$1-h-\bar{h} = 0.7364(83) \qquad \text{for } A_3. \tag{6.8}$$

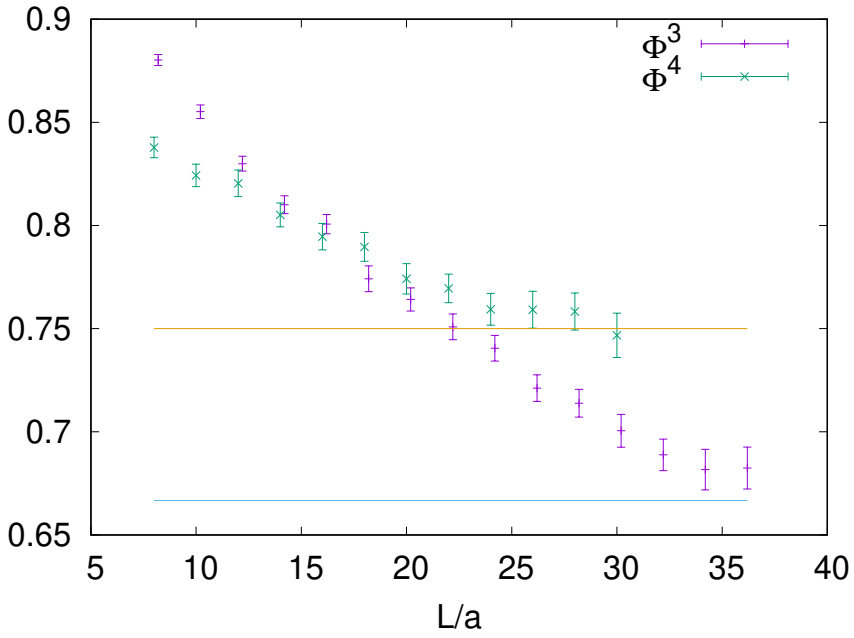

Figure 6.2: Scaling dimensions obtained for A_2 and A_3 with various box sizes.

We also plotted in Fig. 6.2 the scaling dimension obtained by the above method but with different box sizes L/a. Two horizontal lines show the expected values of $1-h-\bar{h}$ from the LG correspondence: $1-h-\bar{h} = 0.666\ldots$ for A_2 and $1-h-\bar{h} = 0.75$ for A_3. We clearly see the tendency that the measured scaling dimension approaches the expected value as L/a increases. The approach appears not quite smooth, however, so we do not try any fitting of this plot to extract the $L \to \infty$ value; we suspect that this non-smoothness is due to statistical fluctuations as we observed for the SUSY WT relation in the previous section.

From the $1-h-\bar{h}$ case presented in Fig. 6.2, we estimated the systematic error associated with the finite-volume effect. We estimate it by the maximum deviation of the central values at the three largest volumes; the values obtained in this way are presented in the second parentheses of $1-h-\bar{h}$ in Table 6.1.

It is also interesting to see the "effective scaling dimension" that is obtained from the fitting in some restricted intermediate region of the momentum norm $|p|$. This is shown in Fig. 6.3. In both panels, the "effective scaling dimension" smoothly changes from that in the IR region (which is summarized in Table 6.1) and approaches $1-h-\bar{h} \to 1$ in the UV limit. This behavior is consistent with the expectation that the 2D $\mathcal{N}=2$ WZ models become the free $\mathcal{N}=2$ SCFT in the UV limit, in which the chiral multiplet should have the scaling dimension $1-h-\bar{h}=1$.

6.2 Central charge

In this section we consider the measurement of the central charge c, an important quantity that characterizes CFT. This appears, in the first place, in the operator product expansion

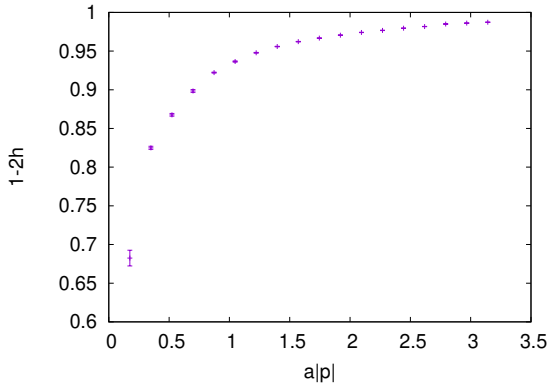

(a) A_2, $L/a = 36$.

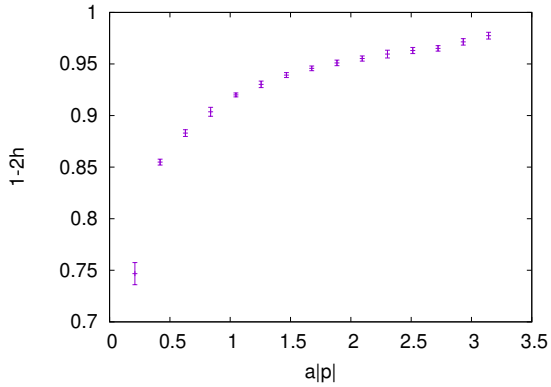

(b) A_3 $L/a = 30$.

Figure 6.3: Scaling dimensions obtained for A_2 and A_3 from the linear fitting in various momentum regions from IR to UV, $\frac{2\pi}{L}n \leq |p| < \frac{2\pi}{L}(n+1)$, for $n \in \mathbb{Z}^+$.

(OPE) of the energy–momentum tensor (EMT) in Eqs. (2.33) and (3.95),[1]

$$T(z)T(0) \sim \frac{c}{2z^4} + \frac{2}{z^2}T(0) + \frac{1}{z}\partial T(0), \tag{6.9}$$

where "$\sim$" implies "$=$" up to non-singular terms. The central charge of the A_n minimal model is

$$c = \frac{3(n-2)}{n} = 1, 1.5, 1.8, \ldots, \tag{6.10}$$

for $n = 3, 4, 5, \ldots$.

From Eq. (6.9), assuming rotational invariance,

$$\langle T(z)T(0)\rangle = \frac{c}{2z^4}. \tag{6.11}$$

Similarly, in $\mathcal{N} = 2$ SCFT, the two-point functions of the supercurrent $S^{\pm}$ (3.99) and the $U(1)$ current J (3.101) are given by

$$\langle S^+(z)S^-(0)\rangle = \frac{2c}{3z^3}, \tag{6.12}$$

$$\langle J(z)J(0)\rangle = \frac{c}{3z^2}. \tag{6.13}$$

Thus, the central charge may also be obtained by computing these two-point functions.

To find the appropriate expression for the supercurrent, the EMT , and the $U(1)$ current such that they form the superconformal multiplet in $\mathcal{N} = 2$ SCFT is itself an intriguing problem, because in our system the $\mathcal{N} = 2$ superconformal symmetry is expected to emerge only in the IR limit. As explained in Chapter 3, we adopt the expressions of the former two which become (gamma-) traceless for the free massless WZ model, $W = 0$. It appears that those expressions work as expected (see also Ref. [75]).

[1] In this chapter we follow the convention of Refs. [53,85]; this convention is different from that of Ref. [75].

As in the previous section, we numerically compute the correlation function in the momentum space. We consider the two-point functions of the supercurrent, the EMT, and the $U(1)$ current. As we explained in Chapter 3, these Noether currents are related to each other by SUSY, which is an exact symmetry of our formulation. Using this fact, the computation of the whole correlation function can be reduced to that for the supercurrent correlator.

6.2.1 Central charge in A-type theories

Central charge from the supercurrent correlator

We first focus on the A_2 and A_3-type WZ model, and measure the central charge from the supercurrent, the EMT, the $U(1)$ current in turn [80]. The argument in Chapter 3 gives the supercurrent in the momentum space,

$$S^+(p) = S_z^+(p) = \frac{4\pi}{L_0 L_1} \sum_q i(p-q)_z A(p-q)\bar{\psi}_{\dot{2}}(q), \tag{6.14}$$

$$S^-(p) = S_z^-(p) = -\frac{4\pi}{L_0 L_1} \sum_q i(p-q)_z A^*(p-q)\psi_2(q). \tag{6.15}$$

We thus compute the two-point function $\langle S^+(p)S^-(-p)\rangle$. The Fourier transformation of Eq. (6.12) is, on the other hand,

$$\begin{aligned}
\left\langle S^+(p)S^-(-p)\right\rangle &= L_0 L_1 \int_{L_0 L_1} d^2x\, e^{-ipx} \left\langle S^+(x)S^-(0)\right\rangle \\
&= L_0 L_1 \int_{L_0 L_1} d^2x\, e^{-ipx} \frac{2c\bar{z}^3}{3(x^2+\delta^2)^3} \\
&= L_0 L_1 \frac{-i\pi c}{6} \frac{\partial^3}{\partial p_{\bar{z}}^3} \left(\frac{|p|}{\delta}\right)^2 K_2(|p|\delta),
\end{aligned} \tag{6.16}$$

where we have introduced a regulator δ to tame the singularity at $x = 0$; K_2 is the modified Bessel function of the second kind. Since we are interested in the IR limit, taking the limit $|p|\delta \to 0$, we have

$$\left\langle S^+(p)S^-(-p)\right\rangle \to L_0 L_1 \frac{i\pi c}{3} \frac{p_z^2}{p_{\bar{z}}}. \tag{6.17}$$

We fit the measured two-point function $\langle S^+(p)S^-(-p)\rangle$ in the IR region by this function.

We plot the two-point function $\langle S^+(p)S^-(-p)\rangle$ in Figs. 6.4 and 6.5 for the maximal box size, that is, $L/a = 36$ for A_2 and $L/a = 30$ for A_3. In each figure, the left panel is the real part of the correlation function and the right one is the imaginary part. The spatial momentum p_1 is fixed to the positive minimal value, $p_1 = 2\pi/L$. In these figures we also show the function on the right-hand side of Eq. (6.17) with the central charge c obtained from the fit in the IR region $\frac{2\pi}{L} \le |p| < \frac{4\pi}{L}$; the central charges obtained in this way are tabulated in Table 6.2.

Compared to the result of Ref. [75] for A_2,

$$c = 1.09(14)(31), \tag{6.18}$$

the central charge we obtained is somewhat closer to the expected value with the smaller statistical error.

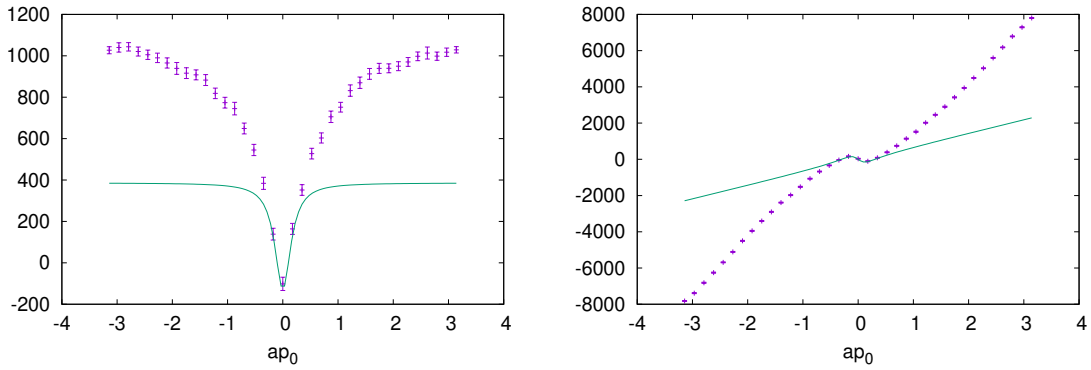

(a) Real part (b) Imaginary part

Figure 6.4: $\langle S^+(p)S^-(-p)\rangle$ for A_2, $L/a = 36$, and $ap_1 = \pi/18$. The fitting curves from Eq. (6.17) are also depicted.

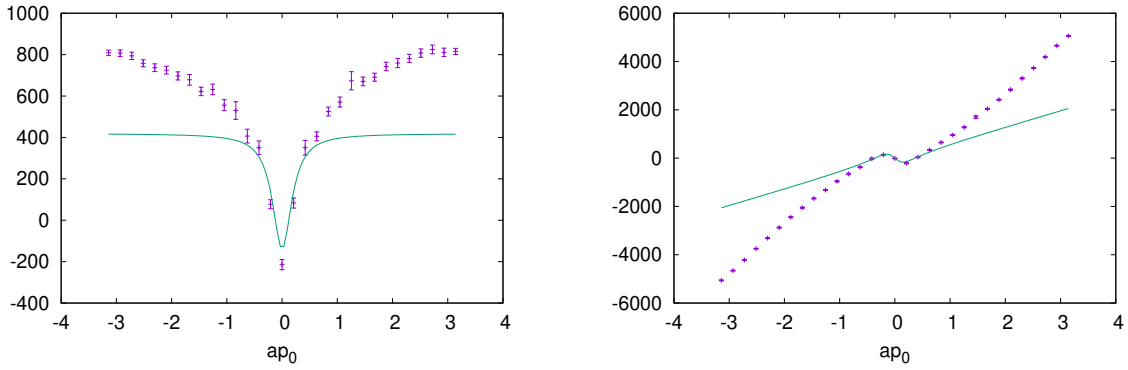

(a) Real part (b) Imaginary part

Figure 6.5: $\langle S^+(p)S^-(-p)\rangle$ for A_3, $L/a = 30$, and $ap_1 = \pi/15$. The fitting curves from Eq. (6.17) are also depicted.

In Fig. 6.6 we have plotted how the fitted central charge changes as a function of the box size L/a. From the central charge c presented in Fig. 6.6, we estimated the systematic error associated with the finite-volume effect. We estimate it by the maximum deviation of central values at the largest three volumes; the values obtained in this way are presented in the second parentheses for c in Table 6.2.

As for Fig. 6.3 in the previous section, it is interesting to see how the central charge obtained by the fit changes as a function of the fitted momentum region [75]. The result is shown in Fig. 6.7. This "effective central charge" depending on the momentum region is analogous to the supersymmetric version of the Zamolodchikov C-function given in Eq. (4.27). As expected, the "effective central charge" changes from the IR value to $c = 3$ in the UV limit in which the system is expected to become a free $\mathcal{N} = 2$ SCFT.

Table 6.2: The central charges for A_2 and A_3 obtained from the fit of the supercurrent correlator. The fitting momentum region is $\frac{2\pi}{L} \leq |p| < \frac{4\pi}{L}$.

Algebra	L/a	χ^2/d.o.f.	c	Expected value
A_2	36	0.928	1.087(68)(56)	1
A_3	30	4.606	1.413(65)(31)	1.5

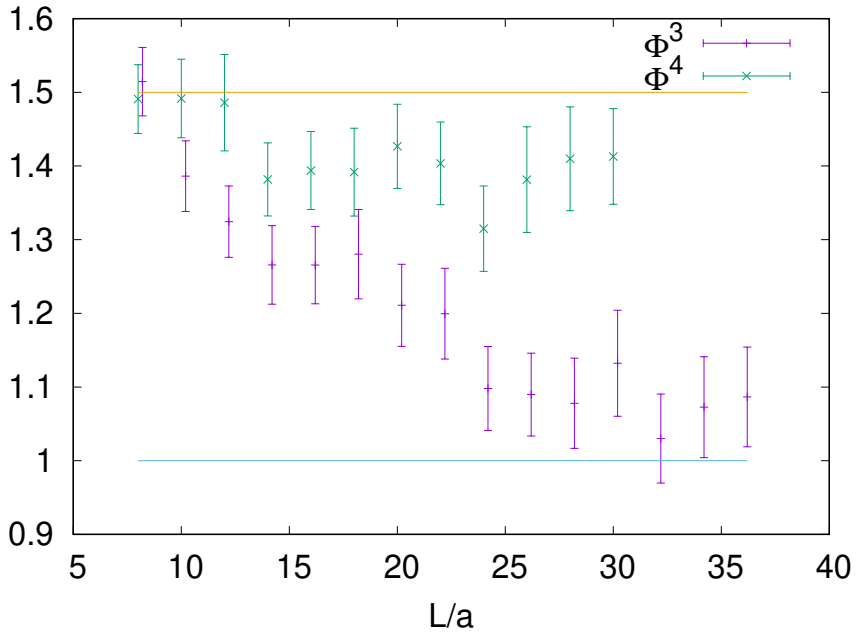

Figure 6.6: Central charges obtained by the fit for A_2 ($W = \Phi^3$) and A_3 ($W = \Phi^4$) as a function of the box size $L/a = 8$–36.

Central charge from the EMT correlator

As discussed in Chapter 3, the EMT $T = T_{zz}$, which is expected to be consistent with the conformal symmetry, is given in the momentum space by

$$T(p) = \frac{\pi}{L_0 L_1} \sum_q \Big[4(p-q)_z q_z A^*(p-q) A(q) - i q_z \psi_2(p-q) \bar{\psi}_{\dot{2}}(q) + i(p-q)_z \psi_2(p-q) \bar{\psi}_{\dot{2}}(q) \Big]. \tag{6.19}$$

It turns out that this expression as it stands leads to a very noisy two-point correlation function. Fortunately, as discussed in Chapter 3, noting the fact that the EMT of Eq. (6.19) is the SUSY transformation of the supercurrent in Eqs. (6.14) and (6.15),

$$T(p) = \frac{1}{4} Q_2 S^+(p) - \frac{1}{4} \bar{Q}_{\dot{2}} S^-(p), \tag{6.20}$$

where the SUSY transformation is given in Chapter 3, we can express the two-point function of the EMT by a linear combination of two-point functions of the supercurrent which are less

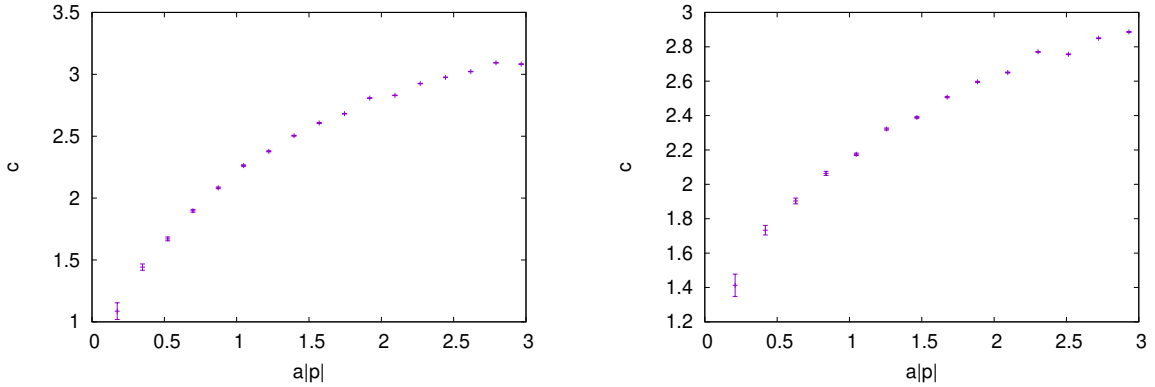

(a) A_2 and $L/a = 36$. (b) A_3 and $L/a = 30$.

Figure 6.7: "Effective central charge" obtained by the fit for A_2 and A_3 in various momentum regions, $\frac{2\pi}{L}n \le |p| < \frac{2\pi}{L}(n+1)$ $(n = 1, \ldots, L-1)$.

Table 6.3: The central charges for A_2 and A_3 obtained from the fit of the EMT correlator. The fitting momentum region is $\frac{2\pi}{L} \le |p| < \frac{4\pi}{L}$.

Algebra	L	χ^2/d.o.f.	c	Expected value
A_2	36	1.017	1.061(36)(34)	1
A_3	30	0.916	1.415(36)(36)	1.5

noisy:

$$\langle T(p)T(-p)\rangle = -\frac{2ip_z}{16}\left\langle S^+(p)S^-(-p) + S^-(p)S^+(-p)\right\rangle. \tag{6.21}$$

Note that this relation holds exactly in our formulation that preserves SUSY.

The Fourier transformation of Eq. (6.11) is, by the same procedure as Eqs. (6.16) and (6.17),

$$\begin{aligned}\langle T(p)T(-p)\rangle &= L_0L_1\frac{\pi c}{2\cdot 4!}\frac{\partial^4}{\partial p_{\bar z}^4}\left(\frac{|p|}{\delta}\right)^3 K_3(|p|\delta)\\ &\to L_0L_1\frac{\pi c}{12}\frac{p_z^3}{p_{\bar z}}.\end{aligned} \tag{6.22}$$

We plot the two-point function $\langle T(p)T(-p)\rangle$ of Eq. (6.21) in Figs. 6.8 and 6.9 for the maximal box size, that is, $L/a = 36$ for A_2 and $L/a = 30$ for A_3. In each figure, the left panel is the real part of the correlation function and the right one is the imaginary part. The spatial momentum ap_1 is fixed to the positive minimal value, $p_1 = 2\pi/L$. In these figures we also show the function in Eq. (6.22) with the central charge c obtained from the fit in the IR region $\frac{2\pi}{L} \le |p| < \frac{4\pi}{L}$. The central charges obtained in this way are tabulated in Table 6.3; this is one of the main results of this section.

We repeated the computation of the central charge c by using only the $(2,0)_2$-type solutions for A_2 $(L/a = 36)$ and the $(3,0)_3$-type solutions for A_3 $(L/a = 30)$, to see how the values are

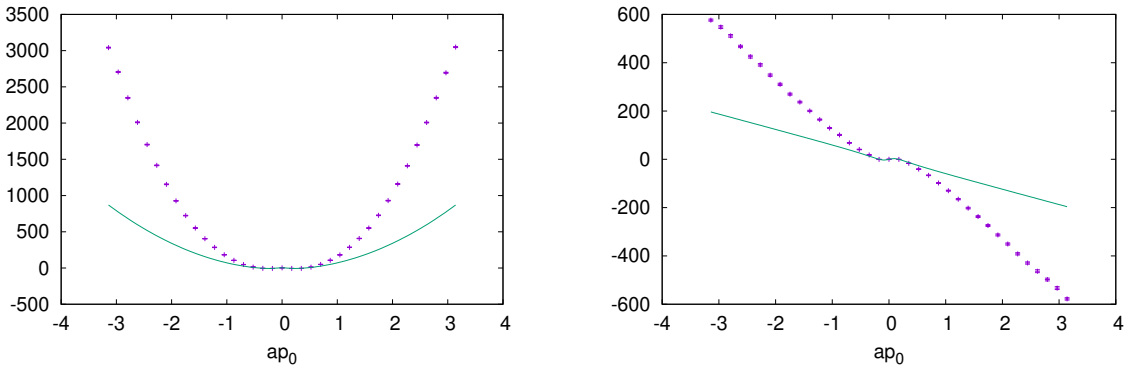

(a) Real part (b) Imaginary part

Figure 6.8: $\langle T(p)T(-p)\rangle$ for A_2, $L/a = 36$, and $ap_1 = \pi/18$. The fitting curve of Eq. (6.22) is also depicted.

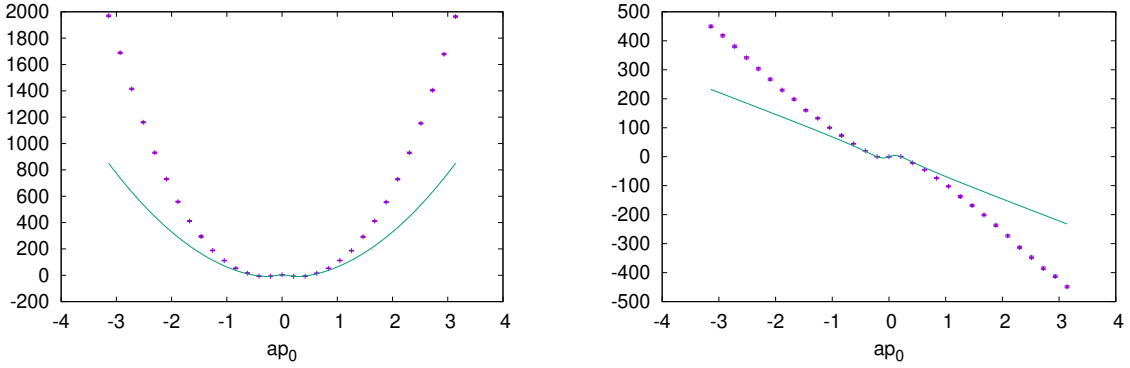

(a) Real part (b) Imaginary part

Figure 6.9: $\langle T(p)T(-p)\rangle$ for A_3, $L/a = 36$, and $ap_1 = \pi/15$. The fitting curve by Eq. (6.22) is also depicted.

changed if we do not include a few percent "strange solutions." The results are:

$$c = 1.057(34) \qquad \text{for } A_2, \tag{6.23}$$

$$c = 1.288(28) \qquad \text{for } A_3. \tag{6.24}$$

One may note that the fit in Table 6.3 is better than that in Table 6.2, in the sense that χ^2/d.o.f. is very close to 1 in the former. This is due to the fact that the real and imaginary parts of the two-point correlation function of Eq. (6.21) are exactly (anti-)symmetric under $p \to -p$, while the numerical data of $\langle S^+(p)S^-(-p)\rangle$ itself does not possess this property.[2] The number of data points is thus effectively doubled.

[2]This (anti-)symmetry under $p \to -p$ is fulfilled within the margin of the statistical error; one may also (anti-)symmetrize the two-point function $\langle S^+(p)S^-(-p)\rangle$ by hand.

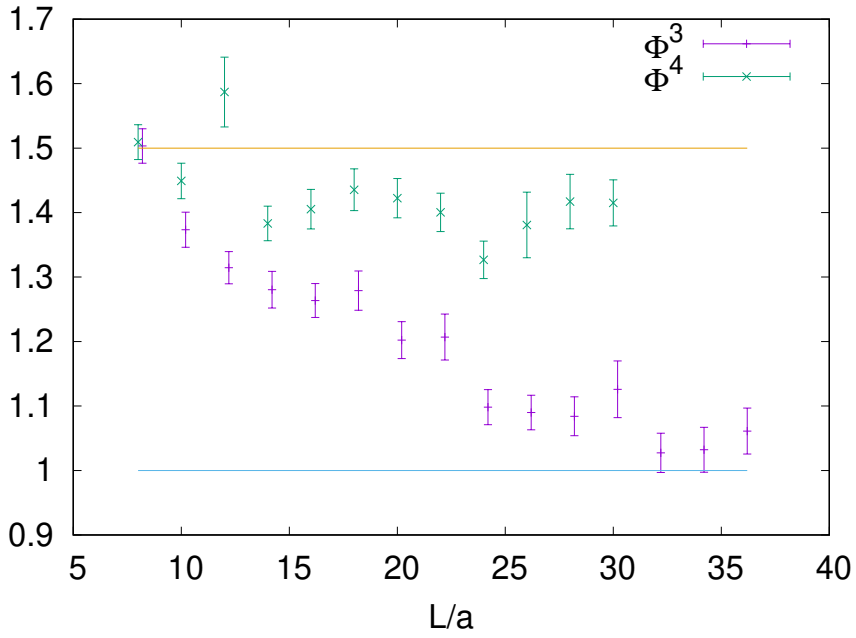

Figure 6.10: Central charges obtained by the fit for A_2 ($W = \Phi^3$) and A_3 ($W = \Phi^4$) as a function of the box size $L/a = 8$–36.

In Fig. 6.10, we plotted how the fitted central charge changes as a function of the box size L. From c presented in Fig. 6.10, we again estimated the systematic error associated with the finite-volume effect. The values obtained in this way are presented in the second parentheses for c in Table 6.3.

Also, in Fig. 6.11 the "effective central charge" obtained from the fit in various momentum regions is depicted; from IR to UV, it again shows the expected behavior analogously to the Zamolodchikov C-function (4.14).

Central charge from the $U(1)$ current correlator

Finally, we consider the $U(1)$ current correlator. As discussed in Chapter 3, the $U(1)$ current is given by

$$J(p) = \frac{2\pi}{L_0 L_1} \sum_q \bar{\psi}_{\dot{2}}(p-q)\psi_2(q). \tag{6.25}$$

The two-point function of this current is expected to behave in the IR limit as

$$\begin{aligned} \langle J(p)J(-p)\rangle &= L_0 L_1 \frac{-\pi c}{3} \frac{\partial^2}{\partial p_{\bar{z}}^2} \frac{|p|}{\delta} K_1(|p|\delta) \\ &\to L_0 L_1 \frac{-\pi c}{3} \frac{p_z}{p_{\bar{z}}}. \end{aligned} \tag{6.26}$$

We note that the supercurrent $S^{\pm}$ can be rewritten as the SUSY transformation of J,

$$S^+(p) = \bar{Q}_{\dot{2}} J(p), \qquad S^-(p) = Q_2 J(p). \tag{6.27}$$

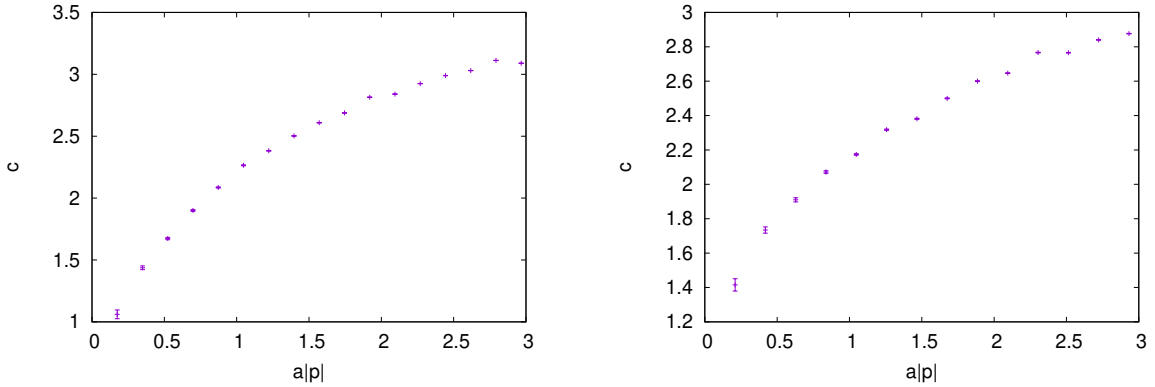

(a) A_2 and $L/a = 36$. (b) A_3 and $L/a = 30$.

Figure 6.11: "Effective central charge" obtained by the fit for A_2 and A_3 in various momentum regions, $\frac{2\pi}{L}n \leq |p| < \frac{2\pi}{L}(n+1)$ $(n \in \mathbb{Z}_+)$.

Therefore,

$$\left\langle S^+(p)S^-(-p) + S^-(p)S^+(-p) \right\rangle = -2ip_z \left\langle J(p)J(-p) \right\rangle . \tag{6.28}$$

This shows that the computation of the $U(1)$ current correlator is identical to the EMT correlator of Eq. (6.21) up to a proportionality factor. We expect that we would obtain almost the same results as the previous subsection, so we do not carry out the analysis on this correlator.

6.2.2 Central charge in DE-type theories

Let us show the result of the numerical determination of the central charge for the D_3, D_4, and E_7 models [81]. We plot the correlation function $\langle T(p)T(-p)\rangle$ in Figs. 6.12–6.14 for the maximal box size with the fitting curve (6.22); the central charge c is obtained from the fit in the IR region $\frac{2\pi}{L} \leq |p| < \frac{4\pi}{L}$. The left panel in each figure is devoted to the real part of the two-point function and the right one is the imaginary part. The horizontal axis indicates the momentum ap_0, and the momentum ap_1 is fixed to the positive minimal value $p_1 = 2\pi/L$. In Table 6.4, we tabulate the numerical results of the central charge for all box sizes in the D_3, D_4, and E_7 models.

The central charge for the maximal box size in Table 6.4 reads

$$c = 1.595(31)(41) \qquad \text{for } D_3, \tag{6.29}$$
$$c = 2.172(48)(39) \qquad \text{for } D_4, \tag{6.30}$$
$$c = 2.638(47)(59) \qquad \text{for } E_7. \tag{6.31}$$

This is the last main result in this section. Here, a number in the second parentheses indicates the systematic error associated with the finite-volume effect. In Eqs. (6.29) and (6.31), we estimate this as follows: We pick out the largest three volumes for each minimal model; from the central values at two smaller ones, we extrapolate to the larger L/a regime as a linear function of the inverse volume $1/(L/a)^2$, and then, obtain an extrapolated value at the

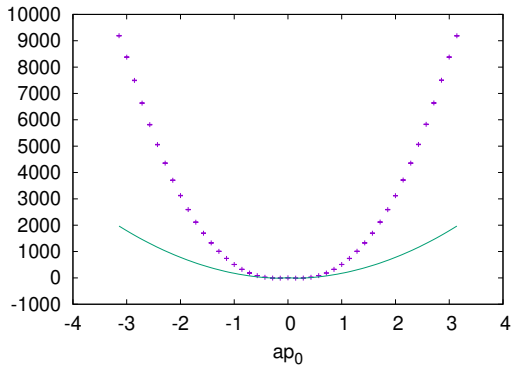

(a) Real part

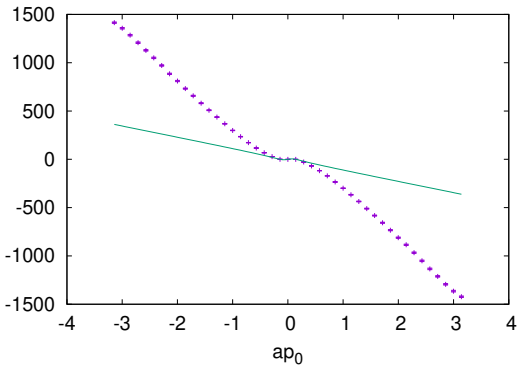

(b) Imaginary part

Figure 6.12: $\langle T(p)T(-p)\rangle$ for D_3, $L/a = 44$, and $ap_1 = \pi/22$. The fitting curve (6.22) is depicted at once.

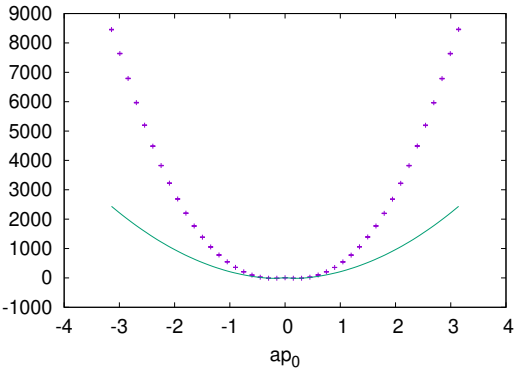

(a) Real part

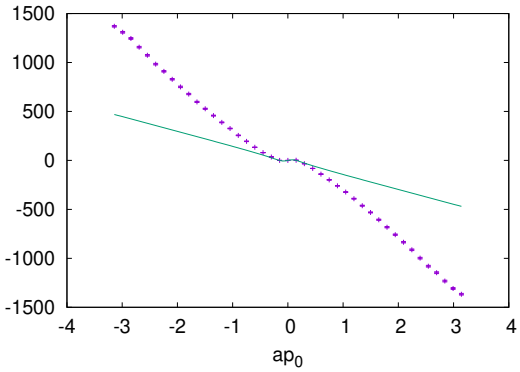

(b) Imaginary part

Figure 6.13: $\langle T(p)T(-p)\rangle$ for D_4, $L/a = 42$, and $ap_1 = \pi/21$. The fitting curve (6.22) is depicted at once.

maximal volume (see Fig. 6.15); the systematic error is identified with the deviation between this and the central value in Eqs. (6.29) and (6.31).[3] In Eq. (6.30), since we have more than two would-be convergent results at large L, the systematic error is estimated by the maximum deviation of the central values at the three largest volumes. Eqs. (6.29)–(6.31) are consistent with the expected values, 1.5 for D_3 within $\sim 1.3\sigma$, 2 for D_4 within 2σ, and $2.666\ldots$ for E_7 within the numerical errors; the standard deviations are evaluated by the sum of the statistical and systematic errors.

As mentioned already, it is interesting to plot the "effective central charge," which is

[3]The fit function $\propto 1/L^2$ is a possible choice, but there would be no theoretical evidence to support this choice. Because the behavior of the $L \to \infty$ limit appears not quite smooth as in Fig. 6.15, we do not attempt to extrapolate to the infinite volume limit.

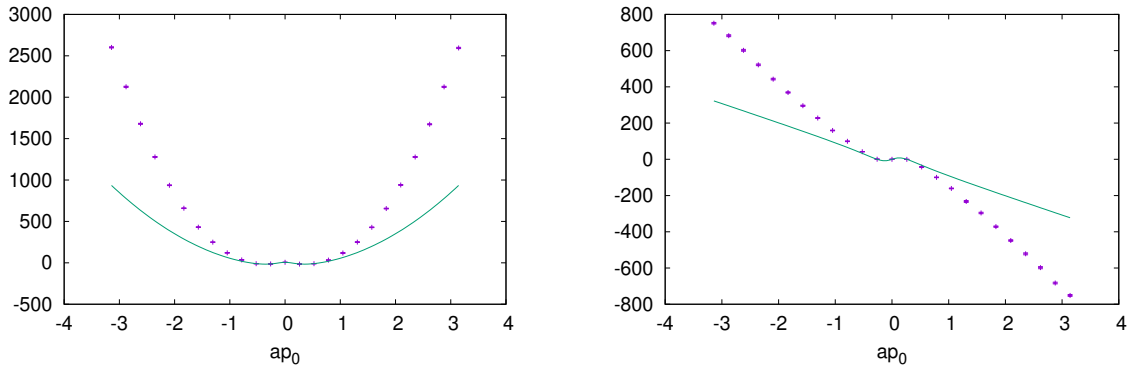

(a) Real part

(b) Imaginary part

Figure 6.14: $\langle T(p)T(-p)\rangle$ for E_7, $L/a = 24$, and $ap_1 = \pi/12$. The fitting curve (6.22) is depicted at once.

Table 6.4: The central charge for D_3, D_4 and E_7 obtained from the fit of the EMT correlator. The fitted momentum range is $\frac{2\pi}{L} \le |p| < \frac{4\pi}{L}$.

Algebra	L/a	χ^2/d.o.f.	c	Expected value
D_3	8	6.056	2.786(34)	1.5
	16	5.496	2.141(31)	
	24	3.122	1.867(28)	
	32	2.682	1.711(29)	
	40	0.476	1.591(32)	
	44	3.598	1.595(31)	
D_4	8	3.216	2.907(36)	2
	16	3.738	2.509(34)	
	24	1.946	2.466(42)	
	32	2.832	2.202(40)	
	36	1.109	2.211(70)	
	40	2.276	2.175(48)	
	42	1.177	2.172(48)	
E_7	8	2.220	2.964(36)	2.666...
	16	1.800	2.639(35)	
	24	1.364	2.638(47)	

analogous to the Zamolodchikov's C-function (4.14). This is obtained from the fit in a variety of momentum regions from IR to UV; we take the fitted momentum regions as $\frac{2\pi}{L}n \le |p| < \frac{2\pi}{L}(n+1)$ for $n \in \mathbb{Z}_+$. Then Fig. 6.16 shows that the "effective central charge" connects the IR central charge to an UV value $c \approx 6$. This number is consistent with the central charge $c = 3N_\Phi$ in the expected free $\mathcal{N} = 2$ SCFT. Recall that N_Φ is the number of supermultiplets in the free $\mathcal{N} = 2$ WZ model, and we have set $N_\Phi = 2$ here.

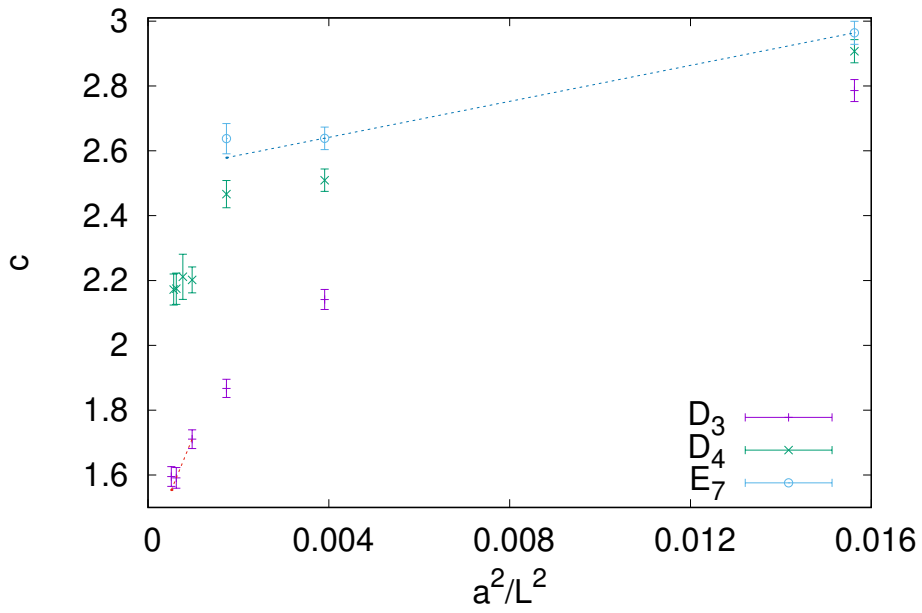

Figure 6.15: Systematic error estimation for the central charge for D_3, D_4, E_7.

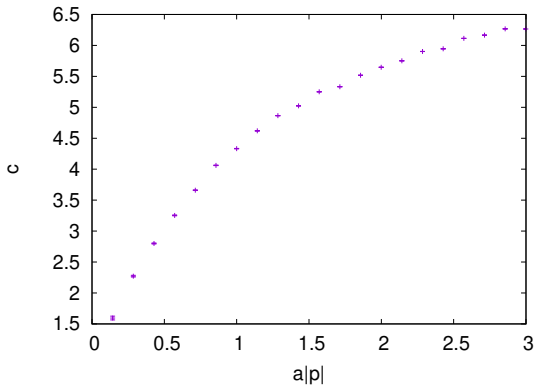

(a) For D_3 and $L/a = 44$.

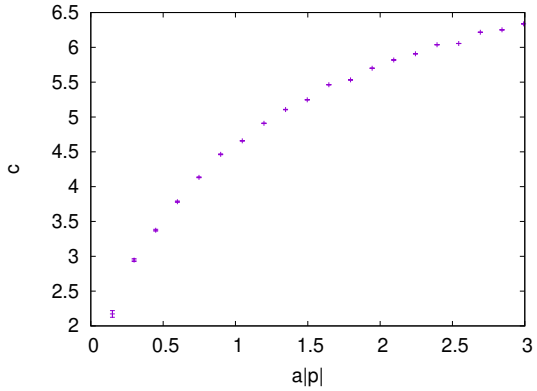

(b) For D_4 and $L/a = 42$.

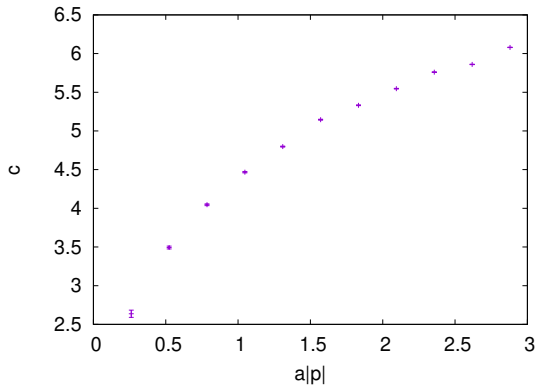

(c) For E_7 and $L/a = 24$.

Figure 6.16: "Effective central charge" for D_3, D_4, and E_7, which changes as the function of $|p| = \frac{2\pi}{L}n$ with fitted momentum regions, $\frac{2\pi}{L}n \leq |p| < \frac{2\pi}{L}(n+1)$, for $n \in \mathbb{Z}_+$.

6.3 Continuum limit analysis for the scaling dimension

In this section the finite-size scaling analysis given in Refs. [61, 75] is developed into an analysis method with continuum-limit extrapolation [84]. The extrapolation also carries out the thermodynamic limit. Then, we numerically simulate the IR behavior of a scalar correlator for the A_2-type WZ model, extrapolate it to the continuum limit, and perform a precision measurement of the scaling dimension [84].

For simplicity, we study a single superfield with the superpotential

$$W(\Phi) = \frac{\lambda}{n+1}\Phi^{n+1}, \tag{6.32}$$

which corresponds to the A_n minimal model, and the system is defined in the box $L_0 \times L_1$, Here, the coupling constant λ is a dimensionful parameter and characterizes the mass scale in this theory.

6.3.1 Continuum limit of the susceptibility of the scalar field

To numerically determine the scaling dimension, we first explain the finite-size scaling analysis in Refs. [61, 75], which is compatible with the continuum limit as we will develop later. Recall that the susceptibility of the scalar field A is defined by

$$\chi(L_\mu) = \frac{1}{a^2}\int_{L_0L_1} d^2x\ \langle A(x)A^*(0)\rangle = \frac{1}{a^2 L_0 L_1}\left\langle |A(p=0)|^2\right\rangle. \tag{6.33}$$

In the IR limit, the scalar field is expected to behave as a chiral primary field with the conformal dimensions $(h, \bar{h})$; the two-point function of A behaves as

$$\langle A(x)A^*(0)\rangle = \frac{1}{z^{2h}\bar{z}^{2\bar{h}}}, \tag{6.34}$$

for large $|x| = \sqrt{x^2}$. Note that the field A is spinless, $h = \bar{h}$. Then, we observe the finite-volume scaling of the scalar susceptibility for large L_μ, as

$$\chi \propto (L_0 L_1)^{1-h-\bar{h}}. \tag{6.35}$$

Numerically simulating the scalar correlator for some different volumes but the same value of the coupling, one can read the exponent, $1-h-\bar{h}$, from the slope of $\ln\chi(L_\mu)$ as a linear function of $\ln(L_0L_1)$. In what follows, for simplicity, we take into account the case of the physical box size $L = L_0 = L_1$.

As already announced, we consider the thermodynamic and continuum limits, $a/L \to 0$. No extrapolation has been done in the preceding numerical studies. In Sect. 6.1 and 6.2 (and Refs. [61, 75]), the grid size L/a is expected to be taken as sufficiently large values, while the coupling λ in the superpotential (6.32) is fixed by $a\lambda = 0.3$; good agreement of the scaling dimension with those of the A_2 and A_3 minimal models was observed. Unlike in the case of QCD, however, the present model does not possess any dynamical scale, so the "sufficiently small" scale of a is not obvious. In fact, we will find that the susceptibility, $\chi(L)$, takes a slow approach to $a/L = 0$. To obtain precise and reliable results, we should extend the above finite-size scaling analysis in order to treat the thermodynamic and continuum limits.

We have also recognized the pathology of the locality in the lattice formulation that is based on the SLAC derivative; the computation of $\ln \chi(L)$ with finite L/a is quite sensitive to this problem [75,80] (see also Sect. 6.3.3). A proposal given in Sect. 6.1 is to directly study the correlation function in the momentum space, $\langle A(p)A^*(-p)\rangle$. Although the measured scaling dimension with the fixed coupling tends to approach expected values as the grid size L/a increases, the approach to the $L/a \to \infty$ limit appears not quite smooth.[4] We would need a more systematic method for the infinite-volume and continuum limits, while the locality should be restored in the limits.

Our strategy for the continuum limit is very similar to that in Ref. [121]. We regard $\ln \chi(L)$ as the same kind of running coupling $\bar{g}^2(L)$ defined on a lattice. To take the continuum limit, various sizes of the lattice spacing $\{a_i\}$ ($i = 1, 2, \dots$) are required; we first prepare various momentum-grid sizes $\{L/a_i\}$, while the lattice parameter $a_i\lambda$ is tuned so that $\ln \chi(L)$ (or $\bar{g}^2(L)$) is kept fixed; we denote $u = \ln \chi(L)$. A system with a different grid size $L'/a' \neq L/a_i$ and the same parameter $a'\lambda' = a_i\lambda$ possesses the physical box size $L' \times L'$ with $a' = a_i$. Then, we compute $\ln \chi(L')$ ($\bar{g}^2(L')$) for L'/a_i and $a_i\lambda$; we observe the a-dependence of $\ln \chi(L')|_a$ ($\bar{g}^2(L')|_a$), and attempt to extrapolate this in the continuum limit, $\lim_{a\to 0} \ln \chi(L')|_a$.

To be more specific, we introduce the scaling function Σ as

$$\Sigma(s, u, a/L) = \ln \chi(sL)|_a. \tag{6.36}$$

The statistical error of Σ would be given by the square root of the sum of squared errors of $\ln \chi(L)$ and $\ln \chi(sL)$, owing to the long-distance behavior in Eq. (6.35). As a consequence of the continuum limit with a to-be-determined fit function, we can obtain the scaling dimension

$$1 - h - \bar{h} = \frac{1}{\ln s^2} \left[\lim_{a\to 0} \Sigma(s, u, a/L) - u \right]. \tag{6.37}$$

The cutoff dependence will be determined from numerical results. Note that the unique mass scale λ in this model should be sufficiently larger than $1/L$ to study the conformal behavior [61], hence $\lambda L \to \infty$ as the continuum limit. This indicates that the extrapolation carries out the thermodynamic limit at the same time. We can apply our extrapolation method to the continuum limit to other non-perturbative formulations, for example the lattice formulation in Ref. [61].

6.3.2 Precision measurement of the scaling dimension

In this subsection, we perform precision measurement of the scaling dimension for the A_2-type theory with the cubic superpotential Φ^3 by using the above continuum-limit analysis. We first summarize the numerical setup we use in this section; the most part of our setup is identical in Chapter 5. L/a is taken as even integers in the interval $[10, 52]$. We employ the Newton–Raphson method with the convergence threshold as

$$\sqrt{\frac{\sum_p |2ip_z A(p) + W'(A)^*(p) - N(p)|^2}{\sum_q |N(q)|^2}} < \begin{cases} 10^{-14} & \text{for } L < 52a \\ 10^{-13} & \text{for } L = 52a. \end{cases} \tag{6.38}$$

[4] In Sect. 6.2, the central charge appears to possess a higher convergence speed than the scaling dimension, though the approach to $L/a \to \infty$ is also not quite smooth.

Table 6.5: Classification of the configurations obtained for the A_2-type theory with tuned λ.

L/a	$a\lambda$	$\mathcal{N}_{\rm conf}$	$(2,0)$	$(3,1)$	$(4,2)$	$(1,0)$	$(2,1)$	$(3,2)$	$(3,0)$	$(4,1)$
10	0.1780	7680	7680	0	0	0	0	0	0	0
12	0.2135	5120	5119	1	0	0	0	0	0	0
14	0.2538	5120	5119	1	0	0	0	0	0	0
16	0.3000	5120	5112	8	0	0	0	0	0	0
18	0.3420	5120	5093	27	0	0	0	0	0	0
20	0.3888	5120	5070	50	0	0	0	0	0	0
22	0.4500	5120	5023	97	0	0	0	0	0	0
24	0.5100	5120	4961	156	3	0	0	0	0	0
26	0.5705	5120	4909	204	6	0	0	0	1	0
20	0.1780	5120	5117	3	0	0	0	0	0	0
24	0.2135	5120	5104	16	0	0	0	0	0	0
28	0.2538	5120	5075	44	1	0	0	0	0	0
32	0.3000	4320	4236	83	1	0	0	0	0	0
36	0.3420	2592	2514	77	1	0	0	0	0	0
40	0.3888	2592	2472	118	0	0	1	1	0	0
44	0.4500	2592	2458	131	2	0	0	0	0	1
48	0.5100	2592	2433	157	2	0	0	0	0	0
52	0.5705	1512	1392	107	4	1	1	1	6	0

In the case of $L = 52a$, which is the most numerically demanding one in this section, the threshold is less accurate (and also the number of obtained configurations is not relatively high). For a fixed configuration $N(p)$, we randomly generate initial trial configurations of $A(p)$ so that we obtain 200 solutions for $L < 52a$, allowing repetition of identical solutions, and 120 solutions for $L = 52a$. Two solutions A_1 and A_2 are regarded as identical if

$$\sqrt{\frac{\sum_p |A_1(p) - A_2(p)|^2}{\sum_q |A_1(q)|^2}} < \begin{cases} 10^{-11} & \text{for } L < 52a \\ 10^{-10} & \text{for } L = 52a. \end{cases} \tag{6.39}$$

We tabulate the classification of the configurations obtained in Table 6.5, where the coupling $a\lambda$ has already been tuned in accordance with the above strategy. $\mathcal{N}_{\rm conf}$ denotes the total number of configurations for each setup. In the upper half of the table, the number of configurations for L is shown; in the lower half, that for $L' = 2L$ is shown. In Table 6.6, we list the numerical results of Δ in Eq. (5.19), which should be identical the Witten index 2; the one-point SUSY Ward–Takahashi identity in Eq. (5.29), which should vanish in the SUSY-invariant system. Whether Δ and δ are correctly reproduced indicates the quality of our configurations. Note that, for $L' = 52a$, the quality of the configurations obtained is poorer due to the computational cost.

We tabulate the numerical results of the scalar susceptibility with the various box sizes of L and $L' = 2L$ in Table 6.7. The third column is devoted to the tuned values of the coupling, $a\lambda$, so that $\ln \chi(L)$ in the fourth column is kept almost fixed. The results of $\Sigma(u, a/L)$ are shown in the last column, where we have omitted the first argument $s = 2$ of $\Sigma(s, u, a/L)$,

Table 6.6: Quality of the configurations obtained for the A_2-type theory with tuned λ.

L/a	L'/a	$a\lambda$	$\Delta(L)$	$\Delta(L')$	$\delta(L)$	$\delta(L')$
10	20	0.1780	2	2	−0.00099(104)	−0.00005(67)
12	24	0.2135	2	2	−0.00063(107)	+0.00046(56)
14	28	0.2538	2	2	−0.00019(94)	−0.00030(48)
16	32	0.3000	2	2	−0.00024(81)	−0.00004(46)
18	36	0.3420	2	2	−0.00109(74)	+0.00020(52)
20	40	0.3888	2	1.9992(5)	−0.00078(67)	+0.00053(55)
22	44	0.4500	2	2.0004(4)	−0.00005(62)	+0.00031(48)
24	48	0.5100	2	2	+0.00041(56)	+0.00000(41)
26	52	0.5705	2.0002(2)	2.002(2)	−0.00058(52)	+0.00073(110)

Table 6.7: Scalar susceptibility with $u = 3.9175$.

L/a	L'/a	$a\lambda$	$\ln\chi(L)$	$\ln\chi(L')$	$\Sigma(u, a/L)$
10	20	0.1780	3.9174(59)	4.6338(72)	4.6338(93)
12	24	0.2135	3.9175(73)	4.6642(69)	4.6642(100)
14	28	0.2538	3.9193(70)	4.6844(66)	4.6844(97)
16	32	0.3000	3.9171(69)	4.6913(68)	4.6913(97)
18	36	0.3420	3.9166(68)	4.7223(83)	4.7223(107)
20	40	0.3888	3.9215(65)	4.7251(81)	4.7251(104)
22	44	0.4500	3.9162(62)	4.7400(76)	4.7400(97)
24	48	0.5100	3.9186(60)	4.7610(70)	4.7610(93)
26	52	0.5705	3.9175(56)	4.7823(91)	4.7823(107)

Table 6.8: Scaling dimension measured at finite volumes. The results in the last two rows are obtained by reading the slope of $\ln\chi$ for $(L/a, L'/a) = (24, 48)$ or $(L/a, L'/a) = (26, 52)$ in Table 6.7.

	Fit range of L	$a\lambda$	$1 - h - \bar{h}$
Kamata–Suzuki [75]	From 24 to 36	0.3000	0.603(19)
	From 26 to 36	0.3000	0.609(25)
	From 24 to 48	0.5100	0.6076(66)
	From 26 to 52	0.5705	0.6238(77)

while we set $u = \ln\chi(L)$ as 3.9175. The error of $\Sigma(u, a/L)$ is given by the square root of the sum of the squared errors of $\ln\chi(L)$ and $\ln\chi(L')$.

In Ref. [75] the scaling dimension was obtained from the slope of the susceptibility in the formulation by using data for $24 \le L/a \le 36$ or $26 \le L/a \le 36$ with a fixed coupling; we have a similar slope of $\ln\chi$ for $(L/a, L'/a) = (24, 48)$, though we have used different values of $a\lambda$ (see Table 6.8). We will find a significant difference between such numerical results at a finite cutoff and our result below at $a/L = 0$.

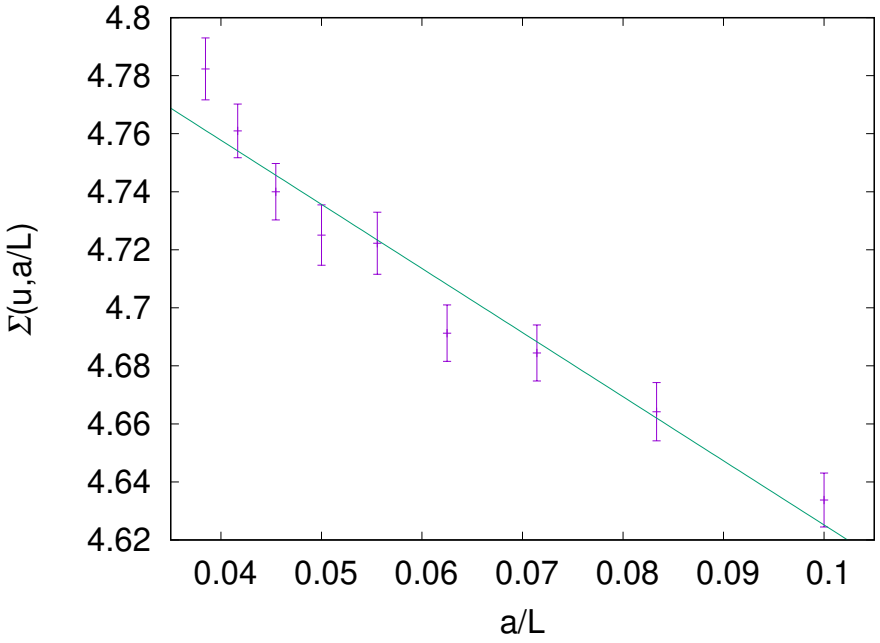

Figure 6.17: $\Sigma(u, a/L)$-(a/L) plot with $u = 3.9175$. The fitting line of Eq. (6.40) is also depicted.

Now we have enough data to clarify the (a/L)-dependence of $\Sigma(u, a/L)$. Figure 6.17 shows $\Sigma(u, a/L)$ as a function of a/L given in Table 6.7. From the plot, we simply apply a linear function of a/L in order to take the continuum limit; then we have

$$\Sigma(3.9175, a/L) = -0.0850(64) \times \frac{26a}{L} + 4.8461(107), \tag{6.40}$$

with $\chi^2/\text{d.o.f.} = 1.417$. From Eq. (6.37), the scaling dimension is given by

$$1 - h - \bar{h} = 0.6699(77). \tag{6.41}$$

This result is consistent with the expected exact value $1 - h - \bar{h} = 2/3 = 0.6666\ldots$ within the statistical error.

Because the quality of configurations with $L/a = 52$ is poorer due to the computational cost, the computation of $\ln \chi$ could be less accurate. In fact, the above result in Fig. 6.17 implies that there is a discrepancy between the central values of $\ln \chi(L)$ and the fit function at $L/a = 52$. To make sure that this discrepancy comes from statistical fluctuations, we show the behavior of $\ln \chi(L)$ for $L/a = 52$ when the number of configurations varies in Table 6.9; the deviation of the central values decreases.

To estimate the systematic error, we may omit the configurations for $L/a = 52$; that is,

$$\Sigma(3.9175, a/L)|_{L/a<52} = -0.0791(69) \times \frac{26a}{L} + 4.8341(120), \tag{6.42}$$

with $\chi^2/\text{d.o.f.} = 0.807$; we obtain

$$1 - h - \bar{h} = 0.6612(86). \tag{6.43}$$

Table 6.9: $\ln \chi(L')$ with $u = 3.9175$ and $L/a = 52$ when the number of configurations, $\mathcal{N}_{\rm conf}$, varies.

$\mathcal{N}_{\rm conf}$	$\ln \chi(L')$
1512	4.7823(91)
756	4.7950(133)
378	4.8087(193)

The main result of the scaling dimension in this section is given by

$$1 - h - \bar{h} = 0.6699(77)(87). \tag{6.44}$$

Here, the number in the second parentheses indicates the systematic error defined by the deviation between the central values of Eq. (6.41) and Eq. (6.43). This result of the scaling dimension is rather consistent with the conjectured WZ/SCFT correspondence.

As shown in Table 6.8 and Fig. 6.17, we observed a significant difference between our net result and the ones at any finite L/a. The scalar susceptibility takes a slow approach to the $a/L = 0$ limit, at least in the present formulation. By using our extrapolation analysis, we can get down to the target SUSY continuum theory with the infinite volume; from a numerical simulation based on the formulation by Kadoh and Suzuki, we obtained the limiting value for the simplest A_2 theory. This result not only has a smaller margin of error in the numerical value, but also would be much more reliable than those of preceding studies, which were computed at finite L/a; it shows a coherence picture being quite consistent with the theoretical conjecture.

6.3.3 Discussion on the fit function

We found that a linear fit of $\Sigma(s, u, a/L)$ with respect to a/L would be good within the numerical error. To convince ourselves of this fact, let us introduce a slightly modified extrapolation method, by which we obtain another result for the scaling dimension from same data. If the two results are similar, our extrapolation method (or fit function) to the continuum limit works well.

The new method is based on the excision of a small region around the contact point of the integrand $\langle A(x)A(0)\rangle$ in $\ln \chi(L)$ in Eq. (6.33) [61]. The modified scalar susceptibility $\tilde{\chi}$ is defined by

$$\tilde{\chi}(L) = \frac{1}{a^2} \int_{|x| \geq \lambda^{-1}} d^2x \ \langle A(x)A^*(0)\rangle \, . \tag{6.45}$$

The coupling λ is the unique mass scale in the WZ model with the superpotential in Eq. (6.32), and the correlations at short lengths $\sim \lambda^{-1}$ would not affect the scaling in Eq. (6.35) of $\chi(L)$ in low-energy regions. Note that the shape of the excised space is slightly different from those in Refs. [61, 75], but the susceptibility should not be sensitive to such UV details *in the continuum limit*; if the grid size L/a is not sufficiently large (i.e. L/a is finite), we suffer from sensitivity to the excised space size; this is the problem that the susceptibility in Ref. [75] is

quite sensitive to the UV ambiguity. In terms of the Fourier modes of A, we have

$$\tilde{\chi}(L) = \frac{1}{a^2L^2}\left\langle |A(p=0)|^2 \right\rangle - \frac{1}{a^2L^4}\sum_p \frac{2\pi\lambda^{-1}}{|p|} J_1(\lambda^{-1}|p|)\left\langle |A(p)|^2 \right\rangle, \tag{6.46}$$

where $|p| = \sqrt{p^2}$ and J_1 is the Bessel function of the first kind.

The parameter tuning above indicates that the dimensionless coupling $a\lambda$ becomes large as $L/a \to \infty$, while $\ln \chi(L)$ is kept fixed. That is, in the small-a limit, the volume of the excised space becomes smaller and smaller; we must have completely the same result of the scaling dimension as in the method of Eq. (6.37), at least analytically. In numerical simulations, however, it is not known a priori what function we should apply to take the continuum limit. Thus, attempting to extrapolate results of $\ln \tilde{\chi}(L)$ and to determine the fit function, one can justify the numerical determination of the scaling dimension from Σ. In the same way as $\ln \chi(L)$, we define the new scaling function $\tilde{\Sigma}$ by

$$\tilde{\Sigma}(s, u, a/L) = \ln \tilde{\chi}(sL). \tag{6.47}$$

Here, u is given by the fixed number $\ln \chi(L)$, which is identical to the value of $\ln \tilde{\chi}(L)$ in the continuum limit, that is, $\lambda^{-1} \to 0$. Similarly, one can measure the scaling dimension by Eq. (6.37) with $\tilde{\Sigma}$ and another to-be-determined fit function.

From the $\tilde{\Sigma}(u, a/L)$-(a/L) plot in Fig. 6.18 we obtain the fitted quadratic curves

$$\tilde{\Sigma}(3.9175, a/L) = -0.091(14) \times \left(\frac{26a}{L}\right)^2 + 0.031(52) \times \frac{26a}{L} + 4.8062(425) \tag{6.48}$$

with $\chi^2/\text{d.o.f.} = 1.600$, or

$$\tilde{\Sigma}(3.9175, a/L) = -0.0823(19) \times \left(\frac{26a}{L}\right)^2 + 4.8317(62) \tag{6.49}$$

with $\chi^2/\text{d.o.f.} = 1.423$. These fitting results give the scaling dimension as

$$1 - h - \bar{h} = 0.641(31), \qquad 1 - h - \bar{h} = 0.6594(45), \tag{6.50}$$

respectively. These two results are consistent with our previous result in Eq. (6.44). We have obtained the precise and reliable result in Eq. (6.44) through the finite-size scaling with the continuum-limit extrapolation.

Our result seems to support the restoration of the locality in the continuum limit. The UV ambiguity in $\chi(L)$ with finite L/a, that is, the sensitivity to the excised space size $\sim \lambda^{-1}$ around the contact point, has disappeared because $\lambda^{-1} \to 0$ in the limit. We indeed found that the results in Eq. (6.50) based on the excision prescription are consistent with Eq. (6.44) without the excision. Also, in addition to the earlier numerical simulations based on the present formulation, it would be exemplified by good agreement between Eq. (6.44) and the expected value that the momentum-cutoff regularization in the 2D theory works quite well. However, the theoretical background of our computational approach is still not clear, so we should observe the locality restoration more carefully; this is a future problem.

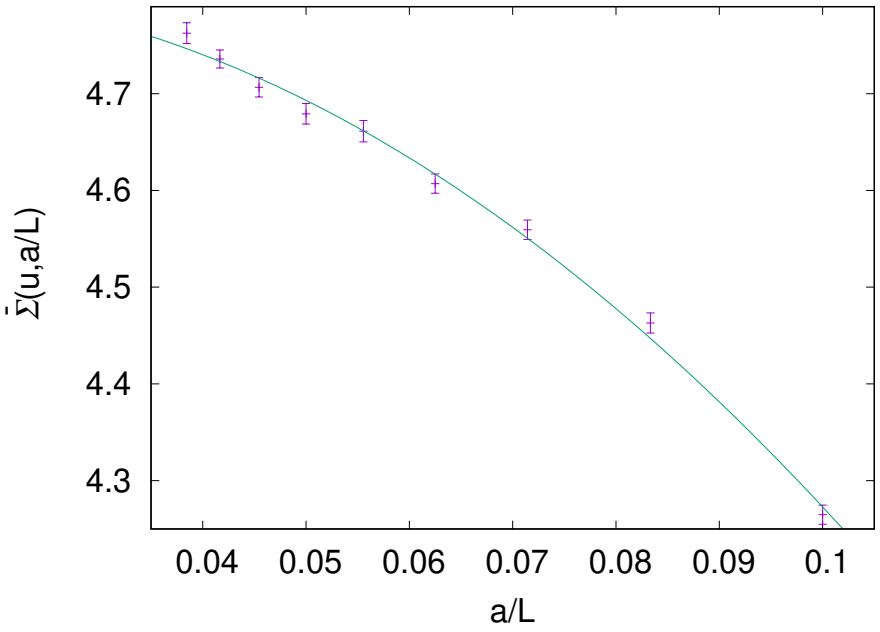

Figure 6.18: $\tilde{\Sigma}(u, a/L)$-(a/L) plot with $u = 3.9175$. The fitting curve of Eq. (6.48) is also depicted.

6.4 Torus compactification of superstring theory

Finally, we attempt to apply our numerical approach to the superstring compactification in a simple way. The most simplest case would be given by the compactification into the complex one-dimensional torus. Such a theory can be described by the Gepner model, $A_2 \otimes A_2 \otimes A_2$, with the central charge $c = 3$. We now consider the $N_\Phi = 3$ WZ model with the superpotential,

$$W(\{\Phi\}) = \lambda \left(\frac{1}{3} \sum_{I=1}^{3} \Phi_I^3 + \beta \Phi_1 \Phi_2 \Phi_3 \right), \tag{6.51}$$

where the cubic terms correspond to the A_2 minimal model, and the last term is the deformation of the torus, which is not included in the ADE classification in Table 4.1. Such a operator bringing about the deformation is believed to be marginal; the central charge would be unchanged under this deformation.

To see this, we numerically simulate the WZ model with the superpotential (6.51), while the deformation parameter β is varied. We set the coupling $a\lambda$ to 0.3, and generate 320 configurations of $\{N\}$ for $\beta = 0.1$, 1280 ones for $\beta = 1$, and 160 ones for $\beta = 10$. L/a is taken as 16, 24, 32, and 40 for $\beta = 0.1$; 16, 24, 32, and 36 for $\beta = 1$; 16 for $\beta = 10$. The other simulation setup is identical to that for the DE-type theories in Sect. 5. We tabulate the classification of obtained configurations in Tables 6.10–6.12. Note that the Witten index is given by $\Delta = 8 = (2^3)$.

As one of the main result of this section, Tables 6.13–6.15 summarize the scaling dimension we obtained in the same way in Sect. 6.1 for each superfield. Also, in the same way in Sect. 6.2,

Table 6.10: Classification of configurations for Eq. (6.51) with $\beta = 0.1$

L/a	16	24	32	40
$(8,0)_8$	319	305	286	276
$(9,1)_8$	0	6	12	12
$(10,2)_8$	1	5	11	13
$(11,3)_8$	0	2	5	7
$(12,4)_8$	0	0	1	9
$(16,8)_8$	0	0	0	1
$(9,0)_9$	0	0	1	0
$(10,1)_9$	0	0	2	1
$(11,2)_9$	0	1	0	0
$(12,3)_9$	0	1	0	1
$(14,5)_9$	0	0	1	0
$(10,0)_{10}$	0	0	1	0
Δ	8	8.006(4)	8.019(9)	8.006(4)
δ	0.0026(19)	0.0032(14)	−0.0002(14)	0.00039(90)

Table 6.11: Classification of configurations for Eq. (6.51) with $\beta = 1$

L/a	16	24	32	36
$(8,0)_8$	1247	1155	1056	497
$(9,1)_8$	27	102	158	102
$(10,2)_8$	6	18	49	23
$(11,3)_8$	0	4	9	5
$(12,4)_8$	0	1	2	5
$(13,5)_8$	0	0	0	1
$(15,7)_8$	0	0	1	0
$(8,1)_7$	0	0	0	1
$(9,0)_9$	0	0	3	2
$(13,4)_9$	0	0	1	2
$(11,2)_9$	0	0	1	1
$(10,1)_9$	0	0	0	1
Δ	8	8	8.004(2)	8.008(4)
δ	0.00158(94)	−0.00020(64)	0.00043(55)	0.00047(80)

the central charge obtained is tabulated in Table 6.16; this is another main result here. Recall again that these numbers in the tables could contain the systematic error from missed solutions, especially for $\beta = 10$. For any cases of β, we see the tendency that the measured scaling dimension approaches the expected value $0.666\ldots$ as L/a becomes large, and also the measured central charge does 3. Therefore, we end up with the conclusion that $\Phi_1\Phi_2\Phi_3$ is a marginal operator in a non-perturbative sense.

Table 6.12: Classification of configurations for Eq. (6.51) with $\beta = 10$

L/a	16
$(8,0)_8$	52
$(9,1)_8$	29
$(10,2)_8$	9
$(11,3)_8$	4
$(12,4)_8$	1
$(8,4)_4$	1
$(6,0)_6$	2
$(7,1)_6$	2
$(8,2)_6$	2
$(7,0)_7$	6
$(8,1)_7$	7
$(9,2)_7$	6
$(10,3)_7$	1
$(9,0)_9$	9
$(10,1)_9$	7
$(11,2)_9$	8
$(12,3)_9$	2
$(13,4)_9$	1
$(10,0)_{10}$	6
$(13,3)_{10}$	1
$(11,0)_{11}$	1
$(12,1)_{11}$	1
$(14,2)_{12}$	1
$(14,1)_{13}$	1
Δ	8.13(8)
δ	0.002(10)

Table 6.13: The scaling dimension obtained from the fit of $\langle A_1 A_1 \rangle$ for Eq. (6.51) with various values of β. The fitted momentum range is $\frac{2\pi}{L} \leq |p| < \frac{4\pi}{L}$.

A_I	L/a	β	χ^2/d.o.f.	$1-h-\bar{h}$	Expected value
A_1	16	0.1	0.043	0.8006(66)	0.666...
	24	0.1	0.178	0.7270(89)	
	32	0.1	0.851	0.703(12)	
	40	0.1	0.165	0.663(13)	
	16	1	0.134	0.7615(21)	
	24	1	1.125	0.7096(30)	
	32	1	0.423	0.6678(37)	
	36	1	0.319	0.6566(66)	
	16	10	0.728	0.666(33)	

Table 6.14: The scaling dimension obtained from the fit of $\langle A_2 A_2 \rangle$ for Eq. (6.51) with various values of β. The fitted momentum range is $\frac{2\pi}{L} \leq |p| < \frac{4\pi}{L}$.

A_I	L/a	β	χ^2/d.o.f.	$1-h-\bar{h}$	Expected value
A_2	16	0.1	0.060	0.7963(63)	0.666...
	24	0.1	0.052	0.7422(88)	
	32	0.1	0.308	0.696(11)	
	40	0.1	0.725	0.663(12)	
	16	1	0.062	0.7612(21)	
	24	1	0.705	0.7100(29)	
	32	1	0.273	0.6719(35)	
	36	1	0.338	0.6616(62)	
	16	10	0.755	0.618(32)	

Table 6.15: The scaling dimension obtained from the fit of $\langle A_3 A_3 \rangle$ for Eq. (6.51) with various values of β. The fitted momentum range is $\frac{2\pi}{L} \leq |p| < \frac{4\pi}{L}$.

A_I	L/a	β	χ^2/d.o.f.	$1-h-\bar{h}$	Expected value
A_3	16	0.1	0.086	0.7979(63)	0.666...
	24	0.1	0.094	0.7460(89)	
	32	0.1	0.299	0.706(14)	
	40	0.1	0.269	0.665(13)	
	16	1	0.201	0.7620(23)	
	24	1	0.941	0.7087(28)	
	32	1	0.269	0.6691(36)	
	36	1	0.403	0.6545(57)	
	16	10	0.531	0.618(23)	

Table 6.16: The central charge obtained from the fit of the EMT correlator for Eq. (6.51) with various values of β. The fitted momentum range is $\frac{2\pi}{L} \leq |p| < \frac{4\pi}{L}$.

L/a	β	χ^2/d.o.f.	c	Expected value
16	0.1	2.176	3.725(62)	3
24	0.1	1.437	3.503(65)	
32	0.1	0.753	3.391(80)	
40	0.1	0.630	2.860(76)	
16	1	7.789	3.642(33)	
24	1	1.514	3.439(35)	
32	1	0.741	3.238(37)	
36	1	0.668	3.203(59)	
16	10	1.068	2.84(23)	

Chapter 7

Conclusions

In this thesis, we numerically studied the 2D $\mathcal{N} = 2$ Wess–Zumino (WZ) model, which is believed to provide the Landau–Ginzburg (LG) description of an $\mathcal{N} = 2$ superconformal field theory (SCFT). We employed the exactly supersymmetric formulation [75] on the basis of the momentum cutoff regularization and the Nicolai map. This formulation allows a straightforward construction of the Noether currents, that is, the supercurrent, the energy-momentum tensor, and the $U(1)$ current.

First, the ADE-type WZ model with one or two superfields was focused [80, 81], which corresponds to the minimal model at the IR fixed point. Then, we observed that the Witten index is reproduced and some SUSY WT relations hold non-perturbatively. From the IR behavior of the two-point functions in the momentum space, we numerically measured the scaling dimension $h+\bar{h}$ and the central charge c (Table 7.1); for the measurement of the central charge, we directly computed the energy-momentum tensor T_{zz}. These results, together with the flow of the "effective central charges," are consistent with the theoretical conjecture of the WZ/minimal-model correspondence. We have the numerical evidences for the various typical minimal models: the A_2, A_3, D_3, D_4, E_6 ($\cong A_2 \otimes A_3$), and E_7 models.

Table 7.1: The scaling dimensions and the central charges obtained.

Algebra	$1 - h - \bar{h}$	Expected value	c	Expected value
A_2	0.682(10)(7)	0.666...	1.061(36)(34)	1
A_3	0.747(11)(12)	0.75	1.415(36)(36)	1.5
D_3			1.595(31)(41)	1.5
D_4			2.172(48)(39)	2
E_7			2.638(47)(59)	2.666...

Second, we considered the continuum limit analysis for the scaling dimension [84]. We developed the extrapolation method to take the continuum/infinite-volume limit, $a/L \to 0$, based on the finite-size scaling. Then, we performed precision measurement of $h + \bar{h}$ in the A_2-type theory, and obtained

$$1 - h - \bar{h} = 0.6699(77)(87). \tag{7.1}$$

This result is quit consistent with the expected value of the A_2 minimal model. Our discussion there supports the restoration of the locality in the continuum limit.

Third, we apply the above method to the non-minimal SCFT associated with the torus compactification of superstring theory. We deformed the geometry of the torus compactification that from the $A_2 \otimes A_2 \otimes A_2$ Gepner model. To do this, we added the operator xyz to the superpotential $x^3 + y^3 + z^3$. It is believed that this operator is marginal, and so, the central charge c is identically equal to 3 under this deformation. We numerically observed this fact, and provided the non-perturbative evidence of the conjecture that the operator xyz is marginal.

All these studies show a coherence picture which is consistent with the conjectured LG description of SCFT. Although the theoretical basis of this numerical approach is not obvious because of the non-locality, our investigations support the validity of the formulation. Of course, it is important to confirm further the theoretical validity of the formulation, that is, the restoration of the locality of the theory. We hope that the numerical approaches, when further developed, will be useful to study dynamics of the superstring compactification via the LG/CY correspondence.

For a possible application to the CY compactification, a simulation of the A_4-type theory with the superpotential $W = \Phi^5$ will be an important starting point. This is because a CY manifold is given by the tensor product of the five A_4 minimal models. A related issue with the continuum-limit analysis is to consider the continuum limit for the central charge. It is also interesting to compute the Zamolodchikov's C-function directly. These could be analyzed by the gradient-flow method [116, 122] in a lattice formulation such as that in Ref. [61, 62].[1].

[1]By employing the gradient-flow method, one can construct a regularization-independent form of the Noether current associated spacetime symmetries [123–127]. There also are various analyses for the relation between the gradient flow and the renormalization group flow [128–138]

Appendix A

A fast algorithm for the Jacobian computation

A.1 Jacobian in the $N_\Phi = 1$ WZ model

We can accelerate the computation of $\mathrm{sign}\det\frac{\partial(N,N^*)}{\partial(A,A^*)}$ by effectively halving the size of the matrix,

$$\frac{\partial(N,N^*)}{\partial(A,A^*)} = \begin{pmatrix} 2ip_z & W''(A)^* * \\ W''(A) * & 2ip_{\bar{z}} \end{pmatrix}, \tag{A.1}$$

whose p,q element is

$$\begin{aligned}\left[\frac{\partial(N,N^*)}{\partial(A,A^*)}\right]_{p,q} &= \begin{pmatrix} 2ip_z\delta_{p,q} & \frac{1}{L_0L_1}W''(A)(q-p)^* \\ \frac{1}{L_0L_1}W''(A)(p-q) & 2ip_{\bar{z}}\delta_{p,q} \end{pmatrix} \\ &= \begin{pmatrix} 2ip_z\delta_{p,q} & \frac{1}{L_0L_1}W''(A)(p-q)^\dagger \\ \frac{1}{L_0L_1}W''(A)(p-q) & 2ip_{\bar{z}}\delta_{p,q} \end{pmatrix}. \end{aligned} \tag{A.2}$$

Note that Eq. (A.2) is a $[2(N_0+1)(N_1+1)]\times[2(N_0+1)(N_1+1)]$ matrix when the momentum takes the values

$$p_\mu = \frac{2\pi}{L_\mu}n_\mu, \qquad n_\mu = 0, \pm 1, \ldots, \pm\frac{N_\mu}{2a}, \tag{A.3}$$

where we have assumed that both integers N_0 and N_1 are even,

We write the matrix in Eq. (A.2) as

$$\frac{\partial(N,N^*)}{\partial(A,A^*)} \equiv \begin{pmatrix} iP & W^\dagger \\ W & iP^\dagger \end{pmatrix}. \tag{A.4}$$

It should be noted that the diagonal matrix P, whose p,q element is $2p_z\delta_{p,q}$, does not have an inverse because it has zero at $p=0$; what we want to do is to remove this zero.

Considering the case that P and W are 3×3 matrices for simplicity, we can confirm that the determinant of the matrix in Eq. (A.4) can be deformed as

$$\det \begin{pmatrix} \lambda_1 & & & & W^\dagger & \\ & 0 & & & & \\ & & \lambda_2 & & & \\ W_{11} & W_{12} & W_{13} & \lambda_3 & & \\ W_{21} & W_{22} & W_{23} & & 0 & \\ W_{31} & W_{32} & W_{33} & & & \lambda_4 \end{pmatrix} = -|W_{22}|^2 \det \begin{pmatrix} \lambda_1 & & \widetilde{W}^*_{11} & \widetilde{W}^*_{31} \\ & \lambda_2 & \widetilde{W}^*_{13} & \widetilde{W}^*_{33} \\ \widetilde{W}_{11} & \widetilde{W}_{13} & \lambda_3 & \\ \widetilde{W}_{31} & \widetilde{W}_{33} & & \lambda_4 \end{pmatrix}, \tag{A.5}$$

where

$$\widetilde{W}_{ij} \equiv \frac{1}{W_{22}} \det \begin{pmatrix} W_{ij} & W_{i2} \\ W_{2j} & W_{22} \end{pmatrix}. \tag{A.6}$$

In an analogous way, we can write, for the general case,

$$\det \begin{pmatrix} iP & W^\dagger \\ W & iP^\dagger \end{pmatrix} = -|W_{0,0}|^2 \det{}' \begin{pmatrix} iP & \widetilde{W}^\dagger \\ \widetilde{W} & iP^\dagger \end{pmatrix}, \tag{A.7}$$

where $W_{0,0}$ is the component at $(p, q) = (0, 0)$, $\det'$ is the determinant in the subspace in which the components with $p = 0$ or $q = 0$ are omitted, and

$$\widetilde{W}_{p,q} = \frac{1}{W_{0,0}} \det \begin{pmatrix} W_{p,q} & W_{p,0} \\ W_{0,q} & W_{0,0} \end{pmatrix}. \tag{A.8}$$

Note that this is simply the determinant of a 2×2 matrix.

Since the right-hand side of Eq. (A.7) refers to the subspace in which P has an inverse, the Jacobian can be expressed as

$$\det \begin{pmatrix} iP & W^\dagger \\ W & iP^\dagger \end{pmatrix} = -|W_{0,0}|^2 \det{}' \begin{pmatrix} iP & 0 \\ \widetilde{W} & I \end{pmatrix} \det{}' \begin{pmatrix} I & (-i)P^{-1}\widetilde{W}^\dagger \\ 0 & iP^\dagger - \widetilde{W}(-i)P^{-1}\widetilde{W}^\dagger \end{pmatrix} \tag{A.9}$$

$$= -|W_{0,0}|^2 \det{}' \left(-PP^\dagger - P\widetilde{W}P^{-1}\widetilde{W}^\dagger \right). \tag{A.10}$$

Here, the inverse of P is given by

$$\left(P^{-1}\right)_{p,q} = \frac{1}{2p_z}\delta_{p,q} = \frac{p_{\bar{z}}}{2|p_z|^2}\delta_{p,q}. \tag{A.11}$$

Thus, substituting the matrix elements in Eq. (A.2), we have

$$\det \begin{pmatrix} iP & W^\dagger \\ W & iP^\dagger \end{pmatrix} = -\det{}'(-1) \left| \frac{1}{L_0 L_1} W''(A)(0) \right|^2 \times \det{}' \left[4|p_z|^2\delta_{p,q} + \left(\frac{1}{L_0 L_1} \right)^2 \sum_{l \neq 0} \frac{p_z}{l_z} \widetilde{W}''(A)(p-l)\widetilde{W}''(A)(l-q)^\dagger \right], \tag{A.12}$$

where for $p \neq 0$,

$$\begin{aligned}\widetilde{W}''(A)(p-l) &\equiv \frac{1}{W''(A)(0)} \det \begin{pmatrix} W''(A)(p-l) & W''(A)(p-0) \\ W''(A)(0-l) & W''(A)(0-0) \end{pmatrix} \\ &= \frac{1}{W''(A)(0)} \left[W''(A)(p-l)W''(A)(0) - W''(A)(pW''(A)(-l) \right]. \end{aligned} \tag{A.13}$$

Here, the factor $\det'(-1)$ is

$$\det'(-1) = (-1)^{(N_0+1)(N_1+1)-1} = +1, \tag{A.14}$$

for N_0 and N_1 are even.

Thus, finally, the sign of the Jacobian is given by the sign of the determinant of a matrix with smaller dimensions $[(N_0+1)(N_1+1)-1] \times [(N_0+1)(N_1+1)-1]$, as

$$\begin{aligned} &\operatorname{sign}\det \begin{pmatrix} iP & W^\dagger \\ W & iP^\dagger \end{pmatrix} \\ &= -\det'(-1) \operatorname{sign}\det' \left[4|p_z|^2 \delta_{p,q} + \left(\frac{1}{L_0 L_1} \right)^2 \sum_{l \neq 0} \frac{p_z}{l_z} \widetilde{W}''(A)(p-l) \widetilde{W}''(A)(q-l)^* \right]. \end{aligned} \tag{A.15}$$

Since the computational cost required for the matrix determinant is $O(N^3)$ for a matrix of size N, this representation reduces the cost by $\sim 1/8$.

It turns out that the above sign is mainly negative for most of configurations of $A(p)$. Since the overall sign of $\operatorname{sign}\det \frac{\partial(N,N^*)}{\partial(A,A^*)}$ is irrelevant in the expectation value of Eq. (5.20), we regard Eq. (A.15) as[1]

$$-\operatorname{sign}\det \frac{\partial(N,N^*)}{\partial(A,A^*)}. \tag{A.16}$$

A.2 Jacobian in the $N_\Phi = 2, 3$ WZ model

For the WZ model with multiple superfields, we write the Jacobian as

$$\det \frac{\partial(\{N\},\{N^*\})}{\partial(\{A\},\{A^*\})} = \det \begin{pmatrix} 2i\delta_{IJ} p_z \delta_{p,q} & \frac{1}{L_0 L_1} \partial_I \partial_J W(A)(p-q)^\dagger \\ \frac{1}{L_0 L_1} \partial_I \partial_J W(A)(p-q) & 2i\delta_{IJ} p_{\bar{z}} \delta_{p,q} \end{pmatrix} \tag{A.17}$$

$$\equiv \det \begin{pmatrix} iP & W_{11}^\dagger & 0 & W_{12}^\dagger & \dots \\ W_{11} & iP^\dagger & W_{12} & 0 & \dots \\ 0 & W_{21}^\dagger & iP & W_{22}^\dagger & \dots \\ W_{21} & 0 & W_{22} & iP^\dagger & \dots \\ \vdots & \vdots & \vdots & \vdots & \ddots \end{pmatrix}, \tag{A.18}$$

where I, J run over 1, 2, …, N_Φ, and $\partial_I \equiv \partial/\partial A_I$ This Jacobian is the determinant of a $[2N_\Phi(N_0+1)(N_1+1)] \times [2N_\Phi(N_0+1)(N_1+1)]$ matrix and the momentum takes the values given in (A.3)

[1] Or we may simply say that the partition function (5.15) is defined with another negative sign.

Note the for the determinant of invertible block matrices M_{ij},

$$\det \begin{pmatrix} M_{11} & M_{12} \\ M_{21} & M_{22} \end{pmatrix} = \det M_{22} \det \left(M_{11} - M_{12} M_{22}^{-2} M_{21} \right), \tag{A.19}$$

and

$$\begin{aligned} &\det \begin{pmatrix} M_{11} & M_{12} & M_{13} \\ M_{21} & M_{22} & M_{23} \\ M_{31} & M_{32} & M_{33} \end{pmatrix} \\ &= \det M_{33} \det \left(M_{22} - M_{23} M_{33}^{-1} M_{32} \right) \\ &\quad \times \det \Big[\left(M_{11} - M_{13} M_{33}^{-1} M_{31} \right) \\ &\qquad - \left(M_{12} - M_{13} M_{33}^{-1} M_{32} \right) \left(M_{22} - M_{23} M_{33}^{-1} M_{32} \right)^{-1} \left(M_{21} - M_{23} M_{33}^{-1} M_{31} \right) \Big]. \end{aligned} \tag{A.20}$$

Thus, we have the Jacobian as the determinant of a matrix with smaller dimensions $[2(N_\Phi - 1)(N_0 + 1)(N_1 + 1)] \times [2(N_\Phi - 1)(N_0 + 1)(N_1 + 1)]$ for $N_\Phi = 2$,

$$\det \frac{\partial(\{N\}, \{N^*\})}{\partial(\{A\}, \{A^*\})}$$

$$= (-1)^2 \det \begin{pmatrix} W_{11} & iP^\dagger & W_{12} & 0 \\ iP & W_{11}^\dagger & 0 & W_{12}^\dagger \\ W_{21} & 0 & W_{22} & iP^\dagger \\ 0 & W_{21}^\dagger & iP & W_{22}^\dagger \end{pmatrix} \tag{A.21}$$

$$= \det \begin{pmatrix} W_{21} & 0 & W_{22} & iP^\dagger \\ 0 & W_{21}^\dagger & iP & W_{22}^\dagger \\ W_{11} & iP^\dagger & W_{12} & 0 \\ iP & W_{11}^\dagger & 0 & W_{12}^\dagger \end{pmatrix} \tag{A.22}$$

$$\begin{aligned} &= |\det W_{12}|^2 \\ &\quad \times \det \left[\begin{pmatrix} W_{21} & \\ & W_{21}^\dagger \end{pmatrix} - \begin{pmatrix} W_{22} & iP^\dagger \\ iP & W_{22}^\dagger \end{pmatrix} \begin{pmatrix} (W_{12})^{-1} & \\ & (W_{12}^\dagger)^{-1} \end{pmatrix} \begin{pmatrix} W_{11} & iP^\dagger \\ iP & W_{11}^\dagger \end{pmatrix} \right], \end{aligned} \tag{A.23}$$

and for $N_\Phi = 3$,

$$
\begin{aligned}
&\det \frac{\partial(\{N\},\{N^*\})}{\partial(\{A\},\{A^*\})} \\
&= (-1)^3 \det \begin{pmatrix}
W_{21} & 0 & W_{22} & iP^\dagger & W_{23} & 0 \\
0 & W_{21}^\dagger & iP & W_{22}^\dagger & 0 & W_{23}^\dagger \\
W_{11} & iP^\dagger & W_{12} & 0 & W_{13} & 0 \\
iP & W_{11}^\dagger & 0 & W_{12}^\dagger & 0 & W_{13}^\dagger \\
W_{31} & 0 & W_{32} & 0 & W_{33} & iP^\dagger \\
0 & W_{31}^\dagger & 0 & W_{32}^\dagger & iP & W_{33}^\dagger
\end{pmatrix} \qquad \text{(A.24)} \\
&= (-1)^3 |\det W_{21}|^2 \\
&\quad \times \det \left[\begin{pmatrix}
W_{12} & 0 & W_{13} & 0 \\
0 & W_{12}^\dagger & 0 & W_{13}^\dagger \\
W_{32} & 0 & W_{33} & iP^\dagger \\
0 & W_{32}^\dagger & iP & W_{33}^\dagger
\end{pmatrix} \right. \\
&\qquad \left. - \begin{pmatrix}
W_{11} & iP^\dagger \\
iP & W_{11}^\dagger \\
W_{31} & 0 \\
0 & W_{31}^\dagger
\end{pmatrix} \begin{pmatrix}
(W_{21})^{-1} & \\
& (W_{21}^\dagger)^{-1}
\end{pmatrix} \begin{pmatrix}
W_{22} & iP^\dagger & W_{23} & 0 \\
iP & W_{22}^\dagger & 0 & W_{23}^\dagger
\end{pmatrix} \right]. \qquad \text{(A.25)}
\end{aligned}
$$

Bibliography

[1] K. Wilson and J. B. Kogut, "The Renormalization group and the ϵ expansion," *Phys. Rept.* **12** (1974) 75–199.

[2] A. M. Polyakov, "Conformal symmetry of critical fluctuations," *JETP Lett.* **12** (1970) 381–383.

[3] A. Zamolodchikov, "Conformal Symmetry and Multicritical Points in Two-Dimensional Quantum Field Theory. (In Russian)," *Sov. J. Nucl. Phys.* **44** (1986) 529–533.

[4] V. Ginzburg and L. Landau, "On the Theory of superconductivity," *Zh. Eksp. Teor. Fiz.* **20** (1950) 1064–1082.

[5] B. Feigin and D. Fuks, "Invariant skew symmetric differential operators on the line and verma modules over the Virasoro algebra," *Funct. Anal. Appl.* **16** (1982) 114–126.

[6] B. Feigin and D. Fuks, "Verma modules over the Virasoro algebra," *Funct. Anal. Appl.* **17** (1983) 241–241.

[7] V. Dotsenko and V. Fateev, "Conformal Algebra and Multipoint Correlation Functions in Two-Dimensional Statistical Models," *Nucl. Phys. B* **240** (1984) 312.

[8] G. Felder, "BRST Approach to Minimal Models," *Nucl. Phys. B* **317** (1989) 215. [Erratum: Nucl.Phys.B 324, 548 (1989)].

[9] J.-L. Gervais and B. Sakita, "Field Theory Interpretation of Supergauges in Dual Models," *Nucl. Phys. B* **34** (1971) 632–639.

[10] Y. Golfand and E. Likhtman, "Extension of the Algebra of Poincare Group Generators and Violation of P Invariance," *JETP Lett.* **13** (1971) 323–326.

[11] D. Volkov and V. Akulov, "Possible universal neutrino interaction," *JETP Lett.* **16** (1972) 438–440.

[12] T. Yoneya, "Quantum gravity and the zero slope limit of the generalized Virasoro model," *Lett. Nuovo Cim.* **8** (1973) 951–955.

[13] T. Yoneya, "Connection of Dual Models to Electrodynamics and Gravidynamics," *Prog. Theor. Phys.* **51** (1974) 1907–1920.

[14] T. Yoneya, "Geometry, Gravity and Dual Strings," *Prog. Theor. Phys.* **56** (1976) 1310.

[15] J. Scherk, "An Introduction to the Theory of Dual Models and Strings," *Rev. Mod. Phys.* **47** (1975) 123–164.

[16] J. H. Schwarz, "Superstring Theory," *Phys. Rept.* **89** (1982) 223–322.

[17] P. Ramond, "Dual Theory for Free Fermions," *Phys. Rev. D* **3** (1971) 2415–2418.

[18] A. Neveu and J. Schwarz, "Quark Model of Dual Pions," *Phys. Rev. D* **4** (1971) 1109–1111.

[19] A. Neveu and J. Schwarz, "Factorizable dual model of pions," *Nucl. Phys. B* **31** (1971) 86–112.

[20] P. Goddard, C. Rebbi, and C. B. Thorn, "Lorentz covariance and the physical states in dual resonance models," *Nuovo Cim. A* **12** (1972) 425–441.

[21] J. Schwarz, "Physical States and Pomeron Poles in the Dual Pion Model," *Nucl. Phys. B* **46** (1972) 61–74.

[22] R. Brower and K. Friedman, "Spectrum Generating Algebra and No Ghost Theorem for the Neveu-schwarz Model," *Phys. Rev. D* **7** (1973) 535–539.

[23] J. H. Schwarz, "Dual resonance theory," *Phys. Rept.* **8** (1973) 269–335.

[24] E. Calabi, "On Kähler manifolds with vanishing canonical class," in *Algebraic Geometry and Topology: A Symposium in Honor of S. Lefschetz*, pp. 78–89. Princeton University Press, 1957.

[25] S.-T. Yau, "Calabi's Conjecture and some new results in algebraic geometry," *Proc. Nat. Acad. Sci.* **74** (1977) 1798–1799.

[26] D. Gepner, "Space-Time Supersymmetry in Compactified String Theory and Superconformal Models," *Nucl. Phys. B* **296** (1988) 757.

[27] D. Gepner, "Exactly Solvable String Compactifications on Manifolds of SU(N) Holonomy," *Phys. Lett. B* **199** (1987) 380–388.

[28] P. Di Vecchia, J. Petersen, and H. Zheng, "N=2 Extended Superconformal Theories in Two-Dimensions," *Phys. Lett. B* **162** (1985) 327–332.

[29] P. Di Vecchia, J. Petersen, and M. Yu, "On the Unitary Representations of N=2 Superconformal Theory," *Phys. Lett. B* **172** (1986) 211–215.

[30] P. Di Vecchia, J. Petersen, M. Yu, and H. Zheng, "Explicit Construction of Unitary Representations of the N=2 Superconformal Algebra," *Phys. Lett. B* **174** (1986) 280–284.

[31] W. Boucher, D. Friedan, and A. Kent, "Determinant Formulae and Unitarity for the N=2 Superconformal Algebras in Two-Dimensions or Exact Results on String Compactification," *Phys. Lett. B* **172** (1986) 316.

[32] D. Gepner, "On the Spectrum of 2D Conformal Field Theories," *Nucl. Phys. B* **287** (1987) 111–130.

[33] A. Cappelli, C. Itzykson, and J. Zuber, "Modular Invariant Partition Functions in Two-Dimensions," *Nucl. Phys. B* **280** (1987) 445–465.

[34] A. Cappelli, "Modular Invariant Partition Functions of Superconformal Theories," *Phys. Lett. B* **185** (1987) 82–88.

[35] D. Gepner and Z.-a. Qiu, "Modular Invariant Partition Functions for Parafermionic Field Theories," *Nucl. Phys. B* **285** (1987) 423.

[36] A. Cappelli, C. Itzykson, and J. Zuber, "The ADE Classification of Minimal and A1(1) Conformal Invariant Theories," *Commun. Math. Phys.* **113** (1987) 1.

[37] A. Kato, "Classification of Modular Invariant Partition Functions in Two-dimensions," *Mod. Phys. Lett. A* **2** (1987) 585.

[38] J. Wess and B. Zumino, "Supergauge Transformations in Four-Dimensions," *Nucl. Phys. B* **70** (1974) 39–50.

[39] E. J. Martinec, "Algebraic Geometry and Effective Lagrangians," *Phys. Lett. B* **217** (1989) 431–437.

[40] S. Cecotti, "Geometry of N=2 Landau-Ginzburg families," *Nucl. Phys. B* **355** (1991) 755–775.

[41] B. R. Greene, C. Vafa, and N. Warner, "Calabi-Yau Manifolds and Renormalization Group Flows," *Nucl. Phys. B* **324** (1989) 371.

[42] E. Witten, "Phases of N=2 theories in two-dimensions," *AMS/IP Stud. Adv. Math.* **1** (1996) 143–211, `arXiv:hep-th/9301042`.

[43] D. Kastor, E. Martinec, and S. Shenker, "RG Flow in N=1 Discrete Series," *Nucl. Phys. B* **316** (1989) 590–608.

[44] C. Vafa and N. P. Warner, "Catastrophes and the Classification of Conformal Theories," *Phys. Lett. B* **218** (1989) 51–58.

[45] W. Lerche, C. Vafa, and N. P. Warner, "Chiral Rings in N=2 Superconformal Theories," *Nucl. Phys. B* **324** (1989) 427–474.

[46] P. S. Howe and P. C. West, "$N = 2$ Superconformal Models, Landau-ginzburg Hamiltonians and the ϵ Expansion," *Phys. Lett. B* **223** (1989) 377–385.

[47] S. Cecotti, L. Girardello, and A. Pasquinucci, "Nonperturbative Aspects and Exact Results for the $N = 2$ Landau-ginzburg Models," *Nucl. Phys. B* **328** (1989) 701–722.

[48] P. S. Howe and P. C. West, "Chiral Correlators in Landau-ginzburg Theories and $N = 2$ Superconformal Models," *Phys. Lett. B* **227** (1989) 397–405.

[49] S. Cecotti, L. Girardello, and A. Pasquinucci, "Singularity Theory and $N = 2$ Supersymmetry," *Int. J. Mod. Phys. A* **6** (1991) 2427–2496.

[50] S. Cecotti, "N=2 Landau-Ginzburg versus Calabi-Yau sigma models: Nonperturbative aspects," *Int. J. Mod. Phys. A* **6** (1991) 1749–1814.

[51] P. S. Howe and P. C. West, "Fixed points in multifield Landau-Ginsburg models," *Phys. Lett. B* **244** (1990) 270–274.

[52] E. Witten, "On the Landau-Ginzburg description of N=2 minimal models," *Int. J. Mod. Phys. A* **9** (1994) 4783–4800, arXiv:hep-th/9304026.

[53] J. Polchinski, *String theory. Vol. 2: Superstring theory and beyond*. Cambridge Monographs on Mathematical Physics. Cambridge University Press, Cambridge, 1998.

[54] K. Hori, S. Katz, A. Klemm, R. Pandharipande, R. Thomas, C. Vafa, R. Vakil, and E. Zaslow, *Mirror symmetry*. Clay mathematics monographs. AMS, Providence, USA, 2003.

[55] K. G. Wilson, "Confinement of Quarks," *Phys. Rev. D* **10** (1974) 2445–2459.

[56] G. Curci and G. Veneziano, "Supersymmetry and the Lattice: A Reconciliation?," *Nucl. Phys. B* **292** (1987) 555–572.

[57] D. B. Kaplan, "Dynamical Generation of Supersymmetry," *Phys. Lett. B* **136** (1984) 162–164.

[58] **DESY-Munster-Roma**, F. Farchioni, C. Gebert, R. Kirchner, I. Montvay, A. Feo, G. Munster, T. Galla, and A. Vladikas, "The Supersymmetric Ward identities on the lattice," *Eur. Phys. J. C* **23** (2002) 719–734, arXiv:hep-lat/0111008.

[59] S. Ali, H. Gerber, I. Montvay, G. Münster, S. Piemonte, P. Scior, and G. Bergner, "Analysis of Ward identities in supersymmetric Yang–Mills theory," *Eur. Phys. J. C* **78** no. 5, (2018) 404, arXiv:1802.07067 [hep-lat].

[60] D. Kadoh, "Recent progress in lattice supersymmetry: from lattice gauge theory to black holes," *PoS* **LATTICE2015** (2016) 017, arXiv:1607.01170 [hep-lat].

[61] H. Kawai and Y. Kikukawa, "A Lattice study of N=2 Landau-Ginzburg model using a Nicolai map," *Phys. Rev. D* **83** (2011) 074502, arXiv:1005.4671 [hep-lat].

[62] Y. Kikukawa and Y. Nakayama, "Nicolai mapping versus exact chiral symmetry on the lattice," *Phys. Rev. D* **66** (2002) 094508, arXiv:hep-lat/0207013.

[63] M. Beccaria, G. Curci, and E. D'Ambrosio, "Simulation of supersymmetric models with a local Nicolai map," *Phys. Rev. D* **58** (1998) 065009, arXiv:hep-lat/9804010.

[64] S. Catterall and S. Karamov, "Exact lattice supersymmetry: The Two-dimensional N=2 Wess-Zumino model," *Phys. Rev. D* **65** (2002) 094501, arXiv:hep-lat/0108024.

[65] J. Giedt, "R-symmetry in the Q-exact (2,2) 2-D lattice Wess-Zumino model," *Nucl. Phys. B* **726** (2005) 210–232, arXiv:hep-lat/0507016.

[66] G. Bergner, T. Kaestner, S. Uhlmann, and A. Wipf, "Low-dimensional Supersymmetric Lattice Models," *Annals Phys.* **323** (2008) 946–988, arXiv:0705.2212 [hep-lat].

[67] T. Kastner, G. Bergner, S. Uhlmann, A. Wipf, and C. Wozar, "Two-Dimensional Wess-Zumino Models at Intermediate Couplings," *Phys. Rev. D* **78** (2008) 095001, arXiv:0807.1905 [hep-lat].

[68] N. Sakai and M. Sakamoto, "Lattice Supersymmetry and the Nicolai Mapping," *Nucl. Phys. B* **229** (1983) 173–188.

[69] H. Nicolai, "On a New Characterization of Scalar Supersymmetric Theories," *Phys. Lett. B* **89** (1980) 341.

[70] H. Nicolai, "Supersymmetry and Functional Integration Measures," *Nucl. Phys. B* **176** (1980) 419–428.

[71] G. Parisi and N. Sourlas, "Supersymmetric Field Theories and Stochastic Differential Equations," *Nucl. Phys. B* **206** (1982) 321–332.

[72] S. Cecotti and L. Girardello, "STOCHASTIC AND PARASTOCHASTIC ASPECTS OF SUPERSYMMETRIC FUNCTIONAL MEASURES: A NEW NONPERTURBATIVE APPROACH TO SUPERSYMMETRY," *Annals Phys.* **145** (1983) 81–99.

[73] J. Giedt and E. Poppitz, "Lattice supersymmetry, superfields and renormalization," *JHEP* **09** (2004) 029, arXiv:hep-th/0407135.

[74] D. Kadoh and H. Suzuki, "Supersymmetry restoration in lattice formulations of 2D $\mathcal{N} = (2, 2)$ WZ model based on the Nicolai map," *Phys. Lett. B* **696** (2011) 163–166, arXiv:1011.0788 [hep-lat].

[75] S. Kamata and H. Suzuki, "Numerical simulation of the $\mathcal{N} = (2, 2)$ Landau-Ginzburg model," *Nucl. Phys. B* **854** (2012) 552–574, arXiv:1107.1367 [hep-lat].

[76] D. Kadoh and H. Suzuki, "Supersymmetric nonperturbative formulation of the WZ model in lower dimensions," *Phys. Lett. B* **684** (2010) 167–172, arXiv:0909.3686 [hep-th].

[77] J. Bartels and J. Bronzan, "SUPERSYMMETRY ON A LATTICE," *Phys. Rev. D* **28** (1983) 818.

[78] S. Drell, M. Weinstein, and S. Yankielowicz, "Variational Approach to Strong Coupling Field Theory. 1. Phi**4 Theory," *Phys. Rev. D* **14** (1976) 487.

[79] S. Drell, M. Weinstein, and S. Yankielowicz, "Strong Coupling Field Theories. 2. Fermions and Gauge Fields on a Lattice," *Phys. Rev. D* **14** (1976) 1627.

[80] O. Morikawa and H. Suzuki, "Numerical study of the $\mathcal{N} = 2$ Landau–Ginzburg model," *PTEP* **2018** no. 8, (2018) 083B05, arXiv:1805.10735 [hep-lat].

[81] O. Morikawa, "Numerical study of the $\mathcal{N} = 2$ Landau–Ginzburg model with two superfields," *JHEP* **12** (2018) 045, arXiv:1810.02519 [hep-lat].

[82] A. Zamolodchikov, "Irreversibility of the Flux of the Renormalization Group in a 2D Field Theory," *JETP Lett.* **43** (1986) 730–732.

[83] A. Cappelli and J. I. Latorre, "Perturbation Theory of Higher Spin Conserved Currents Off Criticality," *Nucl. Phys. B* **340** (1990) 659–691.

[84] O. Morikawa, "Continuum limit in numerical simulations of the $\mathcal{N} = 2$ Landau–Ginzburg model," *PTEP* **2019** no. 10, (2019) 103B03, arXiv:1906.00653 [hep-lat].

[85] J. Polchinski, *String theory. Vol. 1: An introduction to the bosonic string*. Cambridge Monographs on Mathematical Physics. Cambridge University Press, Cambridge, 1998.

[86] H. Weyl, "Gravitation and electricity," *Sitzungsber. Preuss. Akad. Wiss. Berlin (Math. Phys.)* **1918** (1918) 465.

[87] H. Weyl, "A New Extension of Relativity Theory," *Annalen Phys.* **59** (1919) 101–133.

[88] D. Capper and M. Duff, "Trace anomalies in dimensional regularization," *Nuovo Cim. A* **23** (1974) 173–183.

[89] S. Deser, M. Duff, and C. Isham, "Nonlocal Conformal Anomalies," *Nucl. Phys. B* **111** (1976) 45–55.

[90] M. Duff, "Twenty years of the Weyl anomaly," *Class. Quant. Grav.* **11** (1994) 1387–1404, arXiv:hep-th/9308075.

[91] J. C. Ward, "An Identity in Quantum Electrodynamics," *Phys. Rev.* **78** (1950) 182.

[92] Y. Takahashi, "On the generalized Ward identity," *Nuovo Cim.* **6** (1957) 371.

[93] A. Belavin, A. M. Polyakov, and A. Zamolodchikov, "Infinite Conformal Symmetry in Two-Dimensional Quantum Field Theory," *Nucl. Phys. B* **241** (1984) 333–380.

[94] M. Virasoro, "Subsidiary conditions and ghosts in dual resonance models," *Phys. Rev. D* **1** (1970) 2933–2936.

[95] D. Verma, "Structure of certain induced representations of complex semisimple Lie algebras," *Bull. Amer. Math. Soc.* **70** (1968) 160–166.

[96] I. Bernstein, I. Gelfand, and S. Gelfand, "Structure of representations generated by vectors of highest weight," *Funkts. Anal. Prilozh.* **5** (1971) 1–9.

[97] V. Kac, "Contravariant Form for Infinite Dimensional Lie Algebras and Superalgebras," in *7th International Group Theory Colloquium: The Integrative Conference on Group Theory and Mathematical Physics*, pp. 441–445. 1, 1978.

[98] G. Andrews, R. Baxter, and P. Forrester, "Eight vertex SOS model and generalized Rogers-Ramanujan type identities," *J. Statist. Phys.* **35** (1984) 193–266.

[99] D. A. Huse, "Exact exponents for infinitely many new multicritical points," *Phys. Rev. B* **30** (1984) 3908–3915.

[100] E. Witten, "Constraints on Supersymmetry Breaking," *Nucl. Phys. B* **202** (1982) 253.

[101] S. Cecotti and L. Girardello, "Functional Measure, Topology and Dynamical Supersymmetry Breaking," *Phys. Lett. B* **110** (1982) 39.

[102] F. Ravanini and S.-K. Yang, "Modular Invariance in $N = 2$ Superconformal Field Theories," *Phys. Lett. B* **195** (1987) 202–208.

[103] J. Polchinski, "Scale and Conformal Invariance in Quantum Field Theory," *Nucl. Phys. B* **303** (1988) 226–236.

[104] Y. Nakayama, "Scale invariance vs conformal invariance," *Phys. Rept.* **569** (2015) 1–93, `arXiv:1302.0884 [hep-th]`.

[105] A. A. Tseytlin, "Conditions of Weyl Invariance of Two-dimensional σ Model From Equations of Stationarity of 'Central Charge' Action," *Phys. Lett. B* **194** (1987) 63.

[106] K. Osterwalder and R. Schrader, "AXIOMS FOR EUCLIDEAN GREEN'S FUNCTIONS," *Commun. Math. Phys.* **31** (1973) 83–112.

[107] K. Osterwalder and R. Schrader, "Axioms for Euclidean Green's Functions. 2.," *Commun. Math. Phys.* **42** (1975) 281.

[108] M. T. Grisaru, W. Siegel, and M. Rocek, "Improved Methods for Supergraphs," *Nucl. Phys. B* **159** (1979) 429.

[109] N. Seiberg, "Naturalness versus supersymmetric nonrenormalization theorems," *Phys. Lett. B* **318** (1993) 469–475, `arXiv:hep-ph/9309335`.

[110] N. Seiberg, "The Power of holomorphy: Exact results in 4-D SUSY field theories," in *Particles, Strings, and Cosmology (PASCOS 94)*, pp. 0357–369. 5, 1994. `arXiv:hep-th/9408013`.

[111] P. Fayet and J. Iliopoulos, "Spontaneously Broken Supergauge Symmetries and Goldstone Spinors," *Phys. Lett. B* **51** (1974) 461–464.

[112] P. Dondi and H. Nicolai, "Lattice Supersymmetry," *Nuovo Cim. A* **41** (1977) 1.

[113] L. H. Karsten and J. Smit, "The Vacuum Polarization With {SLAC} Lattice Fermions," *Phys. Lett. B* **85** (1979) 100–102.

[114] M. Kato, M. Sakamoto, and H. So, "Taming the Leibniz Rule on the Lattice," *JHEP* **05** (2008) 057, `arXiv:0803.3121 [hep-lat]`.

[115] G. Bergner, "Complete supersymmetry on the lattice and a No-Go theorem," *JHEP* **01** (2010) 024, `arXiv:0909.4791 [hep-lat]`.

[116] M. Lüscher, "Trivializing maps, the Wilson flow and the HMC algorithm," *Commun. Math. Phys.* **293** (2010) 899–919, `arXiv:0907.5491 [hep-lat]`.

[117] "Eigen." http://eigen.tuxfamily.org/.

[118] "The julia programming language." http://julialang.org/.

[119] V. B. S. J. Bezanson, S. Karpinski and A. Edelman, "Julia: A fast dynamic language for technical computing," arXiv:1209.5145 [cs.PL].

[120] S. K. J. Bezanson, A. Edelman and V. B. Shah, "Julia: A fresh approach to numerical computing," arXiv:1411.1607 [cs.MS].

[121] M. Lüscher, P. Weisz, and U. Wolff, "A Numerical method to compute the running coupling in asymptotically free theories," *Nucl. Phys. B* **359** (1991) 221–243.

[122] M. Lüscher, "Properties and uses of the Wilson flow in lattice QCD," *JHEP* **08** (2010) 071, arXiv:1006.4518 [hep-lat]. [Erratum: JHEP 03, 092 (2014)].

[123] H. Suzuki, "Energy–momentum tensor from the Yang–Mills gradient flow," *PTEP* **2013** (2013) 083B03, arXiv:1304.0533 [hep-lat]. [Erratum: PTEP 2015, 079201 (2015)].

[124] H. Makino and H. Suzuki, "Lattice energy–momentum tensor from the Yang–Mills gradient flow—inclusion of fermion fields," *PTEP* **2014** (2014) 063B02, arXiv:1403.4772 [hep-lat]. [Erratum: PTEP 2015, 079202 (2015)].

[125] H. Makino, F. Sugino, and H. Suzuki, "Large-N limit of the gradient flow in the 2D $O(N)$ nonlinear sigma model," *PTEP* **2015** no. 4, (2015) 043B07, arXiv:1412.8218 [hep-lat].

[126] K. Hieda, A. Kasai, H. Makino, and H. Suzuki, "4D $\mathcal{N} = 1$ SYM supercurrent in terms of the gradient flow," *PTEP* **2017** no. 6, (2017) 063B03, arXiv:1703.04802 [hep-lat].

[127] A. Kasai, O. Morikawa, and H. Suzuki, "Gradient flow representation of the four-dimensional $\mathcal{N} = 2$ super Yang–Mills supercurrent," *PTEP* **2018** no. 11, (2018) 113B02, arXiv:1808.07300 [hep-lat].

[128] M. Lüscher, "Future applications of the Yang-Mills gradient flow in lattice QCD," *PoS* **LATTICE2013** (2014) 016, arXiv:1308.5598 [hep-lat].

[129] A. Kagimura, A. Tomiya, and R. Yamamura, "Effective lattice action for the configurations smeared by the Wilson flow," arXiv:1508.04986 [hep-lat].

[130] R. Yamamura, "The Yang—Mills gradient flow and lattice effective action," *PTEP* **2016** no. 7, (2016) 073B10, arXiv:1510.08208 [hep-lat].

[131] S. Aoki, J. Balog, T. Onogi, and P. Weisz, "Flow equation for the large N scalar model and induced geometries," *PTEP* **2016** no. 8, (2016) 083B04, arXiv:1605.02413 [hep-th].

[132] H. Makino, O. Morikawa, and H. Suzuki, "Gradient flow and the Wilsonian renormalization group flow," *PTEP* **2018** no. 5, (2018) 053B02, arXiv:1802.07897 [hep-th].

[133] Y. Abe and M. Fukuma, "Gradient flow and the renormalization group," *PTEP* **2018** no. 8, (2018) 083B02, arXiv:1805.12094 [hep-th].

[134] A. Carosso, A. Hasenfratz, and E. T. Neil, "Nonperturbative Renormalization of Operators in Near-Conformal Systems Using Gradient Flows," *Phys. Rev. Lett.* **121** no. 20, (2018) 201601, arXiv:1806.01385 [hep-lat].

[135] H. Sonoda and H. Suzuki, "Derivation of a gradient flow from the exact renormalization group," *PTEP* **2019** no. 3, (2019) 033B05, arXiv:1901.05169 [hep-th].

[136] A. Carosso, "Stochastic Renormalization Group and Gradient Flow," *JHEP* **01** (2020) 172, arXiv:1904.13057 [hep-th].

[137] A. Carosso, A. Hasenfratz, and E. T. Neil, "Stochastic Renormalization Group and Gradient Flow in Scalar Field Theory," *PoS* **LATTICE2019** (2019) 287, arXiv:1912.01766 [hep-lat].

[138] M. Matsumoto, G. Tanaka, and A. Tsuchiya, "Renormalization group and diffusion equation," arXiv:2011.14687 [hep-th].